

Interference Management in Femtocell Communication System

Von der Fakultät für Elektrotechnik und Informatik

der Gottfried Wilhelm Leibniz Universität Hannover

zur Erlangung des akademischen Grades eines

DOKTORS DER INGENIEURWISSENSCHAFTEN

Dr.-Ing.

genehmigte Dissertation
von

M.Sc. Zhao Zhao

geb. am 19. August 1982 in Shanghai

2012

Referent: Prof. Dr.-Ing. Thomas Kaiser
Korreferent: Prof. Dr. Jürgen Peissig
Vorsitzender: Prof. Dr.-Ing. Jörn Ostermann
Tag der Promotion: 02.03.2012

ABSTRACT

The next generation cellular networks witness the inevitable trend towards network heterogeneity and universal frequency reuse. Given this background, the thesis focuses on the Femtocell and Macrocell coexisting 2-tier cellular systems.

The thesis investigates and proposes innovative Femto subband access algorithms for both uplink and downlink to better manage the interference and improve the coexistence with primary users. By theoretic analysis and computer simulations, the proposed algorithms are proven to be optimal in terms of maximizing the system transmission capacity. By devising a unified framework for both downlink and uplink spectrum access, the proposed algorithms are shown to be practical and implementable for the upcoming mainstream Femtocell designs.

Besides, the thesis also considers practical Femtocell issues and studies the influence of imperfect OFDM sidelobe leakage. The study reveals that, although OFDM sidelobe is in many cases negligible, it can cause substantial system performance loss when channel condition is poor and Femtocell deployment is dense. When revisiting the directional antenna approaches for indoor wireless communication, the thesis finds out that some simple pattern switching schemes, under the regulatory restrictions of EIRP, can achieve much better coexistence compared to omni-directional antennas, with only a slight sacrifice in coverage.

After summarizing the contributions in subband access and deployment issues, the thesis concludes that, even though with stringent budget and limited coordination with Macrocell, the Femtocells with careful study are able to manage its own interference and deemed to play an important roll in the future wireless communication systems.

Keywords

2-tier cellular, coexistence, spectrum access

ZUSAMMENFASSUNG

Die nächste Generation zellulärer Netzwerke bezeugt die unvermeidliche Tendenz zur Netzwerkheterogenität und den universellen Einsatz von Frequenzen. Vor diesem Hintergrund konzentriert sich die Arbeit auf die Koexistenzfähigkeit von 2-Ebenen Mobilfunknetzwerken.

Die vorliegende Dissertation untersucht dabei Algorithmen zur Verminderung der Interferenz und zur Verbesserung der Koexistenz in diesen Szenarien und schlägt innovative Femtozellenzugangsmechanismen für beide Übertragungsrichtungen, Uplink und Downlink, vor. Durch theoretische Analyse und Computersimulationen werden die vorgeschlagenen Algorithmen auf die Maximierung der Systemsübertragungskapazität hin überprüft. Mit Hilfe eines einheitlichen Rahmenwerks für den Downlink und den Uplink wird gezeigt, dass die vorgeschlagenen Algorithmen praktisch einsetzbar und somit für ein massentaugliches Femtozellendesign umsetzbar sind.

Des Weiteren untersucht diese Arbeit auch praktische Probleme beim Einsatz von Femtozellen, wobei der Einfluss der Außerbandstrahlung beim allgemein verwendeten Modulationsverfahren OFDM im Fokus steht. Die Studie zeigt dass, obwohl die Außerbandstrahlung von OFDM-basierten Systemen in vielen Fällen vernachlässigbar ist, sie im Falle eines schlechten Kanals und großer Femtozellendichte einen erheblichen negativen Einfluss auf die Systemperformanz haben können. Zudem werden Ansätze, basierend auf dem Einsatz von Richtantennen überprüft, wobei die Systeme mit umschaltbaren gerichteten Antennen die Koexistenzfähigkeit im Vergleich zu omnidirektionalen Antenne unter Berücksichtigung der regulativen Grenzwerte für die abgestrahlte Leistung wesentlich verbessern und die Abdeckung nur wenig verschlechtern.

Diese Arbeit schließt mit der Aussage, dass die Femtozelle, trotz strikter Limitierung und nur mit begrenzter Koordination mit dem Makrozellennetzwerk, eine wichtige Rolle in zukünftigen Mobilfunknetzwerken spielen wird.

Schlagwörter

2-Ebene Mobilfunknetz, Koexistenzfähigkeit, Zugang zum Spektrum

CONTENTS

1	INTRODUCTION	1
1.1	What is Femto	1
1.2	Technical Challenges	3
1.3	Goal and Scopes	6
1.4	Thesis Statement	9
2	SYSTEM MODELS AND INTERFERENCE TYPES	11
2.1	OFDMA System	11
2.1.1	Resource Allocation in OFDMA	11
2.1.2	Link SINR	12
2.2	Types of Interference	13
2.2.1	Link Types	13
2.2.2	How Strong is Each Type of Interference?	13
2.3	Performance Metrics	16
2.3.1	SINR and Shannon Capacity	16
2.3.2	Power- and Interference-limited System	16
2.3.3	Outage and Transmission Capacity	17
3	FEMTO SPECTRUM ACCESS I: MACRO FFR IN UPLINK	19
3.1	Motivations and Related Works	19
3.2	Contributions	23
3.3	System Models	24
3.4	Analysis and Proposed Algorithms	26
3.4.1	1st-Tier Performance	26
3.4.2	Proposed Algorithms	28
3.4.3	2nd-Tier Performance	32
3.5	Numerical Results	33
3.6	Extensions	37
3.6.1	None 2nd-tier limited Case	37
3.6.2	General Fading Case	39
3.6.3	Sectorized Macrocell Case	42
3.7	Chapter Summary	45
4	FEMTO SPECTRUM ACCESS II: MACRO FFR IN DOWNLINK	47
4.1	Motivations and Discussions	47
4.1.1	Summary from Uplink Case	47
4.1.2	Asymmetric for Downlink Case	48
4.2	Contributions	48
4.3	System Models	49
4.4	Proposed Algorithms	51
4.4.1	Analysis of Outage Probability	51
4.4.2	Transmission Capacity and Access Probability	53
4.4.3	Local MUE Estimations and Proposed Access Algorithms	55
4.5	Numerical Results	56
4.6	Unified Femto Uplink-Downlink Access	57

4.7	Chapter Summary	58
5	FEMTO DEPLOYMENT ISSUE I: OFDM SIDELobe LEAKAGE	61
5.1	Motivations and Related Works	61
5.2	Contributions	62
5.3	Performance Analysis	63
5.3.1	System Models	63
5.3.2	Interference Equivalents	64
5.3.3	Performance of Transmission Capacity	65
5.3.4	Performance of Area Spectral Efficiency	67
5.3.5	Short Summary	70
5.4	Numerical Results	70
5.5	Chapter Summary	74
6	FEMTO DEPLOYMENT ISSUE II: ANTENNA SWITCHING	75
6.1	Motivations and Related Works	75
6.1.1	Directional Antenna for Indoor Coverage	76
6.1.2	Femto Out-of-Building Emission Leakage	76
6.2	Contributions	77
6.3	Outdoor Leakage and Antenna Switching	77
6.3.1	Frequency Selection and TVWS Femto	77
6.3.2	Typical Scenarios	78
6.3.3	Performance Evaluation	80
6.3.4	Proposed Antenna Schemes	81
6.4	Numerical Results	84
6.4.1	Indoor coverage performances	84
6.4.2	Outdoor leakage and co-existence	85
6.5	Chapter Summary	91
7	SYSTEM SIMULATION METHODOLOGIES	93
7.1	General Description	93
7.2	Channel Model	94
7.3	Link-to-System Mapping	96
7.4	Network Simulation	97
7.5	Simulation Summary	97
8	CONCLUSIONS AND FUTURE WORKS	101
8.1	Concluding Remarks	101
8.2	Future Outlook	102
A	APPENDIX: POISSON POINT PROCESS	105
A.1	Definitions	105
A.2	Operations Preserving PPP	105
A.3	Palm Theory	106
A.4	Sum of Poisson Point Process	106
A.5	Shot-Noise Interference	107
	BIBLIOGRAPHY	109

LIST OF FIGURES

Figure 1	Future Heterogeneous Cellular Networks	1
Figure 2	Area Spectral Efficiency Gain by Technologies	2
Figure 3	Femto Revenue Predicted by Infonetics Research	4
Figure 4	Subfloat - Figure	4
Figure 5	Subfloat - Figure	6
Figure 6	Femto communication and interference channel	7
Figure 7	Femto ad-hoc deployment	7
Figure 8	Resource Allocation in OFDMA System	11
Figure 9	Simple Example of Co-Channel Interference	12
Figure 10	Types of Interference in Two-Tiered Cellular	14
Figure 11	Subfloat - Figure	20
Figure 12	F-ALOHA for Femtocell	22
Figure 13	Subfloat - Figure	23
Figure 14	System Model for Study	24
Figure 15	Biased F-ALOHA for Femtos in FFR Macrocell	26
Figure 16	Flowchart of Proposed Optimal Access	30
Figure 17	Transmission Capacity vs. MUE Power Control	35
Figure 18	Transmission Capacity vs. MUE FFR Topology	35
Figure 19	Transmission Capacity vs. MUE Target SIR and Femto Power	36
Figure 20	Second Tier Outage vs. Maximal SIR Target	36
Figure 21	TC vs. MUE FFR Topology in Non-Interference-Limited Case	40
Figure 22	TC vs. MUE FFR Topology in Different Fading	40
Figure 23	Sectorized Case for Macro	43
Figure 24	TC vs. MUE FFR Topology in sector case	46
Figure 25	Subfloat - Figure	47
Figure 26	FUE report the neighboring MBS lists to connected FBS	49
Figure 27	PPP distributed st-and 2nd-tier base stations	50
Figure 28	The Downlink System Map	51
Figure 29	Flowchart of the proposed access algorithm	55
Figure 30	Performance of Proposed Algorithm	57
Figure 31	Subfloat - Figure	58
Figure 32	Sidelobe Leakage for the three Schemes	63
Figure 33	Topology of the System	64
Figure 34	System TC for Accommodating Femtos	71
Figure 35	Macrocell ASE vs. Subband Access	71
Figure 36	Femto ASE in LA channel vs. Subband Access	73
Figure 37	Femto ASE in HA channel vs. Subband Access	73
Figure 38	Subfloat - Figure	75
Figure 39	Primary DVB-T and cognitive LTE-Femtos	79
Figure 40	Subfloat - Figure	79

Figure 41	Subfloat - Figure	80
Figure 42	Azimuth Pattern of Designed Antenna, Omni(left), Patch(mid), and Array(right)	82
Figure 43	Adaptive switching of 1 or 2 patch antenna elements	83
Figure 44	The Training Process of Antenna Switching	83
Figure 45	Throughput of Building A with Omni-Antenna when FBS ₁ is switched on at Freq A, mean data rate is 12.7 Mbit/s, indoor coverage probability is 100%	85
Figure 46	Throughput of Building A with Omni-Antenna when FBS ₁ is switched on at Freq B, mean data rate is 10.7 Mbit/s, indoor coverage probability is 98.9%	86
Figure 47	Throughput of Building A with Omni-Antenna when FBS ₁ is switched on at Freq C, mean data rate is 8.6 Mbit/s, indoor coverage probability is 95.4%	86
Figure 48	Throughput of Building A with Antenna Scheme II when FBS ₁ is switched on at Freq C, mean data rate is 8.1 Mbit/s, indoor coverage probability is 92.2%	87
Figure 49	Throughput of Building A with Antenna Scheme III when FBS ₁ is switched on at Freq C, mean data rate is 8.4 Mbit/s, indoor coverage probability is 93.3%	87
Figure 50	Peripheral emission leakage from Building B when equipped with Omni Antenna	88
Figure 51	Peripheral emission leakage from Building B when equipped with Antenna Scheme I	88
Figure 52	Peripheral emission leakage from Building B when equipped with Antenna Scheme II	89
Figure 53	CDF of leakage power	89
Figure 54	Outage rate vs. LTE-Femto density	91
Figure 55	General Simulation Process	93
Figure 56	Indoor Channel and Raytracing Method	94
Figure 57	Outdoor Leakage and Empirical Channel	95
Figure 58	Subfloat - Figure	98
Figure 59	Generate PPP Positions	99
Figure 60	The Overall Simulation Process	99

LIST OF TABLES

Table 1	Interference Types	15
Table 2	Applications of PPP Modeling in Wireless Communication	21
Table 3	Proposed ALOHA algorithm	23
Table 4	Default Simulation Parameters for 3.5	34
Table 5	Default Simulation Parameters for 4.5	56
Table 6	Default Simulation Parameters for 5.4	72
Table 7	Comparison of the three Schemes	74
Table 8	Indoor Coverage Probability vs. Antenna Schemes	90
Table 9	AMC and Data Rate	96

GLOSSARY

PPP	Poisson Point Process
SOHO	Small Office /Home Office
MCS	Modulation and Coding Scheme
CIR	Channel Impulse Response
FBS	Femtocell Base Station
MBS	Macrocell Base Station
UE	User Equipment
FUE	Femtocell User Equipment
MUE	Macrocell User Equipment
OFDMA	Orthogonal Frequency-Division Multiple Access
LTE	Long Term Evolution
4G	4th-Generaltion Mobile Telecommunication
DAS	Distributed Antenna System
FFR	Fractional Frequency Reuse
EIRP	Equivalent Isotropically Radiated Power
FBMC	Filter Bank Multicarrier
OQAM-OFDM	Offset-QAM OFDM
SIR	Signal-to-Interference Ratio
SINR	Signal-to-Interference and Noise Ratio
AMC	Adaptive Modulation and Coding
WIFI	Wireless Fidelity
TC	Transmission Capacity
ASE	Area Spectral Efficiency
CCI	Co-channel Interference
OCI	Other-cell Interference
ICI	Inter-channel Interference
OOB	Out-of-band

FAP	Femto Access Point
BS	Base Station
EPC	Evolved Packet Core
FCC	Federal Communication Commission
TVWS	TV White Spaces
ISM	Industrial, Scientific, and Medical
CR	Cognitive Radio
ppb	parts-per billion
IRC	Interference Rejection Combining
SIC	Soft/Successive Interference Cancellation
RB	Resource Block
MANET	Mobile Ad-hoc Networks
GPS	Global Positioning System
EESM	Effective Exponential SINR Mapping
IOT	Interference over Thermal
OPEX	Operating Expenditure
CAPEX	Capital Expenditure

MATHEMATICAL ABBREVIATIONS AND NOTATIONS

\mathbb{R}	set of real number
\mathbb{R}^d	Euclidean space of dimension d
\mathbb{Z}	set of integer
\mathbb{N}	set of non-negative integer
$ \cdot $	Lebesgue measure
$\ \cdot\ $	Euclidean norm
$(a)^+$	$\max(0, a)$
$\Pr(\cdot), \Pr^0(\cdot)$	probability, Palm probability
$\mathbf{E}(\cdot), \mathbf{E}^0(\cdot)$	expectation, expectation w.r.t. the Palm probability
$\mathbf{F}_a(\cdot), \mathbf{F}_a^c(\cdot)$	c.d.f., c.c.d.f. of r.v. a
$\mathbf{f}_a(\cdot)$	p.d.f. of r.v. a
$\mathcal{L}_a(\cdot)$	Laplacian transform of r.v. a
$\mathcal{N}(\mu, \delta^2)$	Gaussian law of mean μ and variance δ^2 on \mathbb{R}
$\mathcal{LN}(\mu, \delta^2)$	lognormal law of mean $e^{\mu+\delta^2/2}$ and variance $(e^{\delta^2} - 1)e^{2\mu+\delta^2}$
S, I, N	power of signal, interference, noise
γ, Γ	SIR/SINR, SINR threshold
\mathcal{E}	outage event
λ, Λ	the intensity of a hPPP deployment, the maximal λ that meets outage bounds
(1), (2)	first, second tier (in superscript)
(a), (s), (c)	mainlobe, sidelobe, combined interference (in superscript)
V, A	victim, aggressing link
w.r.t.	with regard to
p.d.f.	probability density function
r.v.	random variable
c.d.f.	cumulative density function
c.c.d.f.	complimentary cumulative density function
i.i.d.	independently and identically distributed
R.H.S.	right hand side
L.H.S.	left hand side

INTRODUCTION

Femto Cellular System, or shortly "*Femto*", is basically a Home Base Station that is apart from the conventional cellular infrastructure for the signal improvement in residential use. With a brief summary of the state-of-the-art Femto market and research, we consequently address the main technical challenges that might jeopardize the Femtocells successful deployment, and cause substantial hazards to already existed Macro Cellular System, or shortly "*Macro*". Among these challenges, we focus on the Femto-Macro interference problems with sheer cost and implementation restrictions. The main research goals and perspectives of this thesis are thus formalized into several specific topics. We will briefly introduce these topics in this chapter and tackle with them one by one in detail in the following chapters. Additionally, we describe the sketch of this thesis at the end of this chapter.

1.1 WHAT IS FEMTO

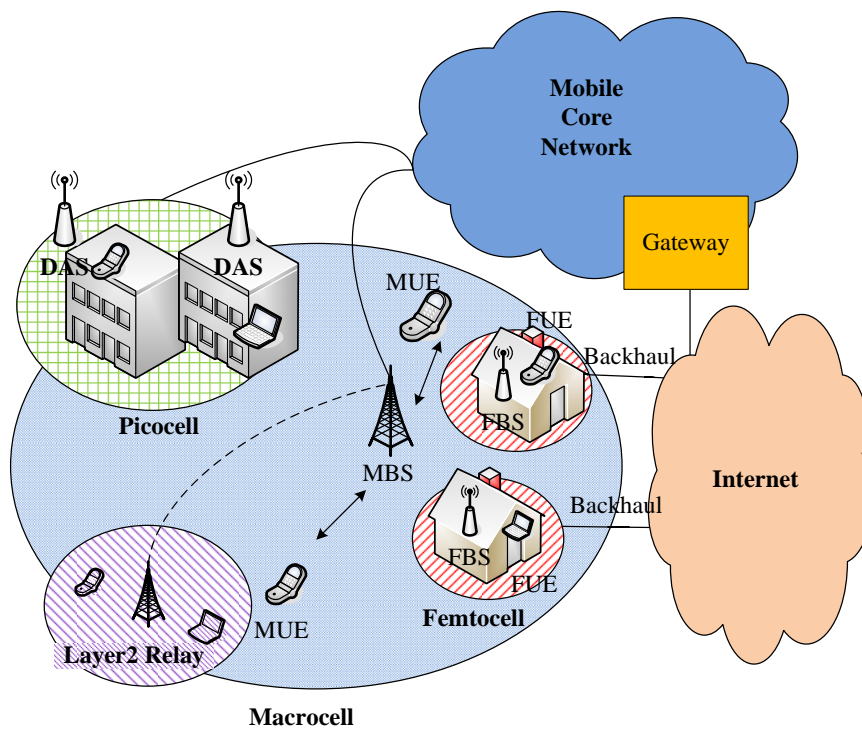


Figure 1: Future Heterogeneous Cellular Networks

Due to the essential nature of uneven distribution of traffic and radio propagation over the terrestrial plain, **hotspots** (where dense user traffic emerges) and **deadzones** (where radio signal is deeply blocked) are the two long standing and formidable obstacles for mobile communication

system to achieve ubiquitous coverage. Even since the very beginning of cellular age, radio **Repeaters** are invented and deployed in specific places to improve the signal coverage for indoor and underground deadzones. In 1990s, **Picocell** or simply "*Pico*" and Distributed Antenna System (**DAS**) are also brought into reality but they were never with a high market portion and massive deployment. With the upcoming era of 4th-Generaltion Mobile Telecommunication (**4G**), radio technologies have been greatly advanced and we witness the roll-out of many powerful coverage solutions such as **Layer 2 Relays** (or simply "*Relays*") and **Femtos**. Relays, Femtos, together with Repeaters, Picos, DASs, and etc. formalize the future cellular system with multi-elements in variety and we are affirmed that this trend towards network heterogeneity is inevitable and will become more and more significant in the next decades, see Fig. 1.

There are many forces in the background compelling the cellular heterogeneity. Among them, the greatest force comes from the exploding data traffic from multi-media applications, thanks to the recent advances in laptops, smart-phones and tablet products.

Other forces are the growing expenditure for operating a Macrocell and the accumulating concerns on Area Spectral Efficiency (**ASE**). It has been shown by many reports that since 1957, the wireless capacity has an approximately million-fold increase, $25\times$ improvement from wider spectrum, $5\times$ improvement from dividing spectrum into smaller slices, $5\times$ improvement by designing better modulation schemes, and a whopping $1600\times$ gain through reduced cell sizes and transmit distance [7], see Fig. 2. Therefore, turning into smaller size and providing various support of traffic demands is indeed the great intuition towards cellular heterogeneity by service providers.

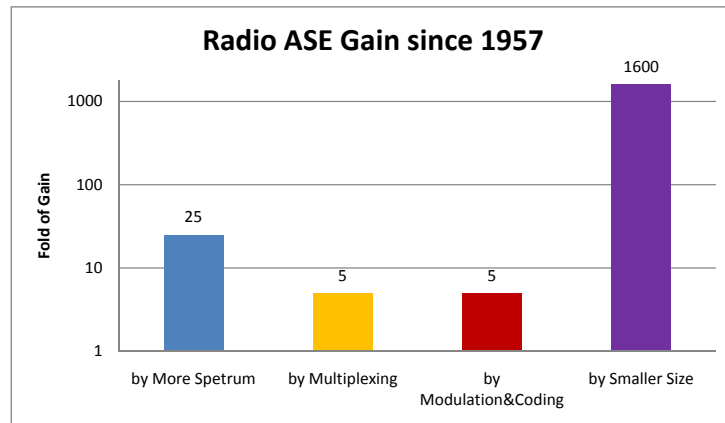


Figure 2: Area Spectral Efficiency Gain by Technologies

As one of the above mentioned cellular elements, Femtos are aimed to improve the residential and Small Office /Home Office (**SOHO**) indoor coverage. Distinguished from Picos, Femtos are apart from the cellular infrastructure, usually back-hauled to Internet and the Core Network via

some gateways. It is supposed to be deployed by end-users and transmit at a much lower power so its coverage range is usually only within 10-15 meters[3]. Other than DAS which is only a radio signal multiplexer, Femto Access Point (FAP) is much complicated. It is literally a Base Station (BS), i.e. Femtocell Base Station (FBS) and possesses the same air interface as Macrocell Base Station (MBS) so that ordinary User Equipment (UE) can connect to it without extra requirements. For simplicity reasons, throughout the thesis, we name the UEs that connected to MBS as Macrocell User Equipment (MUE) and to FBS as Femtocell User Equipment (FUE).

In recent years, Femtos are becoming a very hot topic that attracts many research efforts from both academia and industry. We can summarize the main reasons of this phenomenon as the following:

- According to the market research by Infonetics Research in year 2007 [38], 69% of the cellular data traffic and 58% of the phone calls are predicted to be made from residential indoors in year 2013. Since MBS tower are usually located outdoors, the radio signal penetrated into the buildings are relatively weak, insufficient to support the most of high speed traffic demand. Thereby, indoor hotspot technology is very promising for dense deployment.
- The second reason is coming from the service providers. Wireless Fidelity (WIFI) as another hotspot technology has been a success and dominates the residential market for a long time. The Repeaters, Picos are mainly for enterprise customer, and the providers are facing the huge problem of reduced residential customer's royalty and hoping that Femtos can salvage this situation. Concerning the cost, the providers are also very keen to deploy the Femtocell because great amount Capital Expenditure (CAPEX) and Operating Expenditure (OPEX) can be saved, see [21] for the Femto financial analysis. The report of [28] also addresses the possibility that Femtos might have great potentials in improving the 4G business models. See Fig.3 for the global Femto revenue forecasts conducted by Infonetics Research [39] amid the economic recession in past three years.

1.2 TECHNICAL CHALLENGES

We will first discuss the Femto technical challenges in aspects of Networking, Regulation, and Implementation. Then we will focus ourselves on the coexistence and interference issue for Femtocells.

Networking is difficult for Femtos mainly due to fact that Femtos are back-hauled to Internet, which means a limited signaling bandwidth and latency issues for synchronization and inter-cell coordination. For example, X2 interface in 3GPP Long Term Evolution (LTE) releases has not yet been successfully realized and providers are also worrying about that a large number of Femtos using X2 to connect with local Macros may lead to the great congestion problems for Evolved Packet Core (EPC) network.

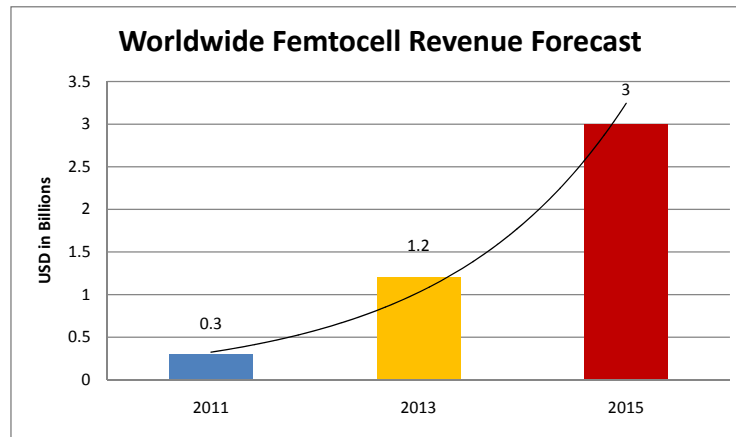


Figure 3: Femto Revenue Predicted by Infonetics Research

Another problem with Networking is how to proceed with the handover and **Access Control** protocol when the subscribers are frequently entering and leaving the coverage region of Femtocells. There are mainly three access modes for Femtocells under discussion, i.e. *Closed Access*, *Open Access*, and *Hybrid Access*.

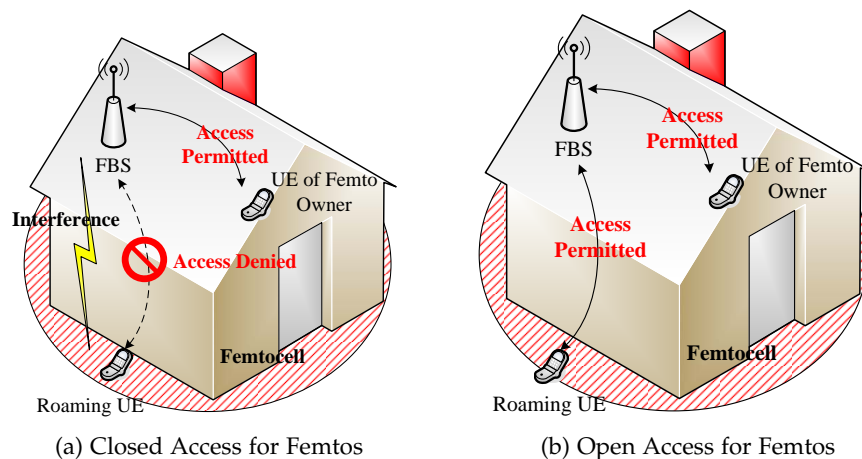


Figure 4: Access Control for Femtocells

- Closed Access, see Fig. 4a, means that Femtocells are only open for subscribers who possesses it and closed to public roaming ones.
- Open Access, see Fig. 4b, on the contrary, allows all the subscribers to access as long as they are in a good coverage of the Femtocell. Apparently, Closed Access suffers from some possible strong co-channel interference problems when the roaming UEs are very close to the FBS. However, customers are not willing to share their own property of Femtocell for public traffic, especially when the safety and security issues are concerned.
- Thereby the Hybrid Access mode is proposed that only allows a very limited bandwidth for public access (only some telephone calls in

strong interference occasions for example) to achieve a "Win-Win" status between the operators and Femto owners.

Regulation for Femtocell is mostly concerned in the following aspects. First concern is the licensing for Femtos. Because Femtos are possessed by end-user, it is possible that a FBS equipment registered in Country A appears in Country B. Operators shall have strict license control to prevent these situations to happen. Additionally, they are also required to own the legal right of terminating the Femtos from service in the cases of technical upgrade, spectrum license expiration etc. Last but not least, as Federal Communication Commission (FCC) has recently ruled, Femtos are also deemed as a part of the provider's communication network so that they are also responsible for accepting emergency calls and some tasks as criminal tracing of locations. Therefore, the locating precision for Femtocells shall be no less than 50m.

Implementation of Femtocell meets a very strict limit in cost because the peer competitor WIFI is extremely cheap in terms of market prices. The current goal of Femto Forum is to make the cost of each FBS as low as 50 US dollars, which also means a practical design against algorithms and mechanisms with too much in complexity [14]. For example, the frequency synchronization for LTE Femtocells [30], as mandated by 3GPP in Rel. 10 [1], the carrier frequency error of LTE Femtocells shall be no more than 250 parts-per billion (ppb), i.e. no less than 50Hz frequency offset at 2.1GHz, which is definitely a challenge at this moment for low-cost realizations.

Finally, we come to the discussion of **Frequency Reuse** and **Interference Management** for Femtocells. At the current stage, the frequency for the Femtocells to access is mostly the same licensed spectrum owned by the service provider because this can rather increase the spectrum efficiency and greatly chop down the cost per bit. We name it here as the *licensed spectrum access* for Femtos, which is favored by the providers as long as the interference coming from the reusing Femtos is at a benign level [44].

There are also some considerations of *unlicensed spectrum access* for Femtos, like its counterpart WIFI in Industrial, Scientific, and Medical (ISM) or even TV White Spaces (TVWS). However, Femtos accessing unlicensed spectrum also mean that the UE radio front-end shall support this unlicensed band as well. This is definitely one critical shortcoming since that the current standardized UEs can only support licensed 3G or 4G bands. However, we do not here exclude the possibility that in a long term future, Femtos might indeed access the unlicensed spectrum like a Cognitive Radio (CR) device. In fact, we discuss some performances for unlicensed spectrum access Femtos in this thesis, see Chapter 5 and 6 of Femto deployment issues.

Let us go back to the licensed spectrum access for Femtocells. There are basically two approaches for allocating the junction of provider-owned licensed frequency bands to the Femtocells, *Orthogonal Access* and *Nonorthogonal Access*[48].

- **Orthogonal Access**, see Fig. 5a, is to simply assign a small fraction of the bands exclusively to the Femtocells, so that no matter how dense

the Femto deployment is, there can be no great influence on the Macro users who are working on the cross-orthogonal bands.

- In **Nonorthogonal Access**, see Fig. 5b, there is no such exclusive assignment, so Femtos need to share the whole band with Macros in a subordinate manner, meaning that spectrum usage of Femtos is strictly inferior to the Macros.

Although some research works reveal that Orthogonal Access in many cases outperforms the Nonorthogonal Access [35] [17], the providers seem to favor the Nonorthogonal Access, because a trunk of dedicated spectrum band is way too expensive and the exclusive assignment does not scale well with the evolving market of Femtos.

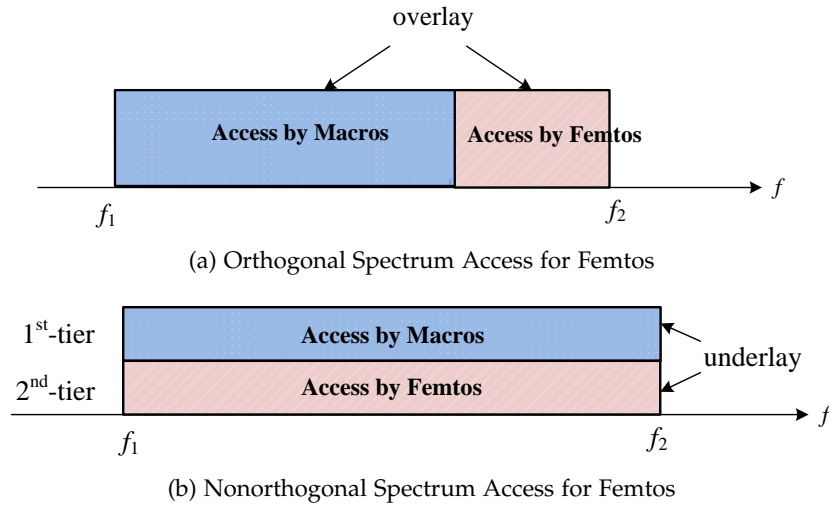


Figure 5: Licensed Spectrum Access for Femtocells

For the Nonorthogonal Access, the Femtos and Macros are sharing the same frequency band with different level of priority. We name such network as *two-tiered* cellular networks, with Macros as the *1st-tier* and Femtos as the *2nd-tier*. The interference management in two-tiered cellular is a very popular topic in research, attracting many contributions from Baccelli, Andrews, Haenggi, Weber, etc. in [12] [9] [11] and [69]. Some works were even extended into a multi-tier domain, capturing the generic heterogeneous network structure of Macros, Picos, and Femtos.

The focus of this thesis is kept also on the case of Nonorthogonal Access. In most of the analysis conducted by this thesis, we will look into both the 1st-tier and the 2nd-tier performances. We introduce the related works in more detail in Chapter 3, 4, and 5.

1.3 GOAL AND SCOPES

The research goal of this thesis is to analyze and devise the interference management algorithms for Femto-Macro coexisting heterogeneous networks within the following scopes:

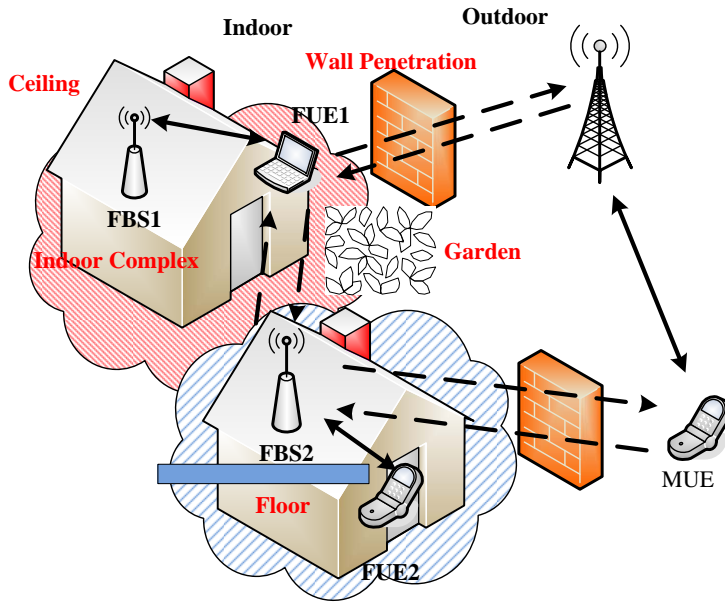


Figure 6: Femto communication and interference channel

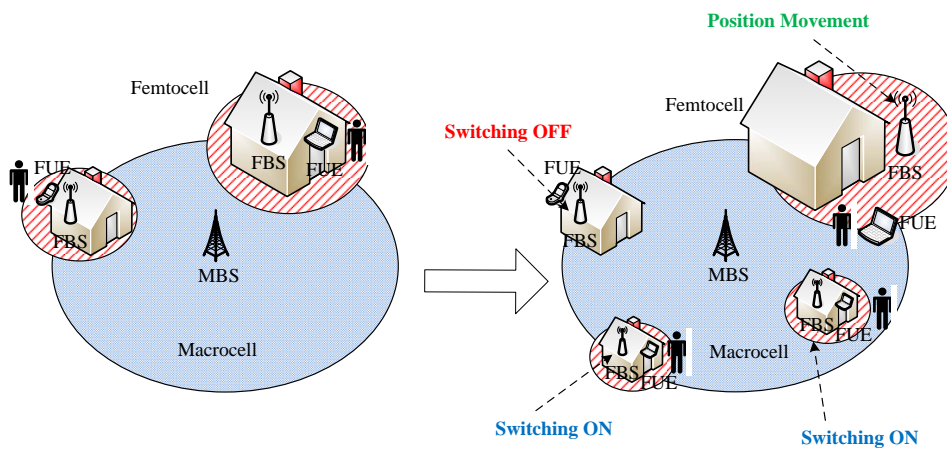


Figure 7: Femto ad-hoc deployment

- **Scope 1:** In this thesis, we will only consider the nonorthogonal spectrum access since it is the mainstream deployment for Femtos. We treat the underlying Femtos as the low cost devices that interference management mechanism is favored to be developed in a distributed manner with controllable parameters and able to adapt to the dynamics of Macrocells. We will try to avoid covering the implementation-oriented schemes by the current efforts from industry. Instead, we deliver a more general and innovative design of Femtos with random access and optimal controlling, which can be the guidelines of the performance bounds for Femto future deployment. We do admit that by the current Femto deployment, inter-tier interference is relatively benign, but for a longer term and more aggressive assumptions, the Femto interference is demonstrated by this work as the true bottleneck of overall system performance. Moreover, we also include the fairly long term TVWS-Femto assumptions in the deployment issue, and discuss the maximal performance bounds for antenna-switching or beam-forming for Femtos using innovative analysis techniques.
- **Scope 2:** In this thesis, we suppose close-access for Femto users. We will consider the interference management issues only for Orthogonal Frequency-Division Multiple Access (OFDMA) based Macro and Femtocells. In OFDMA based communication systems, the intra-cell interference is trivial because resources are orthogonal in frequency or time domain and well scheduled by MAC mechanism to assign to different users. The main performance-influencing interference source is the Other-cell Interference (OCI). Meanwhile, we will mainly concentrate on co-OFDM subcarrier interference (i.e. Co-channel Interference (CCI)) since the inter-subcarrier interference (i.e. Inter-channel Interference (ICI)) due to time offsetting is relative minor in OFDM-like systems. However, in Chapter 5 deployment issues, we do look into some special cases and prove that the imperfect Out-of-band (OOB) of OFDM system can also lead to a substantial performance loss.

To better understand the interference management issue for OFDMA Femtos within the thesis scopes, we summarize the distinctive attributes of Femtocells into the following five remarks.

Remark 1.1 *Femtocells possess a unique indoor wireless channel, e.g. the house shielding effect and the multi-scattering, which is different from the Macro-and Picocells, so it shall be treated in a particular way, see Fig. 6;*

Remark 1.2 *Femtocells are user deployed with ad-hoc manner, while Macro and Picocells are usually provider deployed with a certain plan, see Fig. 7;*

Remark 1.3 *Femtocells have lower traffic demand than Macrocells, the Femto UEs are also lower in number and more symmetry distributed;*

Remark 1.4 *Femtocells are subordinated spectrum user, meaning that their existence shall never exceed the Macro tolerable limit regardless its own performance;*

Remark 1.5 *Femtocells are stringently cost limited. Algorithms with extensive coordination and additional hardware interface requirement are not preferred.*

As we can see from the above, the interference management issue for OFDMA femtos in the scopes of this thesis is very much distinguished from the previous study of inter-cell interference. This indeed justifies the main motivations for this thesis work, and these five remarks essentially play the central roles for the development of algorithms throughout this thesis.

1.4 THESIS STATEMENT

The main contribution of this thesis work can be summarized as follows:

1. In Chapter 3, we analysis the system performance when Femtos are lying under Macros performing Fractional Frequency Reuse (FFR) and propose a partially-biased F-ALOHA spectrum access algorithm which requires the knowledge of macro FFR configuration broadcasted to local Femtos. The proposed scheme is proved to be optimal in the sense of achieving the maximal transmission capacity and it can well adapt to Macro dynamics.
2. In Chapter 4, we analysis the system outage for downlink cases and proposed a totally-biased F-ALOHA algorithm to let the Femtocells achieve the maximal transmission capacity. To enable this algorithm, each FBS shall estimate the local FFR condition and we thus design the mechanism to support these message passing and online inquiry, which is a unified framework for both uplink and downlink.
3. In Chapter 5, we discuss the possibilities of Femtos accessing TVWS and the substitutes of physical layer interfaces. We analyze the effect of OFDM's OOB leakage and derive the analytical performance to make comparisons between several physical layer candidates.
4. In Chapter 6, we discuss the antenna aspects of Femtocells and their influence on the Femto-to-Macro interference. We devise two implementable antenna switching algorithms and designed specified antenna pattern for study. Our findings are that the best-effort performances of antenna switching under EIRP constraints are comparable to Beam-forming and greatly reduce the Femto-to-outdoor interference.
5. In Chapter 7, we propose a joint link- and system-level simulation methodology, which well captures the Femto ad-hoc manner and avoids the inefficiency of empirical propagation model in predicting cross-indoor and outdoor pathloss. We demonstrate this methodology in the simulation for the study cases of Chapter 6, showing a reasonable computation load and the prediction is close to practice.

The thesis is organized as following, in Chapter 1, basic introduction of Femtocell is made together with the motivation of the research and

the basic scopes of the research. In Chapter 2, we address the generic modeling for Femto-Macro (two-tier) coexistence scenarios and classify the interference links into different types. By introducing the industry results, we also explain why inter-tier interference is the main concern of this thesis. In Chapter 3, the F-ALOHA based Femto spectrum access in uplink is investigated with its extension to Macro FFR scenario. In Chapter 4, the work of Chapter 3 is extended to the case of downlink and the unified framework for both links is proposed. In Chapter 5, we discuss the practical deployment issue of sideband leakage in Femtocells. In Chapter 6, adaptive antenna pattern switching is revisited for Femtocell and proved to have excellent performance in the sense of reducing interference. In Chapter 7, we propose an innovative link-and system level simulation methodology and present the simulation results thereafter. Finally in Chapter 8, we draw the conclusion of the thesis work and discuss the future work.

Besides the main contents, the thesis is also provided with an appendix. The appendix is to introduce the fundamentals of stochastic geometry and Poisson Point Process, which supports the analytic work in Chapters 3, 4, 5, and 6.

In this chapter, we formalize the interference management problems of two-tiered cellular system by scenario modeling and interference classification. We define each type of co-channel interference and present the preliminary results done by other parties, mainly from Femto Forum. It is necessary here to shortly introduce the Femto Forum, which is an industrial partnership composed of leading companies in the Femtocell area such as Airvana, Alcatel-lucent, Qualcomm, Samsung, ip.access, etc. It is aiming to promote the concepts and standardize the 2G/3G/4G Femtocell products. Before the roll-out of Femtocell, the newly brought interference is estimated to be serious by the providers. Therefore the Femto Forum has conducted a series of interference studies during year 2008-2010 and published the main results in its white papers, see [29] and [27]. We will first follow the trace of their prototyping method of Femtocell interference and then give a brief discussion to point out the limitation and drawbacks of the industrial efforts. Finally we establish our own modeling method and clarify the performance metrics for the development of the algorithms in this thesis.

2.1 OFDMA SYSTEM

2.1.1 Resource Allocation in OFDMA

Firstly, let us take a look at a typical OFDMA system, see Fig.8 for example.

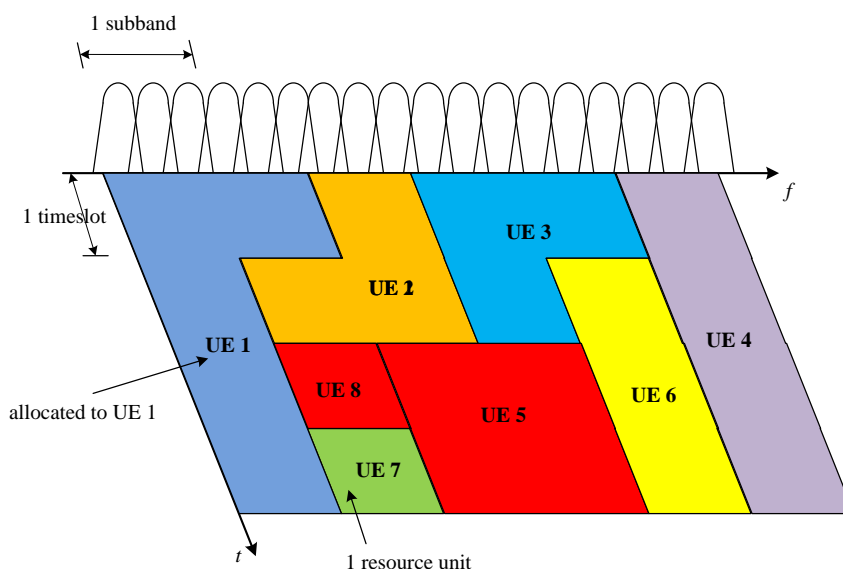


Figure 8: Resource Allocation in OFDMA System

In such system, the resource is slotted in both frequency and time domain. Each of such resource unit is called Resource Block (RB) in this thesis, which can be assigned by the scheduler to one UE within the cell exclusively at the same time. This mechanism precludes the intra-cell interference since each user's resource are orthogonal either in frequency or time domain. As already introduced in the scope of this thesis, both the Macro and Femto are assumed to use the same OFDMA interface with same resource divisions. Although there can be timing offset of the arriving OFDM symbols between Macros and Femtos due to the fact that many of the current FDD Femtos are working at un-synchronized manner, we neglect this effect and look only on one "typical" RB for the observation of a number of sub-frames, where traffic and scheduling decision are assumed to be consistent. This assumption is validated for the case of constant and high data rate traffic with low user mobility which is applicable to the Femto scenario. Moreover, the quasi-constant channel gain assumption on this typical RB is also reasonable since Doppler effect is generally not serious for Femtos, where most users are nomadic or fixed ones.

And throughout the thesis, we name the communication link that is suffered by other-cell interference as the *Interference Victim*, or simply the *victim*, and all the source of interference link as the *Interference Aggressor*, or simply the *aggressor*. We will mostly look only into the traffic channel, although some results might also apply to the control channel of the communication system.

2.1.2 Link SINR

We will take a single link on one specific RB as example:

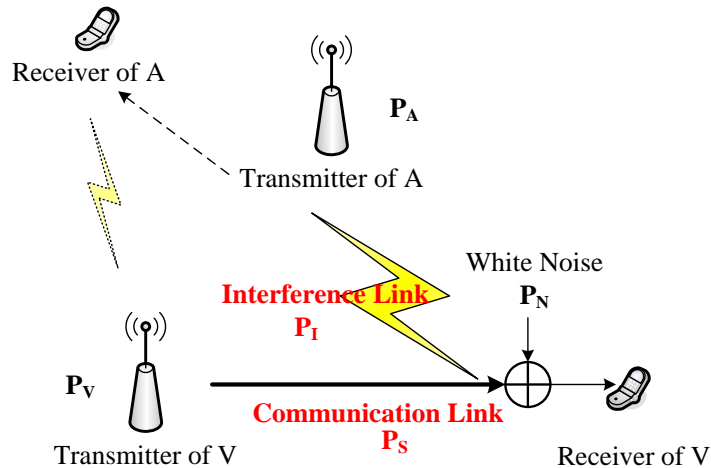


Figure 9: Simple Example of Co-Channel Interference

If we assume the transmit power of victim V and aggressor A transmitter as P_V and P_A respectively and use the empirical radio propagation model as the received signal S seen by the victim receiver is given by:

$$S = P_V K_V W_V X^{-\alpha_V} \quad (2.1)$$

where K_V, W_V, α_V are the penetration loss, large/small-scale fading, pathloss exponent, respectively. X is the distance between communication link pair. Similarly the received interference power, denoted as I , from aggressor A and seen by V equals to:

$$I = P_A K_A W_A Y^{-\alpha_A} \quad (2.2)$$

where K_A, W_A, α_A have the similar definition but on interference link A and Y is the interference distance.

In the case of one victim and one aggressor in the system, the Signal-to-Interference and Noise Ratio (SINR) of victim link, denoted as γ is easily given by:

$$\gamma = \frac{S}{I + N} \quad (2.3)$$

where N is the power of noise, which is modeled as white Gaussian and treated as a constant value throughout the thesis.

Of course, A and V are mutually interfering with each other on the co-channel and usually the interference arrived at one victim can be aggregated from a set of \mathcal{A} interference aggressors. In such case, γ is derived by:

$$\gamma = \frac{S}{\sum_{A \in \mathcal{A}} I_A + N} \quad (2.4)$$

2.2 TYPES OF INTERFERENCE

2.2.1 Link Types

The intuition of dividing interference into different types are quite straightforward. According to Femto Forum, we classify the interference according to the link properties of UL/DL and Femto/Macro, see Fig. 10. The benefit of doing so is that, when we know which type of interference is serious, we can simply devise interference avoidance or mitigation algorithms dedicated to this link and leaving those trivial interference untouched. Therefore the only remaining question is how strong and how significant is each of these interference types. The answer is given in sub-section 2.2.2.

2.2.2 How Strong is Each Type of Interference?

In the following, we will briefly describe if each of the interference types is serious to system performance or not. The results are very similar to the OFDMA interference report by Femto Forum:

1. Femto-to-Femto in UL (intra-2nd-tier):

Aggressor Transmitter: FUE

Victim Receiver: FBS

This type of interference is corresponding to Scenario F1 in Femto Forum white paper [29]. Many simulation-based studies reveal that

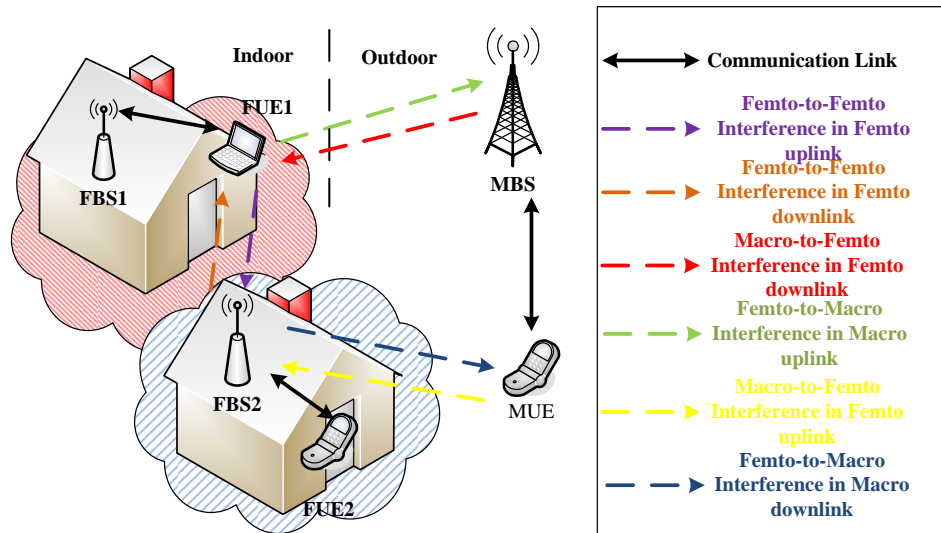


Figure 10: Types of Interference in Two-Tiered Cellular

this type of interference is relative benign because two reasons: 1) FUE transmit power is usually low 2) FUE is in most cases in good coverage of the connecting FBS so uplink power control can further alleviate the interference. On the other hand, great interference can indeed happen when victim FUE or aggressor FUE is placed at the corner of the house. However, this extreme case is very rare. Therefore we treat this type of interference as **minor** at low deployment of Femto.

2. Femto-to-Femto in DL (intra-2nd-tier):

Aggressor Transmitter: FBS

Victim Receiver: FUE

This type of interference is corresponding to Scenario E in Femto Forum white paper [29]. This type of interference is more serious than Type 1 especially when the traffic is of full buffer. Substantial outage is observed by simulation and fairness can also be decreased when a "loud" FBS is always transmitting. However, due to the traffic load of Femto is relative small, Femtos in the vicinity can reuse the frequency at a higher factor. Moreover, Femtos are in lower priority than Macros, thereby, in sum, we treat this type of interference as **medium**, need further investigation in the thesis.

3. Macro-to-Femto in DL (cross-tier):

Aggressor Transmitter: MBS

Victim Receiver: FUE

This type of interference is corresponding to Scenario A1 in Femto Forum white paper [29]. This type of interference is not serious thanks to the high outdoor-to-indoor penetration by walls and ceilings. Moreover, it is not scalable with the increase of Femto deployment. Therefore, we treat this type of interference as **minor**, generally negligible.

4. Femto-to-Macro in UL (cross-tier):

Aggressor Transmitter: FUE

Table 1: Interference Types

Interference Type	Description	Evaluated by Femto Forum
#1	Femto-to-Femto in UL	benign
#2	Femto-to-Femto in DL	medium
#3	Macro-to-Femto in DL	minor
#4	Femto-to-Macro in UL	medium-high
#5	Macro-to-Femto in UL	minor
#6	Femto-to-Macro in DL	medium-high

Victim Receiver: MBS

This type of interference is corresponding to Scenario D2 in Femto Forum white paper [29]. This type of interference is extreme dangerous because the victim is MBS. Conducted simulations suggest that the transmit power of FUE must be capitalized at a low level, otherwise significant harms to the Macro can be done. Another option to mitigate the interference is to secure the usage of Femto from the near region of Macro towers because UE in that region is generally in good coverage of Macro and not necessary to bridged to Femto. We treat this type of interference as **medium-high**, need further investigation in the thesis.

5. Macro-to-Femto in UL (cross-tier):

Aggressor Transmitter: MUE

Victim Receiver: FBS

This type of interference is corresponding to Scenario B1 in Femto Forum white paper [29]. This happens when FBS is located at Macro edges, in the near of MUE with high transmit power. However, in the condition of low Femto deployment, this interference is shown to be minor by simulation study. Therefore, we treat this type of interference as **minor**, not of great impact to system performance.

6. Femto-to-Macro in DL (cross-tier):

Aggressor Transmitter: FBS

Victim Receiver: MUE

This type of interference is corresponding to Scenario C1 in Femto Forum white paper [29]. This is the interference attracting most of the research interest because it can cause the MUE-call to drop and is generally difficult to predict although outage does happen at certain possibility. There are some proposed solutions, such as capitalizing the FBS transmit power, enabling the FBS to sniff the uplink pilot signal by MUE, and also position dependent FBS power control (low transmit power if FBS is at Macro cell edge). However, none of the above solutions can work perfectly alone. We treat this type of interference as **medium-high** and are going to further investigate in the thesis.

To conclude in Tab. 1, interference type 2, 4, and 6, i.e. Femto-to-Femto and Femto-to-Macro interference, are of the major interest because they

can be very harmful to system performance. Therefore, these three types of interference will be the major management object in the thesis. However, it is noted that the above results are generally obtained by computer simulation merely with rather conservative assumptions of Femto deployment. Henceforth, it is still possible that the results do not hold when high market penetration of Femtos are realized in the long term of future. In our study, we will investigate the scenarios and make the performance predictions from a more pessimistic perspective and find out the effective interference management algorithms that can be scalable with different Femto deployment and scenario setups.

2.3 PERFORMANCE METRICS

In the following, we will define the performance metrics in this thesis in a more generic manner. We will begin with the SINR.

2.3.1 SINR and Shannon Capacity

SINR is an important metric for the link performance, since the well known Shannon capacity C of link V in SISO case is given by:

$$C = B \log_2(1 + \gamma) \quad (2.5)$$

where B is the transmission bandwidth.

In practical systems, the link achievable data rate c can be depicted as:

$$c = w B \log_2(1 + \zeta \gamma) \quad (2.6)$$

where $w \in (0,1)$ and $\zeta \in (0,1)$ denote the optimality gap between the Shannon capacity and the performance of practical radio transceivers.

Thanks to the efforts in realizing advanced modulation and coding schemes and link rate adaptation Adaptive Modulation and Coding (AMC), w and ζ for current best-practice transceivers are close 1 meaning that the SISO is nowadays on the verge of the Shannon capacity[51]. Therefore, without too much loss of generality, we simply let the achievable data rate equivalent to the Shannon capacity.

Moreover, the asymptotic behavior of capacity can be shown as $\lim_{\gamma \rightarrow 0} C \approx \gamma$ and $\lim_{\gamma \rightarrow \infty} C \approx \log \gamma$. We name $\gamma \rightarrow 0$ as "low SINR region" and $\gamma \rightarrow \infty$ as "high SINR region".

2.3.2 Power- and Interference-limited System

Then we take a look on the system wise performance. If interference is minor and power control of P_V is resilient with P_A , the capacity can be substantially improved if P_V is increased, we call this as a *power limited* system.

In other cases when interference is very strong ($I \gg N$) so that noise is neglectable, we can simply write as $\Gamma = \frac{S}{I}$, i.e. the SINR degrades to Signal-to-Interference Ratio (SIR). This is named as *interference limited* system.

It is noted that interference signal is actually not white (i.e. correlated in either time, frequency, or spatial domain) and advanced signal processing and interference cancellation algorithms in modern communication systems, such as Interference Rejection Combining (IRC), Soft/Successive Interference Cancellation (SIC) can be used to mitigate the negative influence of interference[10]. In some cases, the influence of interference can be even totally annihilated, see DPC for example. This means a modification on our system model and we will discuss in detail when necessary in the following chapters.

2.3.3 Outage and Transmission Capacity

- **Outage Probability:** Due to the random factor of channel fading and mobility, the SINR observed during certain time interval is actually a random variable. We thereby define the *link outage*, denoted as \mathcal{E} , as a random event that happens when link SINR is falling under a pre-defined threshold Γ . In such cases, the probability of outage for communication link V , denoted as $\Pr(\mathcal{E})$, can be given as:

$$\Pr(\mathcal{E}) = 1 - \Pr(\gamma \geq \Gamma) = 1 - \mathbf{F}_\gamma^c(\Gamma) = \mathbf{F}_\gamma(\Gamma) \quad (2.7)$$

- **Transmission Capacity (TC):** It is obvious that the Macrocell $\Pr(\mathcal{E})$ is a strict monotonically increasing function with the Femto deployment density λ , which is the average number of Femtos within each Macrocell. Therefore, to guarantee that the 1st-tier outage probability by the introduction of 2nd-tier is always greater than a pre-defined threshold ϵ , the deployment density of Femtocell, i.e. λ shall not be greater than a certain value. This is indeed a very important system metric that follows the definition of Remark 1.4, i.e. Femtocells are the strict subordinate users of the sharing spectrum. We name this maximal allowed Femtocell intensity as the *Transmission Capacity* and denote it as Λ :

$$\Lambda \triangleq \sup_{\lambda^{(2)}} : \Pr(\mathcal{E}^{(1)}) \leq \epsilon^{(1)} \quad (2.8)$$

Note that, in the thesis, (1), (2) in superscript denote the 1st-tier and 2nd-tier metrics. respectively.

We remind that the definition of transmission capacity may be not the same as in the other works [69], [70]. However, we point out the similarity between each other and emphasize on the importance of TC being the Femto-Macro coexisting system performance. The detail discussion on the transmission capacity will be given in Chapter 3.

- **Area Spectral Efficiency (ASE):** We assume that there is an approximate link-to-data-rate function of $G(\gamma)$, which denote the achievable rate of link given a specific SINR level γ . For example, $G(\gamma) = wB \log_2(1 + \xi\gamma)$ as defined previously. We also define the sum throughput D of the system, either on 1st-tier or 2nd-tier, as the cumulative

data rate for all the communication links (as the set of \mathcal{V}) within a long term of observation, so that each link data rate reaches ergodicity, i.e.

$$D = \sum_{i \in \mathcal{V}} \mathbf{E}[G_i(\gamma \geq \Gamma)] \quad (2.9)$$

Finally, the ASE of the system, denoted as T , can be derived as:

$$T = \frac{D}{|\mathcal{C}|} \quad (2.10)$$

where $|\mathcal{C}|$ is the area size of the system map $\mathcal{C} \subset \mathbb{R}^2$.

It is true that ASE is another very important system metric since the providers are keen to learn how much payoff can be achieved when Femto-cells are deployed in the area. Those metrics like the 1st-tier ASE $T^{(1)}$, the second-tier ASE $T^{(2)}$, and the overall ASE $T^{(1)} + T^{(2)}$ are helpful to estimate the economic meters such as cost per bit, revenue per Hertz, and so on.

From information theory point of view, random access to radio resource is an efficient way to mitigate the interference, especially when the aggressor is at a relative "blind" status, i.e. it has no clear idea which resource is most vulnerable to the potential interference. This concept is thus implemented into many mechanisms such as frequency hopping, time hopping, random beamforming etc. see [68]. In this chapter, we will briefly introduce the F-ALOHA spectrum access concept to facilitate the later development.

Another long standing problem for wireless communication theory is that, it is extremely tedious to analyze the cellular network performance, even for the most regular BS position like hexagonal or square grid. Thereby many performance predictions can only be made based on computer simulation, which is in many cases not of generality.

Thanks to the successful application of stochastic geometry by Baccelli, Andrews, Weber, and etc., we finally achieve the analytical tractability of Femto modeling. Based on this framework, in this chapter, we derive the optimal Femto subband F-ALOHA access algorithm when the underlying Macros are performing Fractional Frequency Reuse (FFR).

This chapter is organized as follows: related works and a brief history about PPP modeling of Femtos are introduced in Section 3.1, a short description of the contribution by the chapter work is introduced in Section 3.2. Section 3.3 describes how we break down the system model and achieve the optimal access algorithms by analytical proofs in Section 3.4. We then extend the algorithm in more general cases in Section 3.6 and conclude in Section 3.7

3.1 MOTIVATIONS AND RELATED WORKS

- **Classic Cellular Modeling:**

The early cellular system study can be dated back to year 1994, when Wyner in his famous paper [75] successfully models the Other-cell Interference by a deterministic 1-d model and achieves the cellular system capacity in analytic form. Although the mathematical results from Wyner is very beautiful, it is too simple in the sense that the interference from neighboring cell is assumed to be of a constant degradation factor (a), which is only valid for CDMA system because the interference of CDMA system is usually spread and whitened. The later improvement on Wyner's work includes [60], [61], and [63]. However, when these improvements consider a more complex scenario, the initial mathematical tractability is also getting lost. For this reason, the research again has to rely on the computer-based simulation, where the position of cells is often based on some regular or

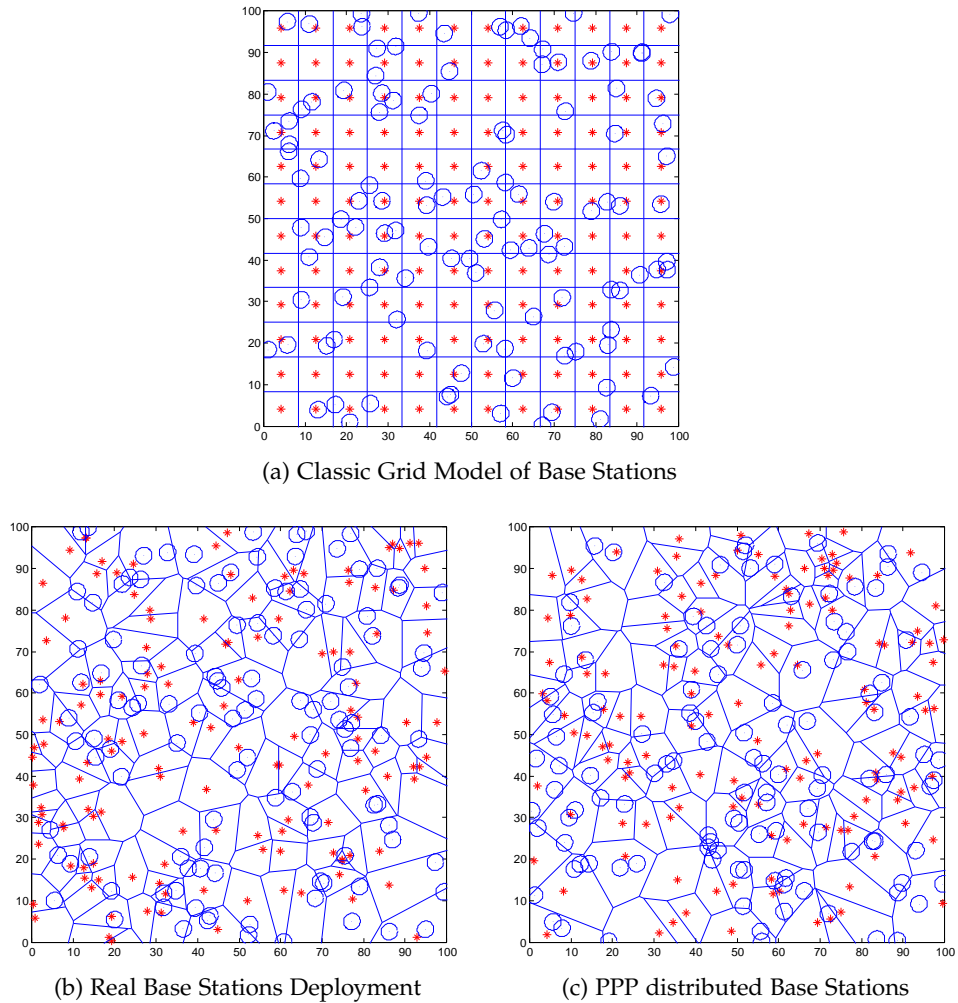


Figure 11: BS Models and Real Cases

real-case pattern. But the problem for computer simulation is that the true performance of system design is difficult to be explicitly revealed and the computation load is enormous when the system is of a large scale.

In short, the classic modeling of cellular system is based on some regular shapes of circles, hexagonal, or square grids. One shall try to improve this modeling approach, because

1. these regular deterministic models are never of good mathematical tractability, in fact, only in rare cases that closed form performance can be found;
2. the deployments of cellular systems in nowadays, even for Macro-cells, are never of regular geometry.

For instance, see the middle subfigure of Fig. 11b, which is the real Macrocell deployments taken from a mid-size city of the US (source: [23]). We find that the regular modeling of cell position in Subfigure 11a is far away from the real case, whereas a snapshot of random Poisson Point Process assumption in the right subfigure is much more

Table 2: Applications of PPP Modeling in Wireless Communication

Generic PPP	independently marked	ALOHA-based access
	Matérn process	CSMA-based access
	germ-grain model	multi-hop coverage
	Voronoi tessellation	cell coverage

accurate. This interesting observation has intrigued the cell modeling by stochastic geometry methods in research [9]. We will introduce it in the following.

- **Stochastic Geometry for Cellular Modeling:**

Stochastic geometry [65] is a mathematical tool for evaluating random spatial distributed locations, which is initially well applied in physics, image processing, astronomy etc. The pioneering successful introduction of stochastic geometry in wireless networks is for study the MAC and routing algorithms of Mobile Ad-hoc Networks (MANET), due to the fact that the nodes in MANETs are close to the assumptions of Poisson Point Process (PPP) distributed [12][43]. Later the work is extended to the random graphs for cell coverage and the Voronoi Tessellation. A good review for this topic can be found in [34], where we summarize that the state-of-art application of stochastic geometry in Tab. 2.

To the best knowledge of the author, poisson arrival of interference modeled as Power-law shot noise can be dated to as early as 1990s in [49] [37]. Nevertheless, the first modeling for Femto location by stochastic geometry is attributed to Chandrasekhar and Andrews in year 2009 [17] [19]. They successfully captured the ad-hoc manner of Femtocell application.

From then on, many results in MANET are reused in the context of Femtocell. For example, [42] proposed the optimal bandwidth partitioning to maximize the number of simultaneous links. [35] pointed out that spectrum overlay is more efficient than spectrum underlay in the sense of increasing the feasible capacity region. [17] proposed a spectrum allocation policy which is optimal according to maximizing area spectral efficiency. [5],[6] consider the network capacity of inhomogeneous MANET deployment.

- **Optimality of F-ALOHA:** When developing distributed spectrum access for ad-hoc networks, one observes that the optimal access scheme for each node in a blind status is to randomly distribute and access the resources. Rigorous mathematical proofs are given in Weber et al.'s paper [71], showing that FH-CDMA is more optimal than DS-CDMA in the sense of maximizing transmission capacity. Theoretic reason behind this finding is that FH-CDMA is the most efficient way of thinning the interference intensity by the spreading factor of

M . Thus the transmission capacity can be scaled by $M^{\frac{2}{\alpha}}$, where α is the pathloss exponent. This finding also verifies that F-ALOHA, i.e. each node randomly access a small portion of the spectrum at each time, is indeed the optimal way to preserving the maximal system transmission capacity. Although most of the current cellular systems only realize frequency hopping in the UL to mitigate the near-far effect, we look into the F-ALOHA case in both DL and UL because it predicts the transmission capacity upper-bounds for blind case. Some computer simulation results also show the similar results [77].

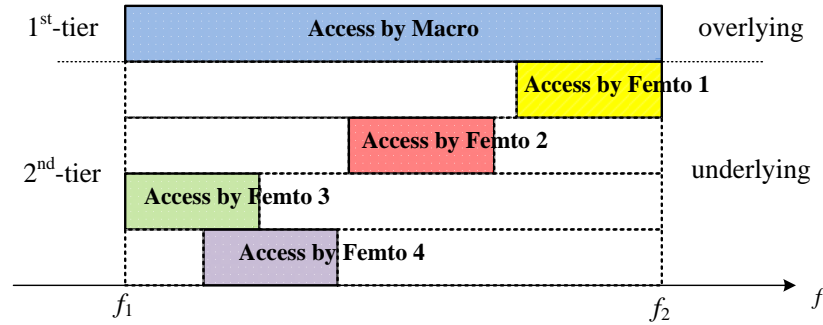


Figure 12: F-ALOHA for Femtocell

- FFR for Cellular:** FFR is an effort of manipulating the frequency resource allocation upon terminal's location to achieve the universal frequency reuse for Macrocell. It is a very simple but effective algorithm that is based on differentiation between cell central and edge MUEs. For the cell central MUEs, since they are close to the connecting MBS, they are mostly robust against OCI in DL thereby the reuse factor is as low as 1. For the cell edge MUEs, since they are near to the neighboring MBS, they are vulnerable to OCI in DL and dangerous in causing OCI to neighboring cell in UL. Therefore, the reuse factor is higher, for example in Fig. 13 the reuse factor for cell edge MUE is 3. The question is which subband (i.e. S_1, S_2, S_3 in the example) for Femto to access when lying under such FFR Macros? One answer is the heuristic approach proposed by Oh et al. [54], that the Femtos in cell edge reuse the subbands that are irrelevant to the subband that the local MUEs are accessing, so that to avoid from causing CCI. This algorithm is later improved in the work of [58] by implementing Load-Spillage power control algorithm to further alleviate the interference. One shortcoming is that precise Femto location information must be acquired to perform this heuristic approach (imagine one FFC located in overlapping area of several Macrocell), which is not always available because Femto is sometimes well isolated in the house that Global Positioning System (GPS) does not work well. As the location precision of Femto mandated by FFC is around 50m, it is too coarse to let the approach to perform well. Additionally, to let one small region of Femtos always access one certain subband also implies a high potential of intra-2nd tier interference.

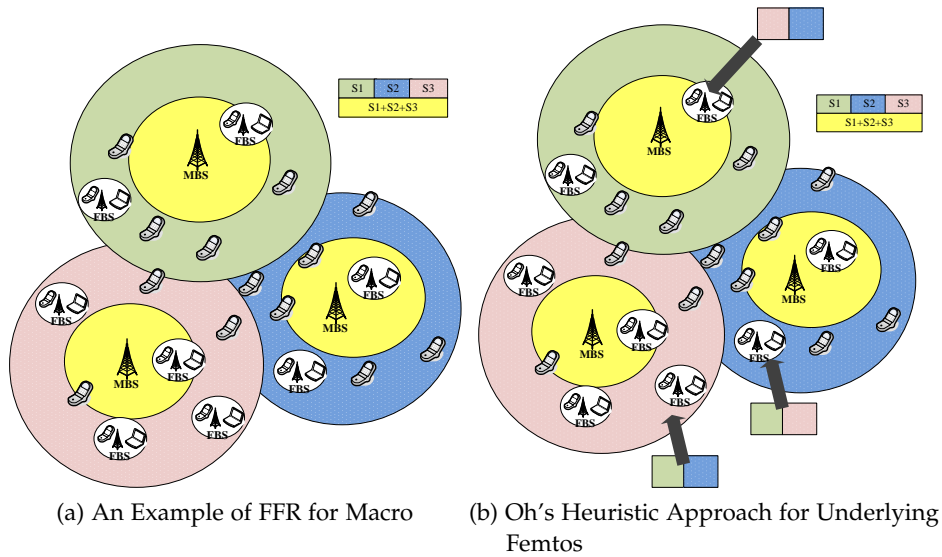


Figure 13: An Example of FFR Macro and Underlying Femtos

Table 3: Proposed ALOHA algorithm

Application	Pre-knowledge	Sub-optimal	Optimal
No specific Macro	No	DS-CDMA etc.	ALOHA with maximal DOF
Macro performing FFR	FFR configuration	Heuristic, blind access	Proposed ALOHA (biased)

Therefore, in this chapter, we study different optimal approaches based on ALOHA access in uplink and deal with downlink in Chapter 4.

3.2 CONTRIBUTIONS

The main contribution ¹ of this chapter's work is that we propose an ALOHA-based algorithm in uplink to optimally access the FFR subband in the sense of maximizing the transmission capacity. The relation between the proposed algorithm and other existing algorithms is shown in Tab. 3.

Besides, the other contributions of this chapter are summarized as follows:

1. The outage probability and transmission capacity on both 1st- and 2nd-tier are derived in analytic forms;
2. The optimal Femto spectrum access rate is analyzed under the condition of different topology and power control schemes;
3. The 1st-tier alleviation mechanism to accommodate bursty rise of Femto traffic is analyzed;
4. The maximized second-tier Signal to Interference Ratio (SIR γ) criteria under constraints is presented;

¹ A part of this chapter's work is presented in [77] and [80].

5. The developed algorithms are extended to many general cases.

3.3 SYSTEM MODELS

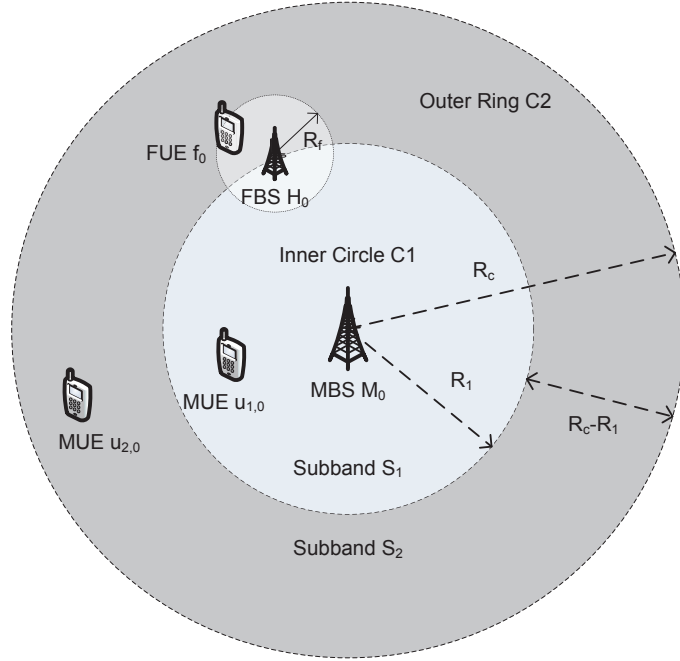


Figure 14: System Model for Study

In this section, we assume a circular shaped Macrocell in the UL, with a simple FFR topology. This is indeed the most straightforward case that analysis can be easily derived. Then we prove the optimality of the devised subband access algorithm for F-Aloha based Femtos in interference-limited cases.

We assume a system map of Euclidean space \mathbb{R}^2 , where a MBS M_0 is located at its origin. The coverage region of this Macrocell is $\mathcal{C} \subset \mathbb{R}^2$, which is a circular disc with a constant radius of R_c , thereby $|\mathcal{C}| = \pi R_c^2$. As shown in Fig. 14, we divide \mathcal{C} into two sub-regions, i.e. Inner Circle \mathcal{C}_1 and Outer Ring \mathcal{C}_2 . We define $\kappa_c \triangleq \frac{|\mathcal{C}_1|}{|\mathcal{C}|}$ so that we have $\kappa_c = \frac{R_1^2}{R_c^2}$, $\kappa_c \in (0, 1)$.

We assume that both first-tier and second-tier systems are using FDMA with a set \mathcal{S} of subchannels within the available bandwidth. We assume that M_0 is adopting FFR policy and that the subchannels in \mathcal{S} are divided into two disjoint subsets (or subbands), denoted as \mathcal{S}_1 and \mathcal{S}_2 . Define ratio $\kappa_s \triangleq \frac{|\mathcal{S}_1|}{|\mathcal{S}|}$, as $|\mathcal{S}|$ denotes the number of subchannels.

Hereby we assume a typical FFR policy for the Macrocell together with the following assumptions:

Assumption 3.1 (Macrocell FFR) *Each MUE can only access the spectrum subset \mathcal{S}_1 or \mathcal{S}_2 depending on whether it is located in \mathcal{C}_1 or \mathcal{C}_2 respectively.*

Consequently, let the set of all the MUEs that are connected to M_0 be \mathcal{U} . \mathcal{U} is submerged into two disjoint subsets, i.e. \mathcal{U}_1 (for users located in

\mathcal{C}_1) and \mathcal{U}_2 (for users located in \mathcal{C}_2). We select one typical MUE from each group and denote them as $u_{1,0}$ and $u_{2,0}$ respectively.

Assumption 3.2 (Position of Femto) *We assume that all the FBSs H_i are randomly distributed over \mathbb{R}^2 , represented by a homogeneous Poisson Point Process (hPPP) $\Omega^{(2)}$ with intensity $\lambda^{(2)}$ (mean FBSs per km^2), simply we denote as Ω and λ in this section since only the 2nd-tier PPP assumption is considered. We assume that all FUEs are i.i.d. randomly located at a radius of R_f ($\kappa_f \triangleq \frac{R_f^2}{R_c^2} \ll 1$) relative to its host FBS, and we pick up one typical Femtocell in region \mathcal{C} (denoted as H_0) and one typical FUE of it (denoted as f_0).*

In this chapter, complicated power control and scheduling algorithms are not considered.

Assumption 3.3 (Power control) *We simply assume that all the UEs within each group have the same transmit power, denoting as P_1 for the users in \mathcal{U}_1 and P_2 for the users in \mathcal{U}_2 respectively. Additionally, all the FUEs have identical transmit power of P_f .*

Assumption 3.4 (Scheduling) *At each time, Macrocell and Femtocell can schedule one subchannel unit to only one UE, and the scheduling is in a channel blind Round Robin (RR) fashion.*

Finally, we assume that the channel power gain can be represented as a combination of penetration loss, path loss (PL), and Rayleigh fading. We denote K_o , K_f , and K_x for outdoor, indoor, and cross-outdoor-indoor penetration loss respectively. Denote by α (> 2) the indoor and outdoor path loss exponent. We denote the power of Rayleigh gain as W , which is assumed be exponentially distributed with mean of unit one.

We assume that each Femtocell has a fixed portion (denote as ρ) of the spectrum requirement compared to $|\mathcal{S}|$. At any time, we assume $\rho \leq \kappa_s$ and $\rho \leq (1 - \kappa_s)$. Each Femtocell decides to use this portion of the spectrum either in subband \mathcal{S}_1 or \mathcal{S}_2 . After deciding which subband to access, each Femtocell access the subchannel in an F-ALOHA fashion where no inter-cell coordination is conducted.

We study the following algorithm for the Femtocells' decision upon the access to subband \mathcal{S}_1 or \mathcal{S}_2 :

Algorithm 3.1 (Location unaware) *Unknown to its geological position, each Femtocell decides which subband between \mathcal{S}_1 and \mathcal{S}_2 to access by tossing a coin, with a biased probability of η to subband \mathcal{S}_1 and $(1 - \eta)$ to \mathcal{S}_2 .*

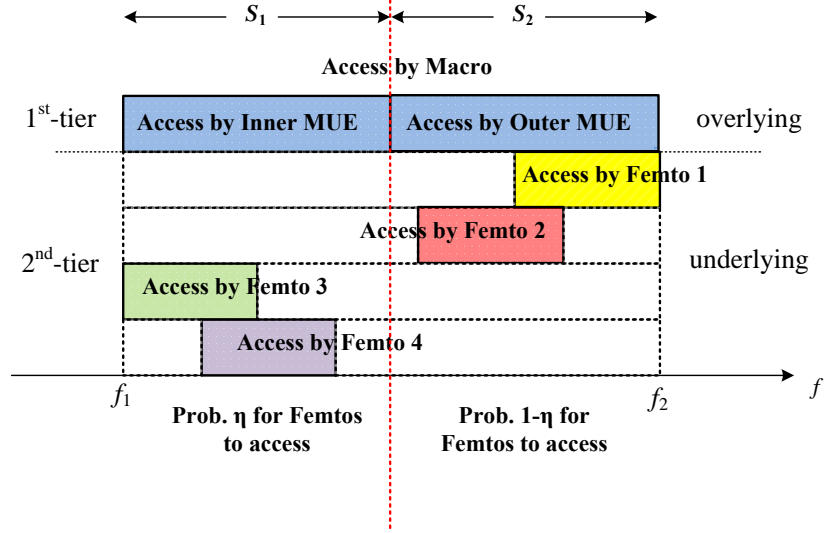


Figure 15: Biased F-ALOHA for Femtos in FFR Macrocell

3.4 ANALYSIS AND PROPOSED ALGORITHMS

3.4.1 1st-Tier Performance

If we denote $s_{1,0}$ as one reference subchannel unit in S_1 , we can derive the received interference power at M_0 as:

$$I_{s_{1,0}}^{(1)} = \underbrace{\sum_{X_i \in \Omega'_1} P_f K_x W_i \|X_i\|^{-\alpha}}_{\text{interference for } U_1 \text{ MUEs from 2nd-tier}} \quad (3.1)$$

where Ω'_1 is an independently marked PPP of Ω due to the fact that, in the F-ALOHA case, each FBS access the subband irrelevantly with its positions and the neighboring conditions. Therefore, due to the thinning property of Poisson process, Ω'_1 is again a hPPP, with a modified intensity of $\frac{\eta\rho\lambda}{\kappa_s}$.

For simplicity, let us first assume the interference limited case and neglect the noise effect. Thereby we can define the SIR $\gamma_{s_{1,0}}^{(1)}$ and the corresponding outage event $\mathcal{E}_1^{(1)}$ for MUE $u_{1,0}$ seen by M_0 , which occurs when:

$$\mathcal{E}_1^{(1)} : \quad \gamma_{s_{1,0}}^{(1)} = \frac{P_1 K_o W_o \|u_{1,0}\|^{-\alpha}}{I_{s_{1,0}}^{(1)}} < \Gamma^{(1)} \quad (3.2)$$

where $\Gamma^{(1)}$ is the first-tier SIR threshold to meet the required QoS of the transmission.

The received interference power at H_0 can be written as:

$$I_{s_{1,0}}^{(2)} = \underbrace{P_1 K_x W_u \|u_{1,0} - H_0\|^{-\alpha}}_{\text{interference from 1st-tier}} + \underbrace{\sum_{X_i \in \Omega'_{1,H_0} \setminus \{f'_0\}} P_m K_x W_i \|X_i\|^{-\alpha}}_{\text{interference from 2nd-tier peers}} \quad (3.3)$$

where f'_0 , Ω'_{1,H_0} are f_0 and Ω_{1,H_0} seen at H_0 . By Slivnyak's theorem, Ω'_{1,H_0} is identical to a marked PPP Ω_h with intensity of $\frac{\eta\rho\lambda}{\kappa_s}$ [34].

Similar to $\mathcal{E}_1^{(1)}$, the outage event $\mathcal{E}_1^{(2)}$ at H_0 occurs when:

$$\mathcal{E}_1^{(2)} : \quad \gamma_{s_{1,0}}^{(2)} = \frac{P_f K_f W_0 R_f^{-\alpha}}{I_{s_{1,0}}^{(2)}} < \Gamma^{(2)} \quad (3.4)$$

where $\Gamma^{(2)}$ is the second-tier SIR threshold.

The interference $I_{s_{2,0}}^{(1)}$, $I_{s_{1,0}}^{(2)}$, and events $\mathcal{E}_2^{(1)}$, $\mathcal{E}_2^{(2)}$ on one reference subband unit in \mathcal{S}_2 (denote as $s_{2,0}$), seen by MUE $u_{2,0}$ can be induced in a similar way, i.e.

$$I_{s_{2,0}}^{(1)} = \underbrace{\sum_{X_i \in \Omega'_2} P_f K_x W_i \|X_i\|^{-\alpha}}_{\text{interference for } \mathcal{U}_2 \text{ MUEs from 2nd-tier}} \quad (3.5)$$

$$I_{s_{1,0}}^{(2)} = \underbrace{P_2 K_x W_u \|u_{2,0} - H_0\|^{-\alpha}}_{\text{1st-to-2nd tier interference}} + \underbrace{\sum_{X_i \in \Omega'_{2,H_0} \setminus \{f'_0\}} P_m K_x W_i \|X_i\|^{-\alpha}}_{\text{interference from 2nd-tier peers}} \quad (3.6)$$

and

$$\mathcal{E}_2^{(1)} : \quad \gamma_{s_{2,0}}^{(1)} = \frac{P_2 K_o W_0 \|u_{1,0}\|^{-\alpha}}{I_{s_{2,0}}^{(1)}} < \Gamma^{(1)} \quad (3.7)$$

$$\mathcal{E}_2^{(2)} : \quad \gamma_{s_{2,0}}^{(2)} = \frac{P_f K_f W_0 R_f^{-\alpha}}{I_{s_{2,0}}^{(2)}} < \Gamma^{(2)}. \quad (3.8)$$

From (3.2), it is obvious that $\gamma_{s_{1,0}}^{(1)}$ is lower-bounded by $\gamma_{s_{1,0}}^{(1)}|_{\|u_{1,0}\|=R_1}$. In the following, we will consider this worst case for the Macrocell outage.

Therefore, we have

$$\begin{aligned} \Pr(\mathcal{E}_1^{(1)}) &\leq 1 - \Pr\left(\frac{P_1 K_o W_0 R_1^{-\alpha}}{I_{s_{1,0}}^{(1)}} \geq \Gamma^{(1)}\right) \\ &= 1 - \Pr\left(W_0 > \frac{\Gamma^{(1)} I_{s_{1,0}}^{(1)}}{P_1 R_1^{-\alpha} K_o}\right) \\ &\stackrel{(a)}{=} 1 - \mathcal{L}_{I_{s_{1,0}}^{(1)}}\left(\frac{\Gamma^{(1)}}{P_1 R_1^{-\alpha} K_o}\right) \end{aligned} \quad (3.9)$$

where step (a) applies for the assumption of Rayleigh fading, i.e. W_0 is exponential distributed and $\mathcal{L}_{I_{s_{1,0}}^{(1)}}(\cdot)$, by definition, is the Laplace-transform of the distribution of interference $I_{s_{1,0}}^{(1)}$ on Ω'_1 [36].

Applying Campbell's Theorem [43], or see appendix, to (3.1) and (3.9), we obtain the following:

$$\begin{aligned} \mathcal{L}_{I_{s_{1,0}}^{(1)}}(s) &= \mathbf{E}_{I_{s_{1,0}}^{(1)}} \left[\exp(-s I_{s_{1,0}}^{(1)}) \right] \\ &= \int_0^\infty \exp\left(-s \sum_{X_i \in \Omega'_1} P_f K_x W_i \|X_i\|^{-\alpha}\right) ds \\ &= \exp\left(\int_{\mathcal{C}} -s P_f K_x W_i \|X_i\|^{-\alpha} \Omega'_1(dX_i)\right) \\ &= \exp\left(\int_0^{R_c} -s P_f K_x W_i \|X_i\|^{-\alpha} \frac{\eta \rho \lambda}{\kappa_s} (d\|X_i\|)\right) \end{aligned} \quad (3.10)$$

therefore,

$$\mathcal{L}_{I_{s_{1,0}}^{(1)}}\left(\frac{\Gamma(1)}{P_1 R_1^{-\alpha} K_o}\right) = \exp\left\{-\frac{\kappa_c}{\kappa_s} \eta \rho \lambda \zeta \left(\frac{P_f K_x \Gamma(1)}{P_1 K_o}\right)^{\frac{2}{\alpha}}\right\} \quad (3.11)$$

where

$$\begin{cases} \zeta = \frac{2}{\alpha} \Gamma\left(\frac{2}{\alpha}\right) \Gamma\left(1 - \frac{2}{\alpha}\right) \\ \Gamma(\cdot) \text{ is the Gamma function.} \end{cases}$$

Similarly on $s_{2,0}$, we have

$$\Pr(\mathcal{E}_2^{(1)}) \leq 1 - \mathcal{L}_{I_{s_{2,0}}^{(1)}}\left(\frac{\Gamma(1)}{P_2 R_c^{-\alpha} K_o}\right) \quad (3.12)$$

where $I_{s_{2,0}}^{(1)}$ is resulted from the similar PPP Ω'_1 with intensity of $\frac{1-\eta}{1-\kappa_s} \rho \lambda$, so that its Laplacian form can be derived as:

$$\mathcal{L}_{I_{s_{2,0}}^{(1)}}\left(\frac{\Gamma(1)}{P_2 R_c^{-\alpha} K_o}\right) = \exp\left\{-\frac{1-\eta}{1-\kappa_s} \rho \lambda \zeta \left(\frac{P_f K_x \Gamma(1)}{P_2 K_o}\right)^{\frac{2}{\alpha}}\right\} \quad (3.13)$$

3.4.2 Proposed Algorithms

Theorem 3.1 (Optimal Access in interference-limited case) *Under this setup, the optimal Femto subband access rate η^* is given by:*

$$\eta^* = \frac{\kappa_s}{\kappa_s + (1 - \kappa_s) \kappa_c a}, \text{ with } a = \left(\frac{P_2}{P_1}\right)^{\frac{2}{\alpha}} \quad (3.14)$$

Proof Suppose that the tolerable outage probability for first-tier users is $\epsilon^{(1)}$, i.e., it is required that $\Pr(\mathcal{E}_1^{(1)}) \leq \epsilon^{(1)}$. To guarantee a reliable communication on subband \mathcal{S}_1 and \mathcal{S}_2 , a sufficient condition is the following:

$$\frac{\kappa_c \eta}{\kappa_s} \rho \lambda \left(\frac{P_f}{P_1}\right)^{\frac{2}{\alpha}} \Gamma(1)^{\frac{2}{\alpha}} \leq -\frac{K_o^{\frac{2}{\alpha}} \ln(1 - \epsilon^{(1)})}{\zeta K_x^{\frac{2}{\alpha}}} \quad (3.15)$$

$$\frac{1-\eta}{1-\kappa_s} \rho \lambda \left(\frac{P_f}{P_2}\right)^{\frac{2}{\alpha}} \Gamma(1)^{\frac{2}{\alpha}} \leq -\frac{K_o^{\frac{2}{\alpha}} \ln(1 - \epsilon^{(1)})}{\zeta K_x^{\frac{2}{\alpha}}} \quad (3.16)$$

As introduced in Chapter 2, *transmission capacity* Λ is defined as the maximal allowable density of FBS deployment in \mathcal{C} without sabotaging the first tier transmission. It can be formulated as the following optimization problem:

$$\begin{aligned} & \text{maximize} && \lambda \\ & \text{subject to} && (3.15), (3.13) \\ & \text{variables} && \lambda, \eta \end{aligned} \quad (3.17)$$

From the geometry of the constraints it is easy to find that this optimization problem has a unique maximum Λ , which is achieved when both the constraints (3.15), (3.13) turn to saturate. In this case, we have

$$\eta^* = \frac{\kappa_s}{\kappa_s + (1 - \kappa_s)\kappa_c a}, \text{ with } a = \left(\frac{P_2}{P_1}\right)^{\frac{2}{\alpha}}$$

and

$$\Lambda = \left[\frac{\kappa_s}{\kappa_c} P_1^{\frac{2}{\alpha}} + (1 - \kappa_s) P_2^{\frac{2}{\alpha}} \right] \frac{-K_0^{\frac{2}{\alpha}} \ln(1 - \epsilon^{(1)})}{\rho \zeta (K_x P_f \Gamma^{(1)})^{\frac{2}{\alpha}}} \quad (3.18)$$

■

(3.14) is indeed a very critical condition for system to maximize its transmission capacity. Observing from that, we realize the optimal subband access rate of Femtocell is only decided by the Macrocell FFR policy parameters such as κ_s, κ_c, a . It is irrelevant to many other system parameters such as the Macrocell threshold $\Gamma^{(1)}$, Femto-specific parameters such as transmit power P_f and so on.

Therefore, we propose the following amendment to Algorithm 3.1.

Algorithm 3.2 (Optimal Access) *As supplementary to Algorithm 3.1, first-tier MBSs periodically broadcast their basic FFR configuration to the local FBSs. The basic FFR configuration includes:*

- 1. Region Factor κ_c
- 2. Bandwidth Partition Factor κ_s
- 3. Power ratio a

Meanwhile the second-tier users accommodate to maximize the transmission capacity by tuning their biased spectrum access rate η^ according to (3.14), see illustration in Fig. 16.*

Besides the amended subband access algorithm, we can draw the following corollaries and remarks.

Corollary 3.1 (PF case) *In most cases, Macrocells allocate proportional fair (PF) of bandwidth resources to one certain area to serve the same proportion of users (if user population is assumed to be uniformly distributed in map), i.e.*

$$\kappa_s \equiv \kappa_c,$$

then we have

$$\eta^* = \frac{1}{1 + (1 - \kappa_c)a} \quad (3.19)$$

Based on the above PF assumption, the following remarks on the Macrocell power control (PC) are due.

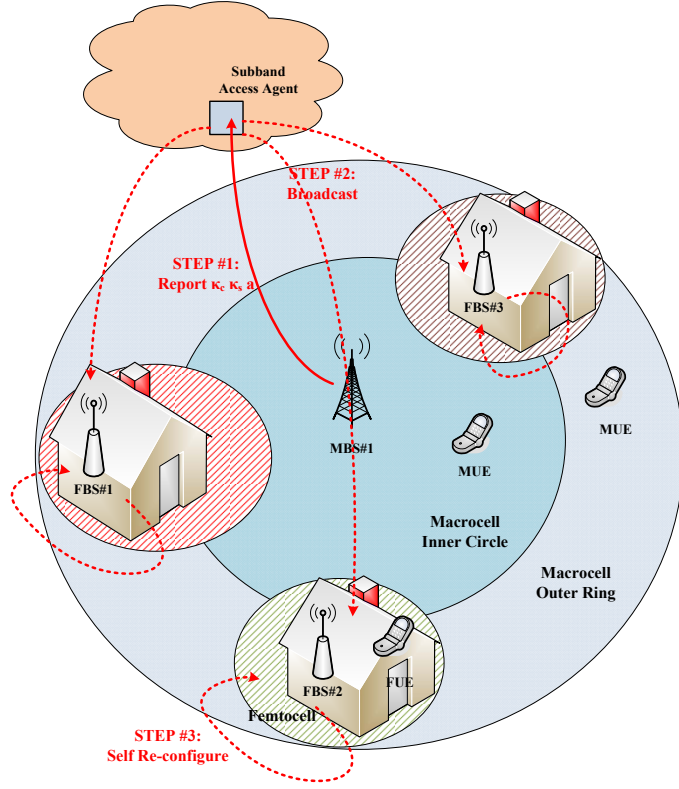


Figure 16: Flowchart of Proposed Optimal Access

Remark 3.1 (Constant PC) If MUEs in U_1 and U_2 are transmitting on a uniform transmit power scheme, i.e., $P_1 = P_2$, we have

$$\eta^* = \frac{1}{2 - \kappa_c} > \frac{1}{2}$$

The FBSs are more optimal to access S_1 than S_2 . However, uniform power allocation is not commonly adopted due to the near-far effect on Macrocell uplink.

Remark 3.2 (PL based PC) To overcome the near-far effect, the far MUEs transmit more power to counter the larger path loss. This is a common technique in FDMA systems with open loop PC. In LTE, it is called Fractional PC and the transmit power P_0 of user o is given by

$$P_{0,\text{dB}} \approx P_{\text{init,dB}} + \beta PL_{0,\text{dB}}, \quad 0 \leq \beta \leq 1$$

In this case, by definition we have $a = (\kappa_c)^{-\beta}$. Therefore,

$$\eta^* = \frac{1}{-\kappa_c^{1-\beta} + \kappa_c^{-\beta} + 1} \in \left[\kappa_c, \frac{1}{2 - \kappa_c} \right] \quad (3.20)$$

At the extreme case that PL is fully compensated ($\beta = 1$), we have

$$\eta^* = \kappa_c$$

which means that, if the received MUE signal power is whitened at MBS, the interference power from FBSs shall also be whitened across subbands.

In common cases, the fractional PL factor β as a cell-specific parameter is between 0 and 1. Therefore, the optimal η is not always equals to κ_s . This phenomenon is discovered by many scenario simulations with different FFR topology and configurations [77]. And here we provide the above analytic proofs.

Let us then consider the maximal transmit capacity for the two-tier system adopting Macrocell FFR. If in real practice that the deployed Femtocells happen to exceed this capacity limit of Λ , directly learning from (3.18), we can obtain the following remarks to solve the urgent capacity starvation problems.

Corollary 3.2 (Bandwidth portion) *When outage constraint on either subband is saturated, decrease of Femto bandwidth portion ρ will accommodate an increased Femto density proportionally, i.e.*

$$\Lambda \sim \mathcal{O}(\rho^{-1}).$$

Corollary 3.3 (Scaling Law of Femto Transmit Power) *The transmission capacity is scaled with the Femtocell transmit power in the law of*

$$\Lambda \sim (P_f)^{-\frac{2}{\alpha}},$$

which is related with the channel pathloss exponent α .

In the case that the channel attenuation is higher, the decrease of Femto transmit power is less effective in increasing the capacity.

When $\epsilon^{(1)}$ is sufficiently small ($\epsilon^{(1)} \rightarrow 0$), which is the case for outage-sensible application e.g. $\epsilon^{(1)} = 1\%$, we have the following linear inequalities for maximal allowable system-specific parameters:

$$\frac{\kappa_c \eta}{\kappa_s} \zeta \rho \lambda \left(\frac{K_x}{P_1 K_o} \right)^{\frac{2}{\alpha}} \leq \epsilon^{(1)} (\Gamma^{(1)} P_f)^{-\frac{2}{\alpha}} + \mathcal{O}(\epsilon^{(1)2}) \quad (3.21)$$

$$\frac{1 - \eta}{1 - \kappa_s} \zeta \rho \lambda \left(\frac{K_x}{P_2 K_o} \right)^{\frac{2}{\alpha}} \leq \epsilon^{(1)} (\Gamma^{(1)} P_f)^{-\frac{2}{\alpha}} + \mathcal{O}(\epsilon^{(1)2}) \quad (3.22)$$

Corollary 3.4 (Decrease 1st-tier QoS Criteria) *From (3.21) and (3.22), the Femtocell capacity Λ grows proportionally with the first-tier outage constraint $\epsilon^{(1)}$, and inverse proportionally with $(\Gamma^{(1)})^{\frac{2}{\alpha}}$.*

The above corollary implies that if the system is over-burdened with too many emerging FBSs, slacking the 1st-tier QoS criteria (i.e. $\epsilon^{(1)}$ and $\Gamma^{(1)}$) can accommodate more FBSs in the system. However, this is with a cost of lower 1st-tier reliability (more often to drop calls) and data rates.

3.4.3 2nd-Tier Performance

From (3.4), we derive the outage probability for Femtocell at subchannel unit $s_{1,0}$ as:

$$\begin{aligned} \Pr(\mathcal{E}_1^{(2)}) &= 1 - \Pr\left(\frac{P_f K_f W_0 R_f^{-\alpha}}{I_{s_{1,0}}^{(2)}} \geq \Gamma^{(2)}\right) \\ &= 1 - \mathcal{L}_{I_{s_{1,0}}^{(2)}}\left(\frac{\Gamma^{(2)}}{P_f R_f^{-\alpha} K_f}\right) \end{aligned} \quad (3.23)$$

Observing the RHS of (3.3) and assuming that the distribution of $u_{1,0}$ and Ω'_{1,H_0} are independent of each other, we obtain the following equation for $\mathcal{L}_{I_{s_{1,0}}^{(2)}}(s)$:

$$\mathcal{L}_{I_{s_{1,0}}^{(2)}}(s) = \mathcal{L}_{I_{s_{1,0}}^{(1)}}(s) \mathcal{L}_{D_1}(s) \quad (3.24)$$

where $D_1 = P_1 K_x W_u y_1^{-\alpha}$, and $y_1 = \|u_{1,0} - H_0\|$ is the Euclidean distance of two uniformly distributed nodes in regions \mathcal{C} and \mathcal{C}_1 respectively.

The p.d.f. of random variable y_1 is given by:

$$\begin{aligned} \mathbf{f}_{y_1}(y_1) &= \frac{4}{\pi R_1^2 R_c^2} \int_0^{R_c} \int_0^{R_1} y_1 y_3 y_4 \frac{1}{\sqrt{[(y_3 + y_4)^2 - y_1^2]}} \\ &\quad \frac{1}{\sqrt{[y_1^2 - (y_3 - y_4)^2]}} dy_3 dy_4, \quad y_1 \in [0, R_1 + R_c] \end{aligned} \quad (3.25)$$

Therefore,

$$\begin{aligned} \mathcal{L}_{D_1}(s) &= \int_{-\infty}^{+\infty} e^{-P_1 K_x s v} \int_{(R_1+R_c)^{-\alpha}}^{+\infty} f_{z_1}(z_1) \frac{e^{-\frac{v}{z_1}}}{z_1} dz_1 dv \\ &= \int_{(R_1+R_c)^{-\alpha}}^{+\infty} \frac{f_{z_1}(z_1)}{z_1} \int_{-\infty}^{+\infty} e^{-P_1 K_x s v - \frac{v}{z_1}} dv dz_1 \\ &= \int_{(R_1+R_c)^{-\alpha}}^{+\infty} \frac{f_{z_1}(z_1)}{z_1} \frac{1}{P_1 K_x s z_1 + 1} dz_1 \end{aligned} \quad (3.26)$$

where $z_1 = y_1^{-\alpha}$.

Similarly, on subband unit $s_{2,0}$, we have

$$\mathcal{L}_{I_{s_{2,0}}^{(2)}}(s) = \mathcal{L}_{I_{s_{2,0}}^{(1)}}(s) \mathcal{L}_{D_2}(s) \quad (3.27)$$

where $D_2 = P_2 K_x W_u y_2^{-\alpha}$, and $y_2 = \|u_{2,0} - H_0\|$ is for two nodes in regions \mathcal{C} and \mathcal{C}_2 respectively.

$$\begin{aligned} \mathbf{f}_{y_2}(y_2) &= \frac{4}{\pi (R_c - R_1)^2 R_c^2} \int_0^{R_c} \int_{R_1}^{R_c} \frac{y_2 y_3 y_4}{\sqrt{[(y_3 + y_4)^2 - y_2^2]}} \\ &\quad \frac{1}{\sqrt{[y_2^2 - (y_3 - y_4)^2]}} dy_3 dy_4, \quad y_2 \in [0, 2R_c] \end{aligned} \quad (3.28)$$

and

$$\mathcal{L}_{D_2}(s) = \int_{(2R_c)^{-\alpha}}^{+\infty} \frac{f_{z_2}(z_2)}{z_2} \frac{1}{P_2 K_x s z_2 + 1} dz_2 \quad (3.29)$$

where $z_2 = y_2^{-\alpha}$.

We use the numerical methods to obtain the value of function $\mathcal{L}_{D_1}(s)$ and $\mathcal{L}_{D_2}(s)$ at $s = \frac{\Gamma^{(2)}}{P_f R_f^{-\alpha} K_f}$.

By using the same method in Equation (3.11), we also derive that

$$\mathcal{L}_{I_{s_{1,0}}^{(1)}}\left(\frac{\Gamma^{(2)}}{P_f R_f^{-\alpha} K_f}\right) = \exp\left\{-\frac{\eta}{\kappa_s} \kappa_f \rho \lambda \zeta \left(\frac{K_x \Gamma^{(2)}}{K_f}\right)^{\frac{2}{\alpha}}\right\} \quad (3.30)$$

and

$$\mathcal{L}_{I_{s_{2,0}}^{(1)}}\left(\frac{\Gamma^{(2)}}{P_f R_f^{-\alpha} K_f}\right) = \exp\left\{-\frac{1-\eta}{1-\kappa_s} \kappa_f \rho \lambda \zeta \left(\frac{K_x \Gamma^{(2)}}{K_f}\right)^{\frac{2}{\alpha}}\right\} \quad (3.31)$$

Finally, the second-tier outage probability constraints can be obtained as:

$$\frac{\eta}{\kappa_s} \kappa_f \rho \lambda \zeta \left(\frac{K_x \Gamma^{(2)}}{K_f}\right)^{\frac{2}{\alpha}} \leq \ln[\mathcal{L}_{D_1}\left(\frac{\Gamma^{(2)}}{P_f R_f^{-\alpha} K_f}\right)] - \ln(1 - \epsilon^{(2)}) \quad (3.32)$$

$$\frac{1-\eta}{1-\kappa_s} \kappa_f \rho \lambda \zeta \left(\frac{K_x \Gamma^{(2)}}{K_f}\right)^{\frac{2}{\alpha}} \leq \ln[\mathcal{L}_{D_2}\left(\frac{\Gamma^{(2)}}{P_f R_f^{-\alpha} K_f}\right)] - \ln(1 - \epsilon^{(2)}) \quad (3.33)$$

Assume that all the FBSs are accessing the subbands at the optimal rate of $\eta = \eta^*$. If the current FBS density is lower than the system transmission capacity ($\lambda \leq \Lambda$), we can see that the maximal second-tier SIR target $\Gamma^{(2)}$ is constrained by the second-tier outage probability in inequalities (3.32) and (3.33).

Nevertheless, in many cases, the 2nd-tier is not so outage sensible as the 1st-tier. In such cases, the 2nd-tier constraints of (3.32) and (3.33) are more slacker than the 1st-tier constraints of (3.15) and (3.13), because

$$\begin{cases} \kappa_f \ll 1 \\ \epsilon^{(2)} \gg \epsilon^{(1)} \end{cases}$$

meaning that the system is mainly constrained by its 1st-tier performance criteria.

3.5 NUMERICAL RESULTS

In this section, we will present the numerical results for the proposed Femto subband access algorithms and the related corollaries.

Firstly, we define the two conventional approaches to make the performance comparisons. They are:

Table 4: Default Simulation Parameters for 3.5

Parameter	Description	Value
R_c	Map Size	1000m
β	MUE Power Control Factor	1/2
κ_c	Macro FFR Region Parameter	1/2
κ_s	Macro FFR Subband Parameter	1/2
\bar{P}	Average Transmit Power of MUE	20dBm
P_f	Transmit Power for FUE	5dBm
α	Pathloss Exponential Factor	4
K_o	Outdoor penetration Loss	-15dB
K_f	Indoor Penetration Loss	-25dB
K_x	In/Outdoor Penetration Loss	-40dB
Γ_m	First Tier SIR Target	5dB
Γ_f	Second Tier SIR Target	15dB
ϵ_m	First Tier Outage Target	1%
ϵ_f	Second Tier Outage Target	5%

- **Blind Access:** or *unbiased access*, as the access scheme of

$$\eta \equiv \frac{1}{2};$$

- **Heuristic Access:** as the access scheme of

$$\eta \equiv \kappa_c.$$

To make clear comparisons with previous conventional approaches, we present the numerical results based on both the analysis and computer simulation. The default setup parameters are listed in Table 4, unless explicitly specified otherwise.

The simulation is based on the Monto-Carlo method of 5×10^4 realizations of FBS locations, with a model of homogeneous PPP over the map are generated. The referred link SIR and its outage rate are calculated accordingly. Only the proportional fair case (i.e. $\kappa_s = \kappa_c$) is considered. Along with the simulation results, corresponding analytical curves given by Equation (3.15) (3.13) (3.32) (3.33) are also depicted in the figures.

- From all the figures Fig. 3.7-10, we see a good match between analytic and simulation results. Both results from Fig. 17 and 18 can proof that Equation (3.20) has precisely predicted the optimal spectrum access rate of $\eta = \eta^*$.

We can find that the blind access scheme in many cases leads to a poor transmission capacity and heuristic access is only close to optimal when β approaches to 1. However the proposed access algorithm can always achieve the optimal transmission capacity, which means a more than 20% and 40% gain of capacity in the cases of ($\kappa_c = \frac{1}{2}$, $\beta = \frac{1}{2}$) and ($\kappa_c = \frac{1}{2}$, $\beta = 0$) respectively.

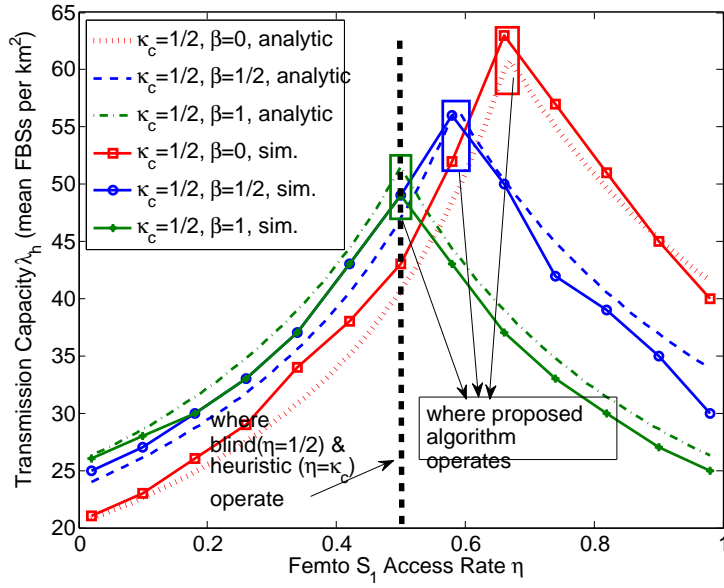


Figure 17: Transmission Capacity vs. MUE Power Control

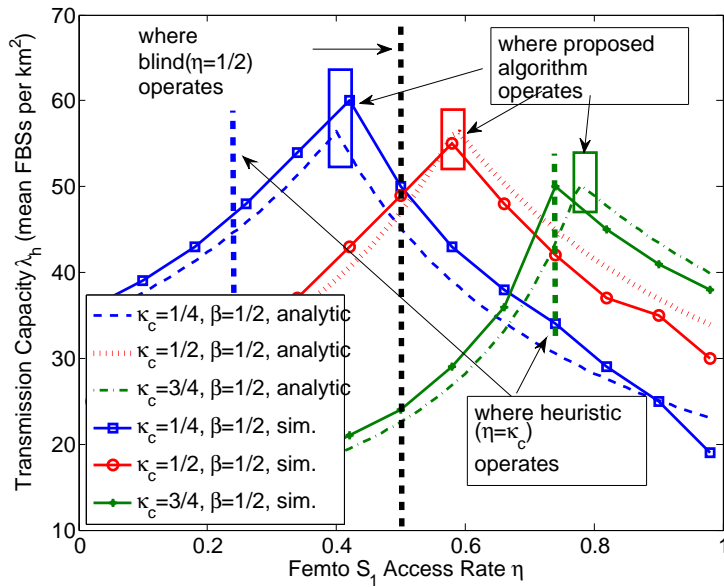


Figure 18: Transmission Capacity vs. MUE FFR Topology

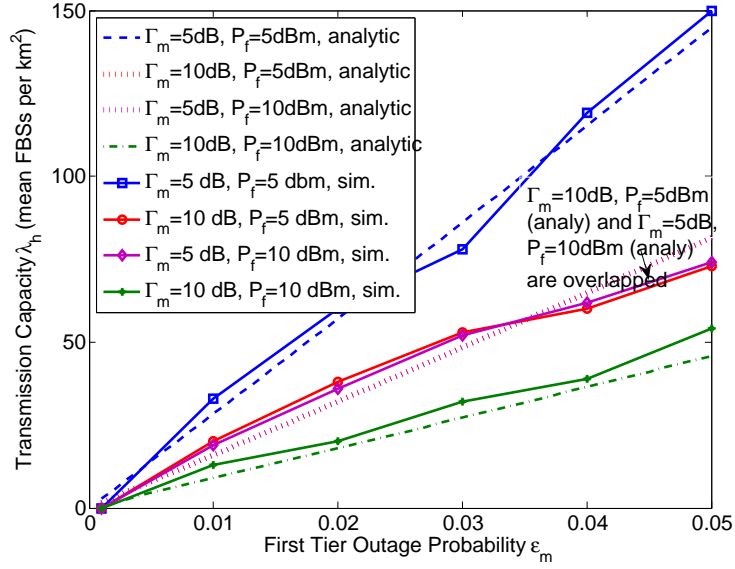


Figure 19: Transmission Capacity vs. MUE Target SIR and Femto Power

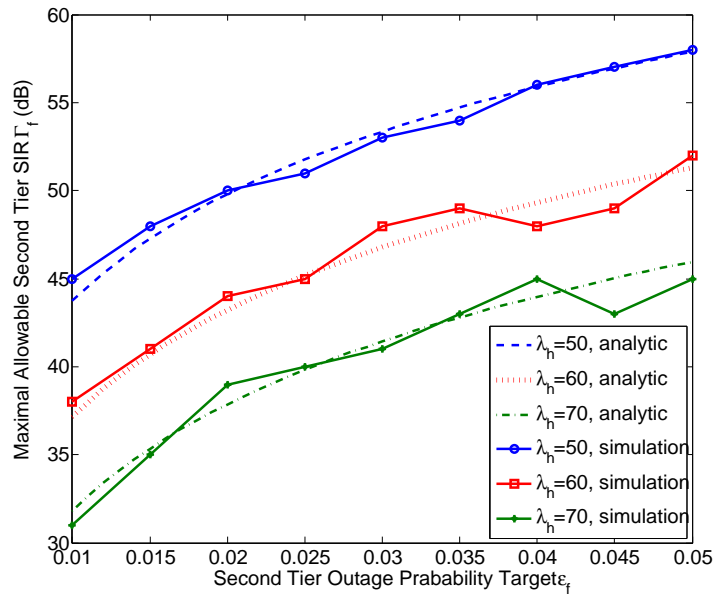


Figure 20: Second Tier Outage vs. Maximal SIR Target

- Fig. 19 illustrates that the tuning of first-tier SIR $\Gamma^{(1)}$, the outage target $\epsilon^{(1)}$, and the second-tier transmit power P_f have a great impact on the system accommodative number of FBSs. Therefore when the first-tier outage probability is overflowed by too many FBSs *in situ*, one effective way to ease the tension is to temporarily reduce the parameters $\Gamma^{(1)}$, P_f or increase $\epsilon^{(1)}$, as predicted in Corollary 3.2, 3.3, and 3.4.
- Fig. 20 shows that the second-tier outage probability along with the FBS density are influential to the second-tier SIR target. Therefore, to maximize the second-tier throughput under the constraints for a given FBS density, the system needs to increase the outage target.

However, the increase of throughput is diminishing in high outage rate region and moreover, it is bounded by the first-tier outage constraints, which is of higher priority in most system design.

To summarize, the good match between the analytical and simulation results confirms that the stochastic geometry is a powerful tool in the study of Femtocell application. Both kinds of results have shown that the optimal spectrum access rate of FBS is closely related to the Macrocell's FFR configuration.

Our proposed algorithm, which optimally adapts Femtocell's spectrum access rate to the FFR configuration of the MBSs in the vicinity, achieves a substantial gain in transmission capacity over blind or heuristic access.

Moreover, the second-tier SIR target is proved to be constrained by the outage probability. Therefore, given a target outage probability, better accessing algorithms can be designed so that the second-tier throughput is also maximized.

3.6 EXTENSIONS

In the previous study of this chapter, the F-ALOHA based spectrum access algorithm for FFR underlying FBS is proposed and its optimality has been proved by simulation. However, the development is based on some critical assumptions that it might not meet in the practical system. Those assumptions include

1. the system is limited by 2nd-tier interference only,
2. the Rayleigh fading for the channel gain,
3. and the simplest case of Macro circular FFR topology.

In this section, we will extend the study and show how does the proposed algorithm work under more general conditions.

3.6.1 None 2nd-tier limited Case

In the previous, we only assume that the system uplink performances (both 1st- and 2nd-tier) are limited by the 2nd-tier Femtocell interference only. In

such case, we overlook the thermal noise at each receiver and the 1st-tier interference that comes from nearby other-cell MUEs, so that the system QoS criteria are represented by SIR $\gamma^{(1)}$ and $\gamma^{(2)}$ defined in (3.2) and (3.4).

However, this assumption only holds when the Femtocell deployment is very dense so that Macro users and the noise figure is much lower. In a more general case, we also take these factors into account and assume the system is also corrupted by additive white Gaussian noise of σ_1 and σ_2 on \mathcal{S}_1 and \mathcal{S}_2 , which are irrelevant to the Femtocell deployment.

Here we somehow abuse the notations and denote the link Signal-to-Interference and Noise Ratio (SINR) also as γ . Correspondingly, (3.2) and the outage event on \mathcal{S}_1 can be written as:

$$\mathcal{E}_1^{(1)} : \gamma_{s_{1,0}}^{(1)} = \frac{P_1 K_o W_o \|u_{1,0}\|^{-\alpha}}{\underbrace{I_{s_{1,0}}^{(1)}}_{\text{interference from 2nd-tier}} + \underbrace{\sigma_1^2}_{\text{thermal + interference from 1st-tier}}} < \Gamma^{(1)} \quad (3.34)$$

Therefore,

$$\begin{aligned} \Pr(\mathcal{E}_1^{(1)}) &\leq 1 - \Pr\left(\frac{P_1 K_o W_o R_1^{-\alpha}}{I_{s_{1,0}}^{(1)} + \sigma_1^2} \geq \Gamma^{(1)}\right) \\ &= 1 - \mathcal{L}_{I_{s_{1,0}}^{(1)} + \sigma_1^2}\left(\frac{\Gamma^{(1)}}{P_1 R_1^{-\alpha} K_o}\right) \end{aligned} \quad (3.35)$$

Because σ_1^2 is a constant,

$$\mathcal{L}_{I_{s_{1,0}}^{(1)} + \sigma_1^2}\left(\frac{\Gamma^{(1)}}{P_1 R_1^{-\alpha} K_o}\right) = \exp\left\{-\frac{\kappa_c}{\kappa_s} \eta \rho \lambda \zeta \left(\frac{P_f K_x \Gamma^{(1)}}{P_1 K_o}\right)^{\frac{2}{\alpha}}\right\} \cdot \exp\left\{-\frac{Q \sigma_1^2}{P_1 R_1^{-\alpha}}\right\} \quad (3.36)$$

where $Q = \frac{\Gamma^{(1)}}{K_o}$.

Consequently, the Femto access constraints of (3.15) and (3.13) now yield to:

$$\frac{\kappa_c \eta}{\kappa_s} \zeta \rho \lambda \left(\frac{P_f K_x}{P_1 K_o}\right)^{\frac{2}{\alpha}} \Gamma^{(1)\frac{2}{\alpha}} + \frac{Q \sigma_1^2}{P_1 R_1^{-\alpha}} \leq -\ln(1 - \epsilon^{(1)}) \quad (3.37)$$

$$\frac{1 - \eta}{1 - \kappa_s} \zeta \rho \lambda \left(\frac{P_f K_x}{P_2 K_o}\right)^{\frac{2}{\alpha}} \Gamma^{(1)\frac{2}{\alpha}} + \frac{Q \sigma_2^2}{P_2 R_c^{-\alpha}} \leq -\ln(1 - \epsilon^{(1)}) \quad (3.38)$$

and the optimal access rate for maximizing the transmission capacity is given by:

$$\eta^* = \frac{\kappa_s}{\kappa_s + (1 - \kappa_s) \kappa_c a b} \quad (3.39)$$

with

$$\begin{aligned} b &= \frac{b_1}{b_2} \\ b_1 &\triangleq -\ln(1 - \epsilon^{(1)}) - \frac{Q \sigma_1^2}{P_1 R_1^{-\alpha}} \\ b_2 &\triangleq -\ln(1 - \epsilon^{(1)}) - \frac{Q \sigma_2^2}{P_2 R_c^{-\alpha}} \end{aligned}$$

The physical meaning of b_1 and b_2 is that the *Femto-free* outage gap between the pre-set criteria and the system thermal and 1st-tier interference.

They are the system parameters characterized by the outage criteria, the Noise-to-Signal Ratio (NSR) of the Macro transceivers, the Macrocell deployment, and so on, which can be estimated by a long term observation from the operator side.

It is easy to derive that, if $b_1 < 0$ or $b_2 < 0$, then the Femto access problem is infeasible because the system is already unable to meet the outage criteria before any deployment of Femtocell.

In conclusion, we see the previous defined Optimal Access Algorithm 3.2 is no longer optimal because the additional term b in the denominator of η^* .

Thereby, we amend the Femto optimal access algorithms as follows:

Algorithm 3.3 (Optimal Access in non-interference-limited case) *As supplementary to Algorithm 3.2, the operator also provide the following information to the local FBSs via the subband access agent. The additional information is:*

- 4. the ratio of the Femto-free outage gaps on \mathcal{S}_1 and \mathcal{S}_2 , i.e. b

Meanwhile the second-tier users accommodate to maximize the transmission capacity by tuning their biased spectrum access rate η^* according to (3.39), i.e.

$$\eta^* = \frac{\kappa_s}{\kappa_s + (1 - \kappa_s)\kappa_c ab}$$

Remark 3.3 *Obviously, if the NSR on subband \mathcal{S}_1 and \mathcal{S}_2 are close in value, $b \approx 1$, the Algorithm 3.3 converges to Algorithm 3.2, the FBSs can access the subband with the same manner as in the interference-limited case.*

To demonstrate the effect of noise, we conduct the simulation and compare with the previous simulation results on FFR topology κ_c in Fig. 18 of Section 3.5. The comparison results are shown in Fig. 21, where we assume that \mathcal{S}_1 is corrupted by a noise of $-95dBm$ and \mathcal{S}_2 is corrupted by a noise of $-90dBm$.

From the simulation results, we do not see any apparent changes on the optimal access rate, due to the fact that in the simulation, we assume the subband resources are slotted so that every FBS can only access an integer number of units. However, we do see a small reduction of TC due to the consideration of noise effect, although the influence is quite marginal.

3.6.2 General Fading Case

In section 3.3, it is assumed that all the channel gains of Femto-to-Femto/Femto-to-Macro interference links and the Femto/Macro victim links are i.i.d Rayleigh distributed. To ease such stringent assumption, in the following, we assume that:

- Femto/Macro victim links are i.i.d faded with an *arbitrary* distribution H_V , i.e. $W_0 \sim H_V$, with $\mathbb{E}[H_V^{\frac{2}{\alpha}}] < \infty$;

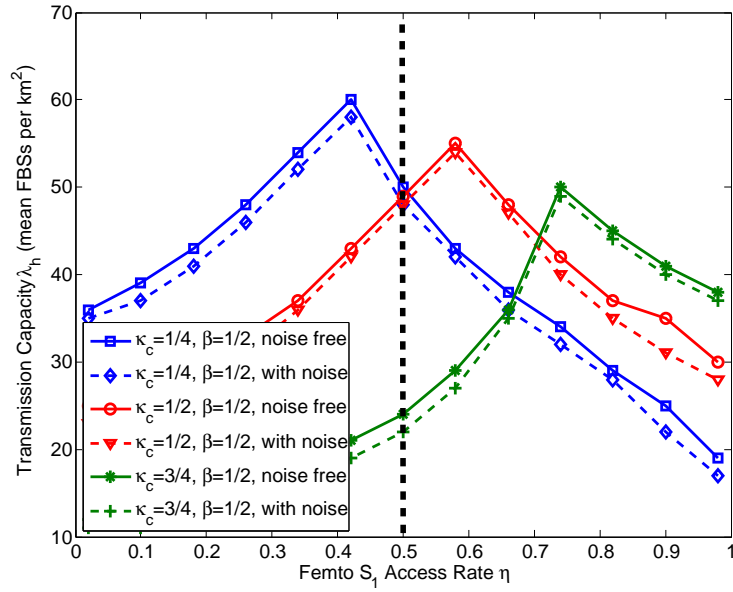


Figure 21: TC vs. MUE FFR Topology in Non-Interference-Limited Case

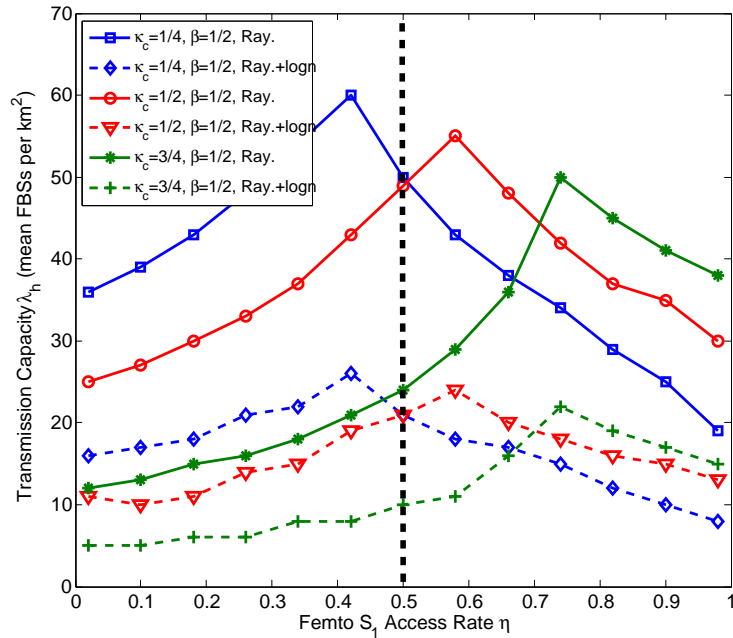


Figure 22: TC vs. MUE FFR Topology in Different Fading

- Femto-to-Femto and Femto-to-Macro interference links are i.i.d. faded with an *arbitrary* distribution H_A , i.e. $W_i \sim H_A$, with $\mathbf{E}[H_A^{-\frac{2}{\alpha}}] < \infty$;
- the pathloss exponent of all the links are identical of α

Theorem 3.2 *The previous proposed frequency access algorithm with access probability given by (3.14), i.e.*

$$\eta^* = \frac{\kappa_s}{\kappa_s + (1 - \kappa_s)\kappa_c a}, \text{ with } a = \left(\frac{P_2}{P_1}\right)^{\frac{2}{\alpha}}$$

is also valid for the above defined general fading case in high target SIR region.

Proof To derive the optimal Femto access algorithm under the above renewed assumptions, we refer to Theorem 2 of [69], which gives that the c.c.d.f. ISR ($1/\gamma^{(1)}$) is lower and upper bounded by $\mathbf{F}_{\gamma^{(1)}}^{c,l}(y)$ and $\mathbf{F}_{\gamma^{(1)}}^{c,\mu}(y)$ respectively:

$$\begin{aligned} \mathbf{F}_{\gamma^{(1)}}^{c,l}(y) &= 1 - \mathbf{E} \left[\exp \left\{ -K\mu y^{-\frac{2}{\alpha}} \right\} \right] \\ \mathbf{F}_{\gamma^{(1)}}^{c,\mu}(y) &= 1 - \mathbf{E} \left[\left(1 - \frac{\frac{\frac{2}{\alpha}}{2-\frac{2}{\alpha}} K\mu y^{-\frac{2}{\alpha}}}{\left(1 - \frac{\frac{2}{\alpha}}{1-\frac{2}{\alpha}} K\mu y^{-\frac{2}{\alpha}}\right)^2} \right)^+ \exp \left\{ -K\mu y^{-\frac{2}{\alpha}} \right\} \right] \end{aligned} \quad (3.40)$$

where

$$\begin{aligned} K &= \pi \mathbf{E}[H_V^{\frac{2}{\alpha}}] H_A^{-\frac{2}{\alpha}} R^2 \lambda \\ \mu &= \frac{\eta \rho \lambda}{\kappa_s} \end{aligned}$$

and the lower bound $\mathbf{F}_{\gamma^{(1)}}^{c,l}(y)$ is asymptotically tight as $y \rightarrow \infty$, while the upper bound is derived by Chernoff Bound, which is not tight.

With the assumption of no too low of SIR target Γ and channel fading gain H_A and H_V are independent, we apply the Jensen's inequality to the lower bound (because $\exp(\cdot)$ is convex) and we obtain the following modified approximation on the 1st-tier outage probability of subband \mathcal{S}_1 and \mathcal{S}_2 respectively, i.e.

$$\begin{aligned} \Pr(\mathcal{E}_1^{(1)}) &\approx 1 - \exp \left\{ -\frac{\kappa_c}{\kappa_s} \eta \rho \lambda \mathbf{E}[H_V^{\frac{2}{\alpha}}] \mathbf{E}[H_A^{-\frac{2}{\alpha}}] \left(\frac{P_f K_x \Gamma^{(1)}}{P_1 K_o} \right)^{\frac{2}{\alpha}} \right\} \\ \Pr(\mathcal{E}_2^{(1)}) &\approx 1 - \exp \left\{ -\frac{1-\eta}{1-\kappa_s} \rho \lambda \mathbf{E}[H_V^{\frac{2}{\alpha}}] \mathbf{E}[H_A^{-\frac{2}{\alpha}}] \left(\frac{P_f K_x \Gamma^{(1)}}{P_1 K_o} \right)^{\frac{2}{\alpha}} \right\} \end{aligned} \quad (3.41)$$

Therefore, the \mathcal{S}_1 and \mathcal{S}_2 outage constraints of access optimization problem (3.15),(3.13) in the previous section can be rewritten as:

$$\frac{\kappa_c \eta}{\kappa_s} \rho \lambda \left(\frac{P_f}{P_1}\right)^{\frac{2}{\alpha}} \Gamma^{(1)\frac{2}{\alpha}} \leq -\frac{K_o^{\frac{2}{\alpha}} \ln(1 - \epsilon^{(1)})}{\mathbf{E}[H_V^{\frac{2}{\alpha}}] \mathbf{E}[H_A^{-\frac{2}{\alpha}}] K_x^{\frac{2}{\alpha}}} \quad (3.42)$$

$$\frac{1-\eta}{1-\kappa_s} \rho \lambda \left(\frac{P_f}{P_2}\right)^{\frac{2}{\alpha}} \Gamma^{(1)\frac{2}{\alpha}} \leq -\frac{K_o^{\frac{2}{\alpha}} \ln(1 - \epsilon^{(1)})}{\mathbf{E}[H_V^{\frac{2}{\alpha}}] \mathbf{E}[H_A^{-\frac{2}{\alpha}}] K_x^{\frac{2}{\alpha}}} \quad (3.43)$$

In the similar way, it is easy to derive that the renewed optimization problem is also maximized by

$$\eta^* = \frac{\kappa_s}{\kappa_s + (1 - \kappa_s)\kappa_c a}.$$

■

Apparently, the derivative corollaries and remarks also hold due for the general fading case and the victim links gain H_V and interference links H_A do not need to be *identically* distributed.

However, one should note that, different from the algorithm derived in the Rayleigh fading case in section 3.3 which applies for the whole SIR region, the results we derive in general fading case are only valid for high SIR or not too low SIR cases.

For FDMA systems, where the SIR threshold is higher than CDMA systems because of no spreading gain, we demonstrate that our proposed algorithm can also approximately capture the optimal access probability.

For the same simulation configs as listed in Tab. 4, we assume that the victim and aggressor link channels are now under a Rayleigh + Lognormal fading, with the standard deviation of the lognormal fading of $8dB$.

As seen from Fig. 22, the simulation results reveal that the new fading model leads to a substantial loss in the transmission capacity. The reason is that because the new fading model involves more randomness for the channel gain, so that the system is more likely to drop. In such condition, the selectivity of TC over the access rate seems to become flat, but we still observe the maximal TC achieved when the Femtos are accessing the subbands with the proposed biased probability, which is identical in value with the Rayleigh fading and Rayleigh+lognormal fading cases.

3.6.3 Sectorized Macrocell Case

While Macrocell sectoring and directional antenna is the common features for the next generation FDMA cells, we in this subsection look into the case that the referred system is sectorized in topology with the angle of Δ . For e.g. in the three-sector case, we simply have $\Delta = 120^\circ$.

We align the reference Macrocell in Fig. 23 to the angular coordinate and set the left axis as 0 degree. For a *typical* MUE of $u_{1,0}$, we assume that the its angle as $\theta_{u_{1,0}}$. Facing to the front region of Δ , the MBS directional antenna gain is assumed to be a function of $f(\theta)$ and perfectly forward-backward isolated. Hereby we assume a common antenna pattern [26] which yields to:

$$f(\theta) = \begin{cases} d \left(\frac{|\theta - \frac{\Delta}{2}|}{\Delta} \right)^p & \text{if } \theta \in [0, \Delta] \\ 0 & \text{otherwise} \end{cases} \quad (3.44)$$

where $d > 0$ and $p \leq 0$ are antenna dependent parameters to characterize how directional the antenna is.

Thereby, the whole region C' can be divided into:

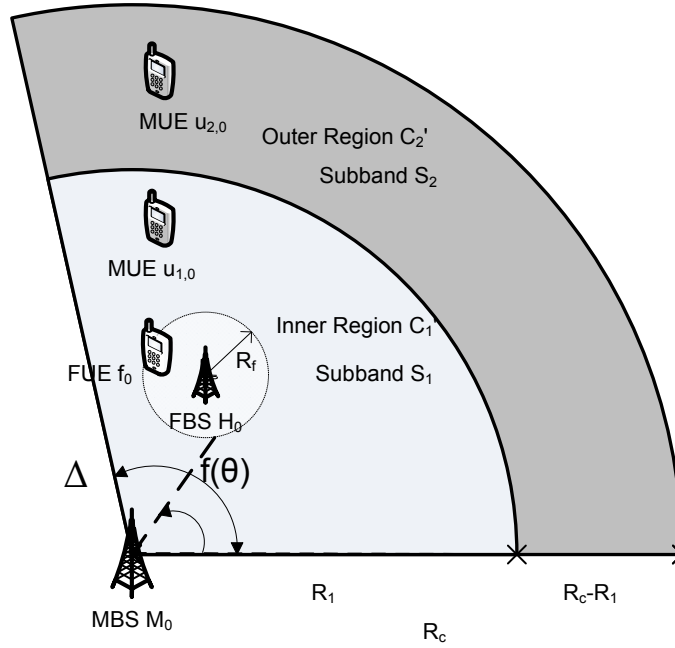


Figure 23: Sectorized Case for Macro

- inner region C'_1 with $|C'_1| = \frac{\Delta}{2\pi} \pi R_1^2$,
- the outer region C'_2 is of $|C'_2| = \frac{\Delta}{2\pi} \pi (R_c^2 - R_1^2)$.

The region factor κ_c remains the same as in Section 3.4.

If we keep other assumptions same as in section 3.4, and define the Femto intensity λ as the average number of FBSs per region area of πR_c^2 .

For the reference MBS, the 2nd-tier interference seen from M_0 on subband S_1 is thus given by

$$I_{s_{1,0}}^{(1)} = \sum_{X'_i \in \Omega'_1 \cap C'} f(\theta_{X'_i}) P_f K_x W_i \|X'_i\|^{-\alpha} \quad (3.45)$$

where according the Restriction Theorem in [43], X'_i is the marked PPP process of Ω'_1 restricted on C' , with the same homogeneous measure.

Therefore, similar to (3.2), the SIR $\gamma_{s_{1,0}}^{(1)}$ and outage event $\mathcal{E}_1^{(1)}$ of one *typical* MUE $u_{1,0}$ can be derived as:

$$\mathcal{E}_1^{(1)} : \quad \gamma_{s_{1,0}}^{(1)} = \frac{f(\theta_{u_{1,0}}) P_1 K_o W_0 \|u_{1,0}\|^{-\alpha}}{I_{s_{1,0}}^{(1)}} < \Gamma^{(1)} \quad (3.46)$$

As all the MUEs and FUEs are assumed to be uniformly distributed in the area of C' , the angular coordinates $\theta_{u_{1,0}}$, $\theta_{X'_i}$ are thus i.i.d. uniformly distributed with distribution:

$$\mathbf{f}(\theta) = \begin{cases} \frac{1}{\Delta} & \theta \in [0, \Delta], \\ 0 & \text{otherwise} \end{cases}$$

$$\begin{aligned}
 \Pr(\mathcal{E}_1^{(1)}) &\leq 1 - \Pr\left(\frac{f(\theta_{u_{1,0}})P_1K_oW_0R_1^{-\alpha}}{I_{s_{1,0}}^{(1)}} \geq \Gamma^{(1)}\right) \\
 &= 1 - \mathbf{E}_{\theta_{u_{1,0}}}\left[\Pr\left(W_0 > \frac{\Gamma^{(1)}I_{s_{1,0}}^{(1)}}{f(\theta_{u_{1,0}})P_1R_1^{-\alpha}K_o} \mid \theta_{u_{1,0}}\right)\right] \\
 &= 1 - \mathbf{E}_{\theta_{u_{1,0}}}\left[\mathcal{L}_{I_{s_{1,0}}^{(1)}|\theta_{u_{1,0}}}\left(\frac{\Gamma^{(1)}}{f(\theta_{u_{1,0}})P_1R_1^{-\alpha}K_o}\right)\right]
 \end{aligned} \tag{3.47}$$

The conditioned interference distribution in Laplacian form $\mathcal{L}_{I_{s_{1,0}}^{(1)}|\theta_{u_{1,0}}}$ can be thus given by:

$$\begin{aligned}
 \mathcal{L}_{I_{s_{1,0}}^{(1)}|\theta_{u_{1,0}}}(s) &= \mathbf{E}_{I_{s_{1,0}}^{(1)}|\theta_{X'_i}}\left[\exp(-sI_{s_{1,0}}^{(1)})\right] \\
 &= \mathbf{E}_{\theta_{X'_i}}\int_0^\infty \left[\exp\left(-s \sum_{X_i \in \Omega'_1} f(\theta_{X'_i})P_fK_xW_i\|X_i\|^{-\alpha}\right) ds\right] \\
 &= \mathbf{E}_{\theta_{X'_i}}\left[\exp\left(\int_{\mathcal{C}'} -sf(\theta_{X'_i})P_fK_xW_i\|X_i\|^{-\alpha} \frac{\eta\rho\lambda}{\kappa_s} \Omega'_1(d\|X_i\|)\right)\right]
 \end{aligned} \tag{3.48}$$

Applying (3.48) to (3.47) and take Jensen's inequality to the upper bound as approximation, we finally get that

$$\begin{aligned}
 \Pr(\mathcal{E}_1^{(1)}) &\approx 1 - \mathbf{E}_{\theta_{u_{1,0}},\theta_{X'_i}}\left[\exp\left(-\frac{\kappa_c\Delta}{\kappa_s\pi}\eta\rho\zeta\left(\frac{P_fK_x\Gamma^{(1)}}{P_1K_o}\right)^{\frac{2}{\alpha}}\left(\frac{f(\theta_{X'_i})}{f(\theta_{u_{1,0}})}\right)^{\frac{2}{\alpha}}\right)\right] \\
 &\approx 1 - \exp\left(-B\frac{\Delta}{2\pi}\int_0^\Delta\int_0^\Delta\left(\frac{|\theta_{X'_i}-\frac{\Delta}{2}|}{|\theta_{u_{1,0}}-\frac{\Delta}{2}|}\right)^{\frac{2p}{\alpha}}d\theta_{X'_i}d\theta_{u_{1,0}}\right) \\
 &= \begin{cases} 1 - \exp\left(-B\frac{\Delta}{2\pi(1+\frac{2p}{\alpha})(1-\frac{2p}{\alpha})}\right) & \text{if } -\frac{\alpha}{2} < p \leq 0 \\ 1 & \text{if } p \leq -\frac{\alpha}{2} \end{cases}
 \end{aligned} \tag{3.49}$$

where

$$B = \frac{\kappa_c}{\kappa_s}\eta\rho\zeta\left(\frac{P_fK_x\Gamma^{(1)}}{P_1K_o}\right)^{\frac{2}{\alpha}}$$

(3.49) tells us that if $p \leq -\frac{\alpha}{2}$, the shot-noise interference will be unbound so that outage will be pervasive. To prevent this, p shall be within the range

of $\in (-\frac{\alpha}{2}, 0)$. If we assume that p obeys this criteria, therefore the outage constraints on subband \mathcal{S}_1 and \mathcal{S}_2 in (3.15) (3.13) can be rewritten as:

$$\frac{\kappa_c \eta}{\kappa_s} \rho \lambda \left(\frac{P_f}{P_1} \right)^{\frac{2}{\alpha}} \Gamma(1)^{\frac{2}{\alpha}} \leq - \frac{K_0^{\frac{2}{\alpha}} \ln(1 - \epsilon^{(1)})}{L \zeta K_x^{\frac{2}{\alpha}}} \quad (3.50)$$

$$\frac{1 - \eta}{1 - \kappa_s} \rho \lambda \left(\frac{P_f}{P_2} \right)^{\frac{2}{\alpha}} \Gamma(1)^{\frac{2}{\alpha}} \leq - \frac{K_0^{\frac{2}{\alpha}} \ln(1 - \epsilon^{(1)})}{L \zeta K_x^{\frac{2}{\alpha}}} \quad (3.51)$$

with

$$L = \frac{\Delta}{2\pi(1 + \frac{2p}{\alpha})(1 - \frac{2p}{\alpha})}, \quad L \geq \frac{\Delta}{2\pi}$$

Consequently, solving the optimal access problems yields to

$$\eta^* = \frac{\kappa_s}{\kappa_s + (1 - \kappa_s)\kappa_c a}$$

and

$$\Lambda = \left[\frac{\kappa_s}{\kappa_c} P_1^{\frac{2}{\alpha}} + (1 - \kappa_s) P_2^{\frac{2}{\alpha}} \right] \frac{-K_0^{\frac{2}{\alpha}} \ln(1 - \epsilon^{(1)})}{L \rho \zeta (K_x P_f \Gamma(1))^{\frac{2}{\alpha}}} \quad (3.52)$$

This means that cell sectorizing will not take influence on the selection of optimal access rate so that Algorithm 3.2 can remain unchanged.

However, cell sectorizing do take effect of increasing the transmission capacity by the fold of $\frac{1}{L}$, which is monotonically decreasing with p , reaches its maximal, i.e. $\frac{2\pi}{\Delta}$ when $p = 0$. In that case, the antenna pattern is omnidirectional within its facing range and completed nullified outside of it, which is too ideal for implementation.

Take a practical case of antenna pattern $p = -\frac{3}{2}$ and $\Delta = \frac{2\pi}{3}$ for channel ($\alpha = 4$) as example, the gain of transmission capacity compared to unsectorized case is

$$\frac{1}{L} \approx 131\% \quad (3.53)$$

To validate the above analysis, we run the computer simulation with the same configuration as in Section 3.5 but in a sectorized map of $\Delta = \frac{2\pi}{3}$. We also assume that the MBS antenna pattern is of $p = -\frac{3}{2}$.

As shown in Fig. 24, the optimal subband access rate for Femtocells are indeed invariant with the cell topology and antenna patterns. However, compared to the circular case, the sectorized case with specified pattern can increase the system transmission capacity by around 30% in overall, which is close to the analytical prediction in (3.53).

3.7 CHAPTER SUMMARY

To conclude, in this chapter, we successfully model the arrival of 2nd-tier interference as PPP and propose the F-ALOHA based optimal frequency access algorithm for Femtocell uplink when underlaid with the

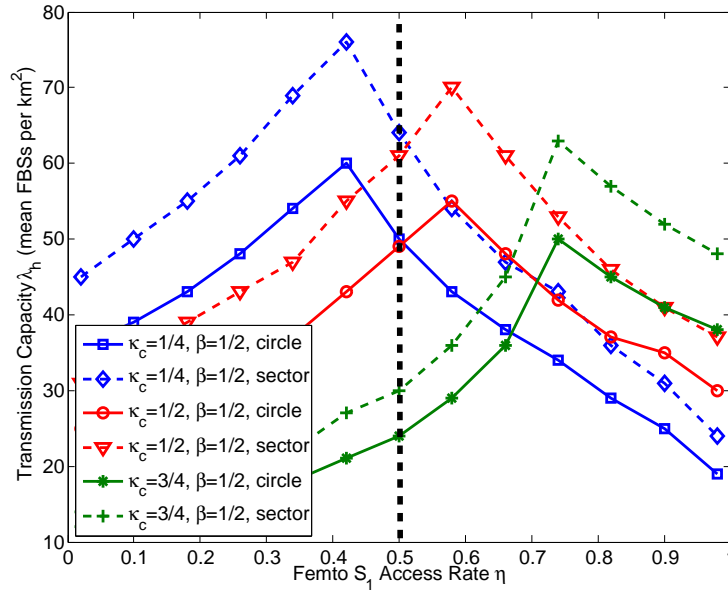


Figure 24: TC vs. MUE FFR Topology in sector case

FFR-performing Macros. The algorithm shows that it is possible for the Femtos to exploit the pre-knowledge of the Macrocell's FFR configuration and access the subbands with *partially bias* (as the access rate is usually not 0 nor 1).

The algorithm is proved by both analysis and simulation that it can always achieve the maximized system transmission capacity.

The later extended investigation also shows that our proposed algorithm works well

- not only for interference-limited case but for non-interference-limited case with some modifications;
- not only for Rayleigh fading, but also for general fading case in high SIR region;
- not only for the circular topology, but also in sectorized topology.

Moreover, the proposed algorithm has been shown to be practically implementable in the current design of Femtocell deployment, with only a low requirement of message broadcasting and coordination.

FEMTO SPECTRUM ACCESS II: MACRO FFR IN DOWNLINK

In Chapter 3, a simple and practical Femto subband access algorithm is devised, which can maximize the transmission capacity of the two-tier coexisting system in uplink. In this chapter, we will investigate whether this designed algorithm can also work efficiently for the downlink scenarios. To proceed, we make comparisons between the uplink and downlink cases for two-tier cellular system in Section 4.1. In Section 4.3, we study a most ideal case and demonstrate that the modified algorithms can also work for such cases. In Section 4.4, we summarize the proposed algorithms and establish a general framework for Femtocells to access the Macro resources. Numerical results are given in Section 4.5 and conclusions are drawn in Section 4.6.

4.1 MOTIVATIONS AND DISCUSSIONS

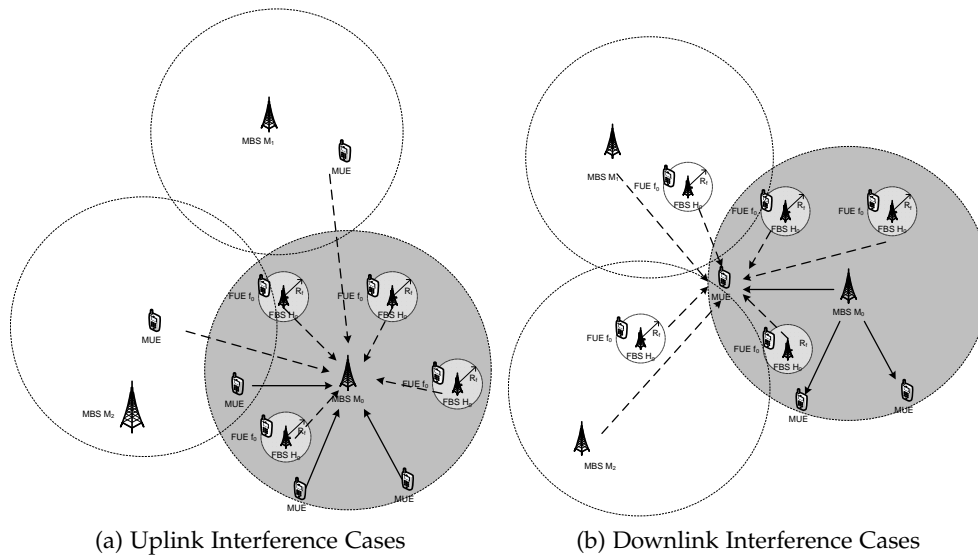


Figure 25: Comparison between UL and DL interference cases

4.1.1 Summary from Uplink Case

Recall from the proposed algorithm in Chapter 3, we can summarize that the general prerequisite for Algorithm 3.2 and 3.3 has the following essentials:

- MBS is able to inform its local parameters to the subband access agent in Internet,
- FBS knows in which Macrocell it is located and listens on the corresponding MBS neighbor's information.

which actually implies that the co-located FBSs are the main interference sources of the 2nd-tier interference.

The above prerequisites are actually compatible with the evolution of Femtocell standardizations. Femto Forum is nowadays actively discussing with 3GPP on the issues that, each LTE FUE can report its neighboring cell-ID (in the descending order of Pathloss or RSSI) to its host FBSs if requested. So that the FBSs are able to learn how many Macrocells are in the near, and estimate the distance between each other.

After knowing this information, the FBS is able to inquire about the necessary information such as subband-access and power control configs from an online access agent. See Fig. 26 for the detail procedure. It is noted that this procedure is also useful and insightful for our later study of downlink cases in this chapter.

4.1.2 *Asymmetric for Downlink Case*

On the other hand, the interference cases for cellular uplink and downlink are **asymmetric**.

- Seen from Subfig. 25a, the 2nd-tier uplink interference victim receiver is the MBS and the interference aggressors are the FUEs that are surrounding the MBS, together with the MUEs that are from the neighboring Macrocells (for 1st-tier universal frequency reuse case). Therefore, the most malicious aggressor are the cell center FUEs and the most vulnerable victims are cell edge MUEs, so that the Algorithm 3.2 and 3.3 of tuning the co-located Femtocells can hold for the uplink scenarios.
- For the downlink cases, the 1st-tier interference victim receiver is the MUEs. If the MUEs are located at the cell edge, it will be corrupted with the co-tier interference from the neighboring MBSs (for 1st-tier universal frequency reuse case), together with the FBSs around it. Those FBSs can be not only from the same Macrocell (as the FBSs in shadow in Subfig. 25b), but also from the neighboring Macrocells (as the FBSs in white circle in Subfig. 25b).

Therefore, the access rate tuned by the Chapter 3 frameworks cannot influence all the involved aggressors and those MUEs are indeed the most vulnerable victims if located at cell edge.

Therefore, for the downlink cases, we will simplify the problem with reasonable assumptions and propose a modified algorithm. One important assumption made is that we model both the 2nd-tier and the 1st-tier with homogeneous Poisson Point Process models. Based on this simplification, we successfully derive the optimal access rate in closed forms.

4.2 CONTRIBUTIONS

The contribution of this chapter's work can be summarized as follows:

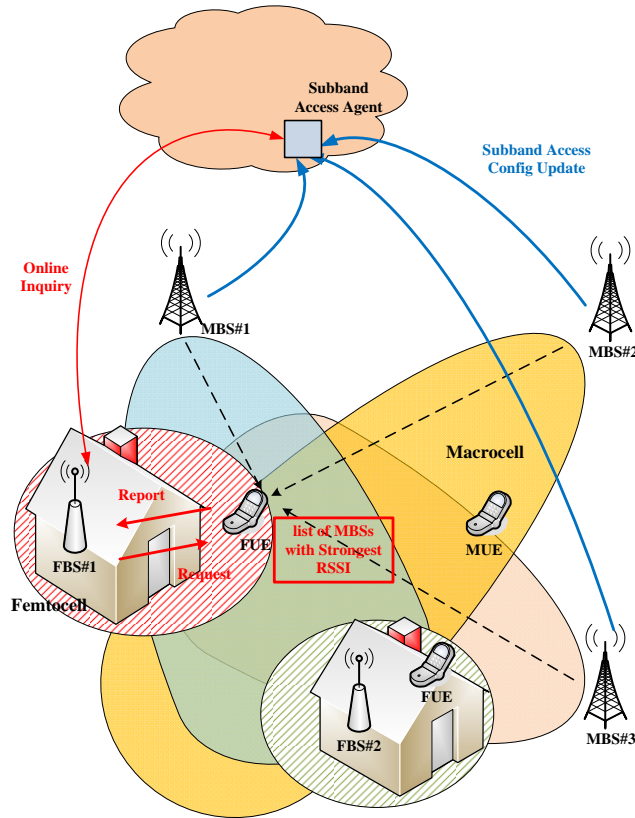


Figure 26: FUE report the neighboring MBS lists to connected FBS

- by proper modeling, we deliver the downlink performance between subband access rate, Femto intensity, and outage criteria in closed forms;
- we thereby propose the optimal downlink Femto subband access algorithms to achieve the maximal transmission capacity;
- we summarize the design essentials of downlink and uplink access algorithms and propose a unified framework at the end of this chapter.

4.3 SYSTEM MODELS

In this chapter, we also assume a circular system map of \mathcal{C} (with radius of R_c), which is Euclidean $\mathcal{C} \subset \mathbb{R}^2$. The definition of Subband \mathcal{S} also follows Chapter 3, which is divided into two disjoint subbands \mathcal{S}_1 and \mathcal{S}_2 , with ratio $\kappa_s \triangleq \frac{|\mathcal{S}_1|}{|\mathcal{S}|}$.

To enable the subsequent analysis in the chapter, we make some important assumptions for the system models.

Assumption 4.1 (PPP for both tiers) *As shown in Fig. 27, we assume that the distribution of the MBSs and FBSs in \mathcal{S} are in the law of two independent PPPs, denoted as Ω_m and Ω_f , respectively. Both Ω_m and Ω_f are assumed to be homogeneous over the map, with the intensity value of λ_m and λ_f , respectively.*

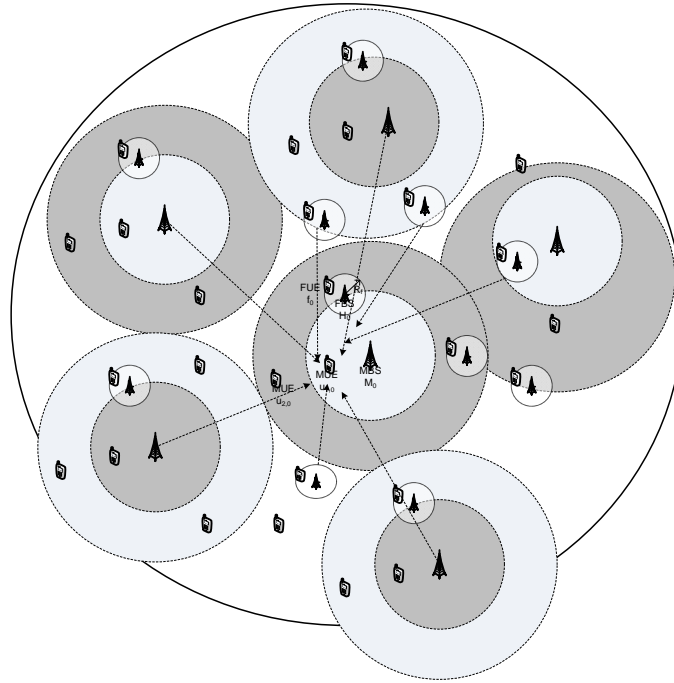


Figure 27: PPP distributed st-and 2nd-tier base stations

Note that different from Chapter 3, we here also assume that 1st-tier MBS is PPP distributed. The reason is that, it can tremendously reduce the analysis tractability. Moreover, in real practice it has also been proved that the PPP assumption is valid for Macrocells in the pioneering paper of [23], which is also introduced in Subfigure 11 of Section 3.1.

Assumption 4.2 (Independent Macro FFR) We assume that each Macrocell can independently perform the Fractional Frequency Reuse (FFR) policies for assigning frequency channel units to the downlink MUEs. Each MBS randomly chooses either subband S_1 or S_2 as its cell-edge subband or cell-center subband with no bias.

Each MUE u is assumed to be connected to one MBS simultaneously. We define the indicator function $S(\cdot, \cdot)$, so that $S(u, S_1) = 1$ if u is assigned by MBS with a channel unit from subband S_1 and 0 if not. Thereby, we can differentiate the MUEs with their accessing subbands.

Assumption 4.3 (Transmit Power for MBS and FBS) We assume that each Macrocell MBS has a constant downlink transmit power of P_m regardless on which subbands and for all the MBSs, we assume that they are transmitting at a constant power of P_f regardless its positions and neighbors.

Combining with Assumption 4.2 and 4.3, we know that the MBSs are independently selecting the FFR and transmitting power for a specific region of MUE receivers, so that the arrival sum of the interference is again an independent thinning process of PPP which can be modeled as shot-noise process.

Assumption 4.4 (A Typical Study Case) As shown in Fig. 28, without loss of generality, we select a typical cell-edge MUE u_0 within a typical MBS M_0 , the distance between u_0 and M_0 are assumed to be R_u . We assume that the FFR policy of Macrocell M_0 (set as the origin of the map) is that: cell-edge MUEs are accessing the subband \mathcal{S}_1 and the cell-center MUEs are accessing the subband \mathcal{S}_2 .

Besides the 1st-tier interference from all other neighboring Macrocells except M_0 , we assume that the u_0 is also exposed to the 2nd-tier interference in the region \mathcal{C}_s of range R_s . The value of R_s is much smaller than the average size of a Macrocell due to the fact that Femto transmit power is much lower and the house shielding effect.

Assumption 4.5 (Uniform FBS decisions within \mathcal{C}_s) We assume the all FBSs in the small region of \mathcal{C}_s (circular with radius R_s) are experiencing the same level of downlink RSSIs reported from its attached FUEs so that they learn exactly the same information of the neighboring MBSs, and how strong the pathloss is between \mathcal{C}_s to each of the neighboring Macrocell.

Therefore, they are able to inquire at the online subband access agent about the FFR configs of the neighboring MBSs and together make a uniform decision on the subband access probability of η to access the \mathcal{S}_1 and probability $(1 - \eta)$ to access \mathcal{S}_2 .

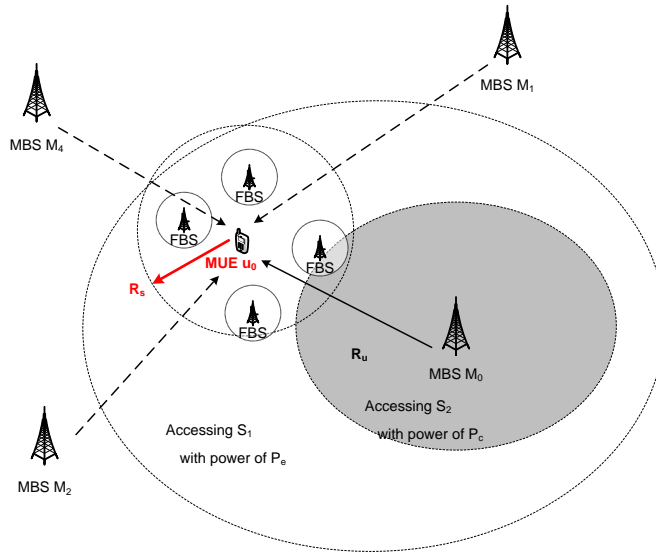


Figure 28: The Downlink System Map

4.4 PROPOSED ALGORITHMS

4.4.1 Analysis of Outage Probability

In this section, we study the optimal access algorithms that can maximize the transmission capacity of the FBSs within the region of \mathcal{C}_s . From the above assumptions, we know that the interference seen from u_0 is consisted of two components: the 1st-tier interference from neighboring MBSs (MBS_1 ,

MBS₂, MBS₃, ... in Fig. 28) and the 2nd-tier interference from the FBSs in region \mathcal{C}_s .

As the FBSs have no idea the MUEs in the region \mathcal{C}_s is assigned with subband \mathcal{S}_1 or \mathcal{S}_2 , it is a random event for them. Conditioned that the u_0 is accessing \mathcal{S}_1 , we have the interference seen by it as:

$$I_{u_0|S(u,\mathcal{S}_1)=1} = \underbrace{\sum_{X_i \in \Omega'_f} P_f K_x W_i \|X_i\|^{-\alpha}}_{\text{2nd-tier interference } \mathbb{X}'} + \underbrace{\sum_{Y_j \in \Omega'_m} P_m K_o W_i \|Y_j\|^{-\alpha}}_{\text{1st-tier interference } \mathbb{Y}'} \quad (4.1)$$

with

$$\begin{aligned} \mathbb{X}' &\triangleq \sum_{X_i \in \Omega'_f} P_f K_x W_i \|X_i\|^{-\alpha} \\ \mathbb{Y}' &\triangleq \sum_{Y_j \in \Omega'_m} P_m K_o W_i \|Y_j\|^{-\alpha} \end{aligned} \quad (4.2)$$

where Ω'_f and Ω'_m stand for the F-ALOHA thinned 2nd-tier and 1st-tier PPP distribution on \mathcal{S}_1 with intensity $\eta\rho\lambda_f$ and $\psi\lambda_m$, respectively. η , and ρ are defined as the same in Chapter 3. ψ is the access probability of MBSs to subband \mathcal{S}_1 , which is $\psi \equiv \frac{1}{2}$ for unbiased macrocell FFR.

Similarly, on subband \mathcal{S}_2 , we have

$$I_{u_0|S(u,\mathcal{S}_2)=1} = \underbrace{\sum_{X_i \in \Omega_f^*} P_f K_x W_i \|X_i\|^{-\alpha}}_{\text{2nd-tier interference } \mathbb{X}^*} + \underbrace{\sum_{Y_j \in \Omega_m^*} P_m K_o W_i \|Y_j\|^{-\alpha}}_{\text{1st-tier interference } \mathbb{Y}^*} \quad (4.3)$$

where Ω_f^* and Ω_m^* are with intensity $(1-\eta)\rho\lambda_f$ and $(1-\psi)\lambda_m$, respectively.

Then conditioned on $S(u, \mathcal{S}_1) = 1$, the 1st-tier SIR γ_1 and outage event \mathcal{E}_1 is defined by:

$$\gamma_1 = \frac{P_m K_o W_0 \|u_0\|^{-\alpha}}{\mathbb{X}' + \mathbb{Y}'} < \Gamma \quad (4.4)$$

where Γ is the 1st-tier SIR criteria and consequently, we have:

$$\begin{aligned} \Pr(\mathcal{E}_1) &\leq 1 - \Pr\left(\frac{P_m K_o W_0 R_u^{-\alpha}}{\mathbb{X}' + \mathbb{Y}'} \geq \Gamma\right) \\ &= 1 - \mathcal{L}_{\mathbb{X}'+\mathbb{Y}'}\left(\frac{\Gamma}{P_m R_u^{-\alpha} K_o}\right) \end{aligned} \quad (4.5)$$

We assume that the FBS and MBS distribution are mutually independent, by the property of Laplacian transform of the sum of two independent r.v.s, (4.5) yields to

$$\begin{aligned} \mathcal{L}_{\mathbb{X}'+\mathbb{Y}'}\left(\frac{\Gamma}{P_m R_u^{-\alpha} K_o}\right) &= \mathcal{L}_{\mathbb{X}'}\left(\frac{\Gamma}{P_m R_u^{-\alpha} K_o}\right) \mathcal{L}_{\mathbb{Y}'}\left(\frac{\Gamma}{P_m R_u^{-\alpha} K_o}\right) \\ &= \underbrace{\exp\left\{-\frac{R_s^2}{R_u^2} \eta \rho \lambda_f \zeta \left(\frac{P_f K_x \Gamma}{P_m K_o}\right)^{\frac{2}{\alpha}}\right\}}_{\text{similar to (3.11)}} \cdot \underbrace{\exp\left\{-\lambda_m \psi \zeta \frac{R_c^2}{R_u^2} \Gamma^{\frac{2}{\alpha}}\right\}}_{\text{irrelevant with } \eta} \end{aligned} \quad (4.6)$$

For the condition of $S(u, \mathcal{S}_2) = 1$, the 1st-tier SIR γ_2 and outage event \mathcal{E}_2 is defined by:

$$\gamma_2 = \frac{P_m K_o W_0 \|u_0\|^{-\alpha}}{\mathbb{X}^* + \mathbb{Y}^*} < \Gamma \quad (4.7)$$

and

$$\Pr(\mathcal{E}_2) \leq 1 - \mathcal{L}_{\mathbb{X}^* + \mathbb{Y}^*} \left(\frac{\Gamma}{P_m R_u^{-\alpha} K_o} \right) \quad (4.8)$$

$$\mathcal{L}_{\mathbb{X}^* + \mathbb{Y}^*} \left(\frac{\Gamma}{P_m R_u^{-\alpha} K_o} \right) = \underbrace{\exp \left\{ -\frac{R_s^2}{R_u^2} (1 - \eta) \rho \lambda_f \zeta \left(\frac{P_f K_x \Gamma}{P_m K_o} \right)^{\frac{2}{\alpha}} \right\}}_{\text{similar to (3.12)}} \cdot \underbrace{\exp \left\{ -\lambda_m (1 - \psi) \zeta \frac{R_c^2}{R_u^2} \Gamma^{\frac{2}{\alpha}} \right\}}_{\text{irrelevant with } \eta} \quad (4.9)$$

From (4.6) and (4.9), we see that the renewed conditional outage probability is only with an additional multiplying component which is same for subband \mathcal{S}_1 and \mathcal{S}_2 (because unbiased 1st-tier FFR $\psi \equiv \frac{1}{2}$), and irrelevant with the Femto access probability η . Thereby, we simply denote

$$A = \exp \left\{ -\lambda_m (1 - \psi) \zeta \frac{R_c^2}{R_u^2} \Gamma^{\frac{2}{\alpha}} \right\}$$

$$B = \frac{R_s^2}{R_u^2} \rho \zeta \left(\frac{P_f K_x \Gamma}{P_m K_o} \right)^{\frac{2}{\alpha}}$$

Therefore, the unconditional outage probability \mathcal{E} for the MUEs located in the region of \mathcal{C}_s can be derived as:

$$\Pr(\mathcal{E}) = \Pr(\mathcal{E}_1) \Pr(S(u, \mathcal{S}_1) = 1) + \Pr(\mathcal{E}_2) \Pr(S(u, \mathcal{S}_2) = 1) \quad (4.10)$$

where $\Pr(S(u, \mathcal{S}_1) = 1)$, $\Pr(S(u, \mathcal{S}_2) = 1)$ is the probability that the MUEs within region \mathcal{C}_s are assigned with subband \mathcal{S}_1 and \mathcal{S}_2 , respectively. Simply we denote $\Pr(S(u, \mathcal{S}_1) = 1)$ as p and $\Pr(S(u, \mathcal{S}_2) = 1)$ as $1 - p$.

4.4.2 Transmission Capacity and Access Probability

Theorem 4.1 (Optimal Subband Access) *In the Femto-Macro coexisting downlink, the optimal subband access strategy for the FBSs are to estimate the probability of the nearby MUEs accessing \mathcal{S}_1 and \mathcal{S}_2 , and opportunistically access the least possible subband to avoid causing interference, i.e.*

$$\eta^* = \begin{cases} 0 & \text{if } 1 \geq p \geq \frac{1}{2} \\ 1 & \text{if } \frac{1}{2} > p \geq 0 \end{cases} \quad (4.11)$$

Proof As the transmission capacity of Femtocell Λ is defined as the maximal intensity of λ_f that satisfies the 1st-tier outage probability criteria, i.e.

$$\begin{aligned} \Lambda : \quad & \max \lambda_f \\ & \text{constrained by} \\ & \Pr(\mathcal{E}) \leq \epsilon \end{aligned} \tag{4.12}$$

for the constraint, we have

$$\left(1 - e^{-B\lambda_f\eta}\right) p + \left(1 - e^{-B\lambda_f(1-\eta)}\right) (1-p) \leq \frac{\epsilon}{A}$$

For the the outage-sensible applications that $\epsilon \rightarrow 0$, similar to Corollary 3.3, we have $1 - e^{-B\lambda_f\eta} \approx B\lambda_f\eta$. Therefore,

$$B\lambda_f\eta p + B\lambda_f(1-\eta)(1-p) \leq \frac{\epsilon}{A}$$

and

$$\lambda_f \leq \frac{\epsilon}{AB[\eta p + (1-\eta)(1-p)]} \tag{4.13}$$

which has the unique maximum when

$$\eta^* = \begin{cases} 0 & \text{if } 1 \geq p \geq \frac{1}{2} \\ 1 & \text{if } \frac{1}{2} > p \geq 0 \end{cases}$$

and the transmission capacity is thus achieved at

$$\Lambda = \frac{\epsilon}{AB \min(\eta, 1-\eta)} \tag{4.14}$$

■

From this theorem, we see that the optimal Femto subband access strategy is no longer a *partially biased* access as in the uplink cases of Algorithms 3.2 and 3.3, but a *totally biased* access which is fully dependent on each Femtocell's estimation of the local FUE subband access conditions, i.e. probability p .

This is a surprising finding, since the optimal scheme in uplink case is revealed to be a partially-biased F-ALOHA access, where as the optimal scheme for downlink is a totally-biased access (η be either 0 or 1).

However, this totally-biased access matches the senses of heuristic approaches, as many reports [54] [77] have already introduced similar algorithms to access the downlink subbands. The analysis in this chapter is only to provide the theoretic supports, showing that such approaches are actually optimal if considering a very low outage probability and a small region of co-behaving FBS neighborhood.

Corollary 4.1 (Multi-subbands) *If the Macro FFR system is consisted of a number of q subbands, i.e. $\mathcal{S}_1, \mathcal{S}_2, \dots, \mathcal{S}_q$, and the probability of MUEs in small region of \mathcal{C}_s is a vector of (p_1, p_2, \dots, p_3) , then optimal subband access strategy for the local FBSs are simple to access the subband of index s , so as*

$$s = \arg \min_i p_i$$

This is a direct derivation from Algorithm 4.1, and for this reason, we will discuss how to estimate this probability p in the next subsection and then propose the full access algorithm for the Femtocells downlink.

4.4.3 Local MUE Estimations and Proposed Access Algorithms

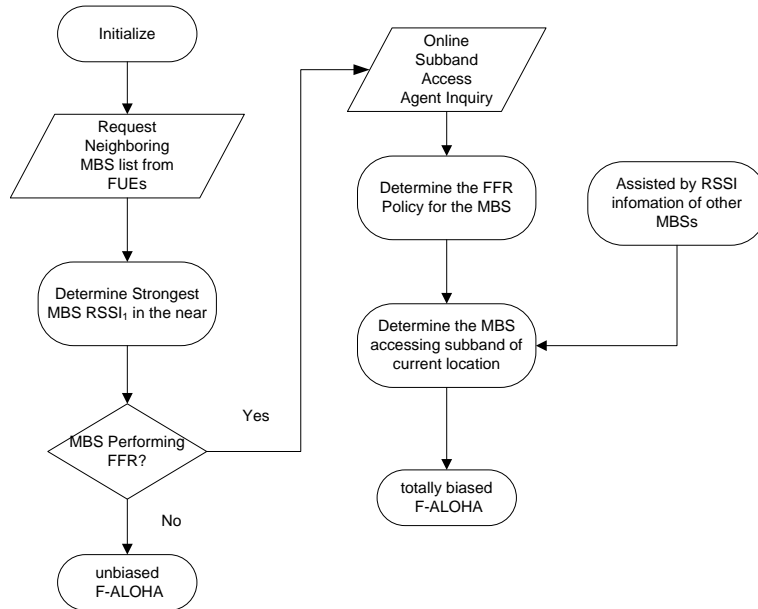


Figure 29: Flowchart of the proposed access algorithm

From the above the analysis, we learn that it is extremely critical for the Femtocells to know the subband access conditions of the MUEs in the near.

However, even though that the Macrocell is adopting a static FFR policy with a clear definition of cell-edge and center, it is not easy in practice for the FBSs to know their closeby because FBSs usually do not possess an accurate position information.

As mentioned before, the FCC requirement is 50m, which is not enough for urban scenarios where Macrocells are small. Let alone the Macrocell FFR policy many change adaptively to adjust the cell breathing or traffic dynamics.

Therefore, we propose the FBS to perform Local MUE Estimations based on the pathloss information to the neighboring MBSs, which is reported by its attached FUEs.

This simple heuristic estimation algorithm can be described as follows:

- **Step 1:** Request Neighboring MBS Pathloss Report from attached FUEs;
- **Step 2:** Inquiry from online subband access agent about Macro FFR, Cell-ID, and Transmit Power;
- **Step 3:** Determine which MBS has strongest local RSSI, denote as MBS A;

Table 5: Default Simulation Parameters for 4.5

Parameter	Description	Value
R_c	Macrocell Size	1000m
R_s	Local Region Size	50m
P_m	Average Transmit Power of MBS	40dBm
P_f	Transmit Power for FBS	20dBm
α	Pathloss Exponential Factor	4
K_o	Outdoor penetration Loss	-15dB
K_f	Indoor Penetration Loss	-25dB
K_x	In/Outdoor Penetration Loss	-40dB
Γ_m	First Tier SIR Target	5dB
ϵ_m	First Tier Outage Target	1%

- **Step 4:** Determine the second strongest local RSSI, denote as MBS B;
- **Step 5:** Determine whether in the cell-edge or cell-center by considering the RSSI of A and B;
- **Step 6:** Inquiry from online subband access agent about the subband for determined cell-edge or center;

Finally, according to the conclusions from Theorem 4.1, each FBS shall

- **Step 7:** Determine which one of the subbands to access, according to (4.11), avoiding the subband known from Step 6.

Algorithm 4.1 (Femto downlink subband access) *With the support from Theorem 4.1 and detail described in Step 1-7., the proposed Femto downlink subband access algorithm in sense of maximizing the local transmission capacity is to perform the procedure according to flow chart in Fig. 29,*

4.5 NUMERICAL RESULTS

To verify the proposed algorithms, we conduct the Mont-Carlo simulations on a two-subbands FFR system and present the results in Fig. 30. The default parameters of the simulation can be found in Table 5 unless explicitly specified otherwise. The baseline algorithm in the Figure is the "blind access" algorithm, which let each FBS access each of the subband with equal probability of $\frac{1}{2}$.

In the simulation, we fixed the subband proportion of κ_s and changes the FFR regional proportion κ_c (i.e. the ratio area of the inner circle). We find out that

- the blind algorithm's performance does not vary with the FFR regional proportion;

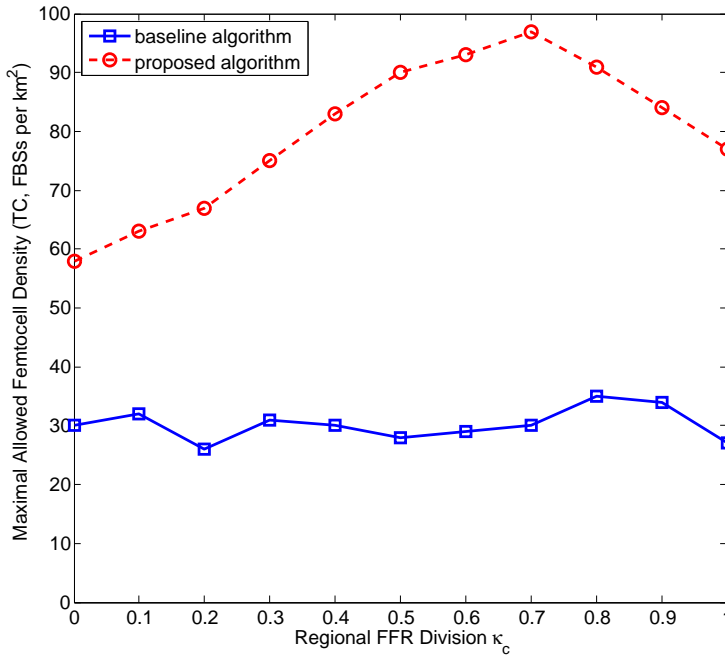


Figure 30: Performance of Proposed Algorithm

- the proposed optimal access algorithm always outperforms the conventional blind access scheme, from around 2 folds of gain in uneven FFR cases to almost 3 folds of gain in even cases;
- interestingly, the κ_c to achieve the highest transmission capacity is not at $\frac{1}{2}$ but at ≈ 0.7 , this is because that the outer circle is more vulnerable to the downlink interference so that making the inner circle area slightly larger will prevent an over-flood in outer circle.

4.6 UNIFIED FEMTO UPLINK-DOWNLINK ACCESS

After achieving the optimal subband access algorithm in downlink as well, we are able to summarize what we have learned in developing the access algorithms for the Femtocells in uplink and downlink cases.

We realize that there is a clear ascending of optimality with the accumulating of available information, and **the subband access agent** is a very important unit serving as the interface between backhauled FBSs and the MBSs and providing the essential information that is required by the FBSs to improve its coexistence performance in the two-tier system.

We see that for the uplink cases, the most essential information for the FBSs is the division of subbands, and the MUE power control parameters. Upon on different level of information cognition, the optimal algorithms for FBSs are:

- **no information at all:** totally blind F-ALOHA;
- **the division of subbands κ_s only:** F-ALOHA biased with κ_s ;
- **κ_c , and power control a :** F-ALOHA biased with Algorithm 3.2;

- $\kappa_c, a,$ and outage gap b : F-ALOHA biased with Algorithm 3.3.

Meanwhile in the downlink, the breakdown of optimal algorithms for FBSs can be:

- **no information at all**: blind F-ALOHA;
- **knowledge of local FFR**: totally biased F-ALOHA to avoid with Algorithm 4.1.

The developed algorithms for downlink and uplink, respectively, can also be interpreted as shown in the subfigures of Fig.31. It is noted that the essence of the optimal uplink access algorithms for Femtocell is to learn the volume of interference level in each subband and water-fill the access rate adaptively, whereas the downlink access algorithm is, by learning the FFR strategies of local Macrocells, to detect the least-interference opportunity among the subbands.

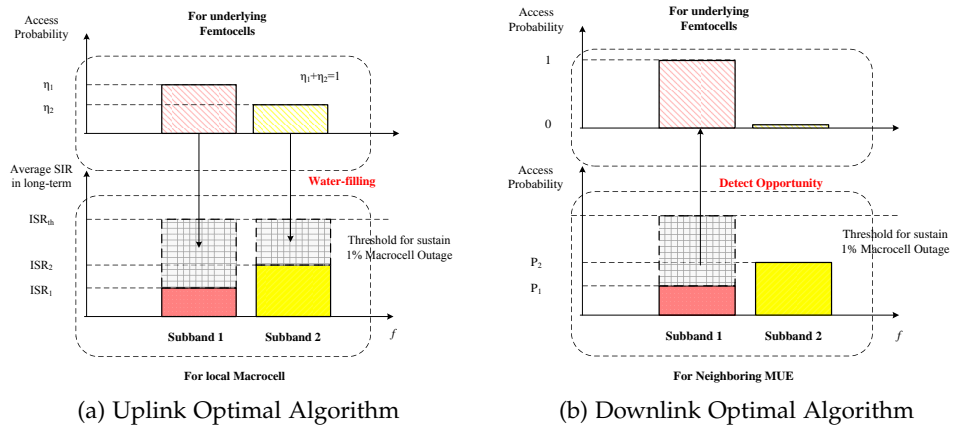


Figure 31: Comparison between UL and DL Optimal Algorithms

Despite the difference from downlink and uplink algorithm, the knowledge of local Macrocell FFR strategies are utilized by both and thus, a framework of MBS periodically uploading this essential information ($\kappa_c, \kappa_s, a, b, RSSI, P_t$) to the subband access agent, the involved FBSs periodically inquiring from the agent to learn these cognition and behaving adaptively as listed above, is a very efficient framework to serve different FFR configurations and maximizing the power of F-ALOHA and achieve the capacity. Moreover, it is a realistic framework with a very limited message passing, definitely realizable within the current Femtocell designs.

4.7 CHAPTER SUMMARY

In this chapter, we investigate the Femto subband access problems in the downlink case when the overlaid 1st-tier is performing FFR. By proper system modeling and outage probability analysis, we find out that, unlike the uplink case, the optimal access strategy for Femtocell downlink is to access the subbands totally biased. Then we develop the heuristic mechanisms

for the FBSs to determine their local FFR subband usage based on the FUE report and propose the complete access algorithm.

In the numerical results part, the computer simulation has shown that the totally-biased subband access are indeed the optimal way to maximize the transmission capacity. This finding provides the backward-engineering to support the previous designs.

After studying both the uplink and downlink cases, we realize that it is possible for the Femtos to optimally perform F-ALOHA access to better co-exist with the Macrocells. Provided only some critical information of Macro FFR configs and some realistic report and inquiry, the proposed algorithms can achieve a substantial gain. Henceforth, we establish the unified framework to support the access decision of Femtocells in both downlink and uplink, which is efficient in performance and implementation with only limited message passing.

FEMTO DEPLOYMENT ISSUE I: OFDM SIDELobe LEAKAGE

It is well known that OFDM signal can have a sidelobe leakage to adjacent channels. This sidelobe leakage is usually not a critical issue for Macrocell because, firstly, a guard band is inserted when defining the Macrocell frequency bands and, secondly, Macro tower is tall mounted that it would be an extreme rare case if it interferes the adjacent channel users. Therefore, as long as a well regulated spectrum mask is respected, the OFDM sidelobe leakage is deemed trivial for Macrocell.

However, this is not always true for Femtocell application. In the case that Femtos are using F-ALOHA to access subbands of the channel, the guard band is usually not considered. And due to the *ad-hoc* manner of Femto deployment, especially for the closed-access Femtos, the imperfect sidelobe leakage may cause considerably performance loss. For these reasons, this chapter is dedicated to study the sidelobe effect for OFDM Femto using F-ALOHA. We will analyze not only the performance of Femtocell (2nd-tier) but also the inverse effect on Macrocell (1st-tier) in a two-tiered cellular network. Additionally, we try to explain the FCC ruling decision of TVWS device's sidelobe leakage from a different perspective and provide guidelines for selecting the appropriate physical layer interface.

5.1 MOTIVATIONS AND RELATED WORKS

To the author's best knowledge, there is no explicit study on the issue of OFDM sidelobe leakage of Macrocell communications so far. The reason has been already mentioned above, i.e. because of the existence of guard band and the low interference chance in practical Macrocell deployment.

Treated similar to the case of Macrocell, the sidelobe effect of Femtocell is not emphasized in [74], [18], [48], [29], [20], [42]. Nevertheless, there are some studies that have covered this issue in the context of OFDM symbol asynchronous and consequent subcarrier interference, see [47], [50], [33]. However, these studies are based on computer simulation only, where the relations between system performances and the sidelobe leakage strength are not thoroughly revealed.

Besides, FCC regulates on the out-of-band emission for portable cognitive devices that access the TVWS as secondly users. The most recent ruling decision [25] is that:

- *TV bands device emissions in channels adjacent to the occupied channel be attenuated at least 72.8 dB below the highest average power in the occupied channel. Emission measurements in the occupied channel are the average emission of the whole 6 MHz bandwidth and emission measurements in the*

adjacent channels are to be made with a minimum resolution bandwidth of 100 KHz and an average detector.

However, the current OFDM air interfaces of LTE and WIFI, i.e. conventional CP-OFDM with rectangular pulse shapes (Scheme I), are not possible to fulfill this emission requirement. On the other hand, the hotspot applications like WIFI and LTE Femto are keen to access TVWS because this band is currently far under utilization in many countries, see COGEU project report [22]. Therefore, it is necessary to consider some alternative PHY interfaces. We show later in this chapter that the concerned PHY schemes of II and III in this chapter are able to fulfill this emission requirements of FCC.

Motivated by this observation, we consider a Femto-Macro coexisting two-tier cellular network in this chapter, where the second-tier users, i.e. Femtos can be densely deployed. Therefore, the interference from the second tier, which is also modeled as a *shot-noise process*, is a dominant factor on both tiers' performance.

5.2 CONTRIBUTIONS

The contributions of this work can be summarized as follows ¹:

1. by scenario modeling and using the superposition theorem of PPP, we successfully formalize the sidelobe interference problem by the shot-noise process framework;
2. we derive the system 1st- and 2nd-tier performance on Transmission Capacity and Area Spectral Efficiency under the OFDM sidelobe leakage effect in analytical form;
3. we demonstrate by computer simulation and explain the cases that substantial system loss can be caused due to OFDM sidelobe leakage;
4. we make comparisons between several OFDM/Filter Bank Multicarrier (FBMC) transmission schemes and discuss the appropriate PHY candidates for Femto and TVWS devices.

More specifically, we investigate the following three OFDM-based transmission schemes with identical subcarrier numbering and spacing:

- **Scheme I:** conventional CP-OFDM with rectangular pulse shape, current PHY interface for LTE, WIFI, etc.
- **Scheme II:** windowed CP-OFDM similar to [73], with roll-off factor $\beta = 0.5$, and
- **Scheme III:** Offset-QAM OFDM (OQAM-OFDM) [62] with the pulse shape presented in [64] based on PHYDYAS project,

where OQAM-OFDM (Offset Quadrature Amplitude Modulation) is of the most interest, achieving best link level spectral efficiency due to its pulse shaping abilities, as discussed in [62] and [13].

¹ A part of this chapter's work is published in [79].

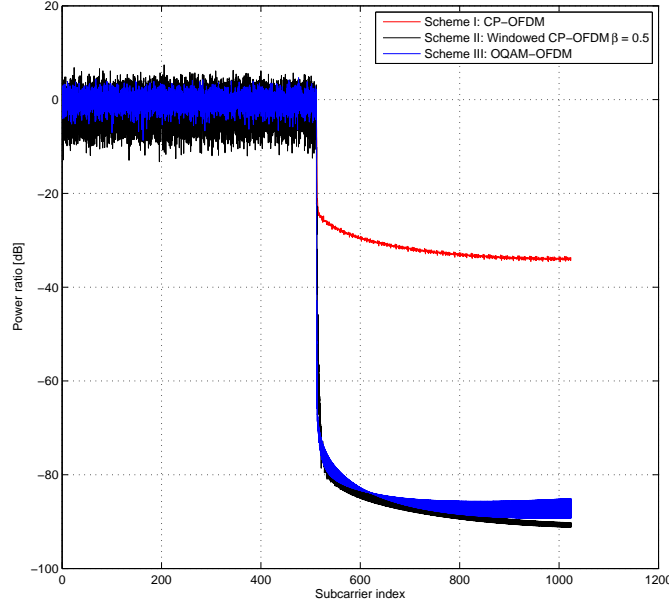


Figure 32: Sidelobe Leakage for the three Schemes

5.3 PERFORMANCE ANALYSIS

5.3.1 System Models

We assume a system with $M \in \mathbb{Z}$ subband units in the whole concerned band. Each subband unit is comprised of a constant number of adjacent OFDM subcarriers. The channel fading gain is assumed to be constant within the subband and uncorrelated across the subbands. As seen in Fig. 33, we further assume that each FBS randomly accesses a consecutive block of $m \in \mathbb{Z}$ subband units at a constant rate of $\frac{m}{M}$ ($\in [0, 1]$). Moreover, we assume that the emission of sidelobe can extend to the neighboring n ($n + m \leq M$) subband units, and maintain a power ratio of ζ ($\ll 1$) compared to the mainlobe.

The concerned 2-D coverage area of a typical Macrocell cite, with the reference MBS located at the origin, is a circular region $\mathcal{C} \in \mathbb{R}^2$ of radius R_c . The FBS intensity is defined as λ (FBSs per unit area). Therefore, each subband unit is

- mainlobe-interferenced by an average intensity of $\rho_m = \frac{m}{M}\lambda$ FBSs,
- and sidelobe-interferenced by an average intensity of $\rho_n = \frac{n}{M}\lambda$ FBSs.

Seen from the sidelobe leakage plot in Fig. 32, the three transmission schemes we choose in this chapter are typical in the sense that:

- **Scheme I:** is unable to achieve the 72.8 dB FCC OOB requirement, it introduces a substantial sidelobe interference of $n = 2$ (if 6 subcarriers are contained in each subband) and $\zeta = -12$ dB;

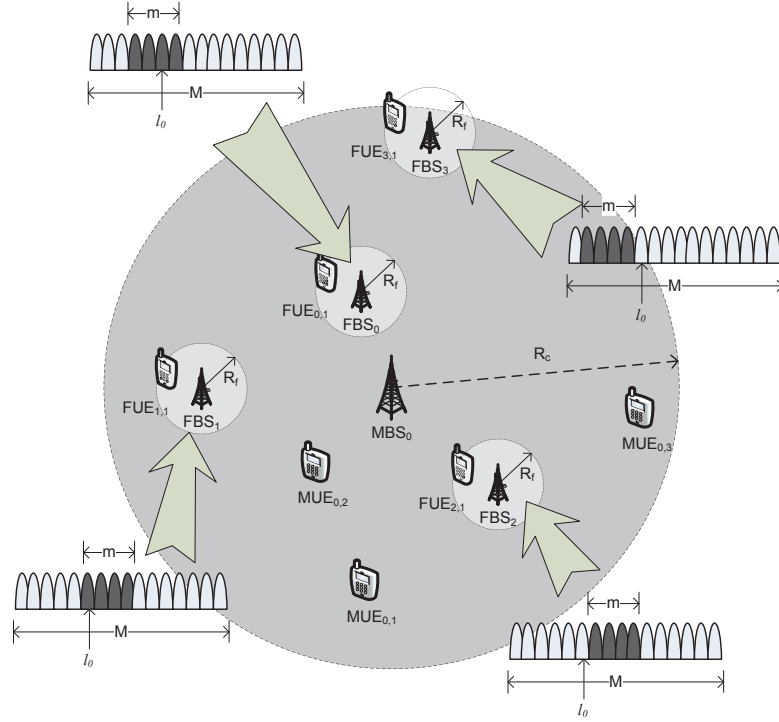


Figure 33: Topology of the System

- **Scheme II:** is almost able to achieve the 72.8 dB FCC OOB requirement, and each link has an efficiency loss of as high as 0.625 due to pooling;
- **Scheme III:** is able to achieve the 72.8 dB FCC OOB requirements, and its link transmission is of the most efficiency among the three schemes due to no cost for cyclic prefix (CP).

Therefore, by comparing Scheme I with Scheme II and III, we are able to interpret the FCC's decisions and clearly see what it can influence on the real system performances.

5.3.2 Interference Equivalents

If we consider one typical subband unit l_0 , the second-tier interference received on this subband unit, denoted as I_0 , is modeled as shot-noise interference in this chapter, which is contributed by a combination of mainlobe and sidelobe interference, i.e.

$$\begin{aligned}
 I_0^{(c)} &= \underbrace{\sum_{i \in \Omega_m} P_f \Psi_i K_f \|X_i\|^{-\alpha_f}}_{I_0^{(a)} \text{ mainlobe interference}} + \underbrace{\sum_{i \in \Omega_n} P_f \zeta \Psi_i K_f \|X_i\|^{-\alpha_f}}_{I_0^{(s)} \text{ sidelobe interference}} \\
 &\stackrel{(a)}{=} \sum_{i \in \Omega} P_f \Theta_i \Psi_i K_f \|X_i\|^{-\alpha_f},
 \end{aligned} \tag{5.1}$$

where superscripts (c), (a), and (s) denote the combined, mainlobe, and sidelobe interference, P_f is the FBS transmit power, Ψ_i is the i.i.d. random

channel fading gain, K_f is the penetration loss, and α_f is the path loss exponent. Ω_m and Ω_n are the set of FBS, represented by the *homogeneous poisson point processes* (PPP) with intensity of ρ_m and ρ_n , respectively. Step (a) follows from the fact that the superposition $\Omega = \Omega_m \cup \Omega_n$ is also a homogeneous PPP over \mathbb{R}^2 [43, Superposition Theorem], with intensity of $\rho = \rho_m + \rho_n = \frac{m+n}{M}\lambda$. Additional mask Θ_i is the manipulated random variable with distribution: $\Pr(\Theta_i = 1) = \eta$, $\Pr(\Theta_i = \zeta) = 1 - \eta$, with $\eta = \frac{\rho_m}{\rho_m + \rho_n} \in (0, 1]$. As we can see from Eq. (5.1), the sidelobe interference has brought two changes to the original shot-noise interferences:

1. increase the interferers' intensity by a factor of $\frac{m+n}{m}$
2. introduce an additional mark of Θ_i .

However, another interpretation of the superposition for the combined interference is that the Laplacian transform of the interference distribution can be written as:

$$\begin{cases} \mathcal{L}_{I_0^{(a)}}(\lambda, y) = \exp \left\{ -\pi \frac{m}{M} \lambda \mathbf{E}[\Psi_i^{\delta_f}] P_f^{\delta_f} y^{-\delta_f} \right\} \\ \mathcal{L}_{I_0^{(s)}}(\lambda, y) = \exp \left\{ -\pi \frac{n}{M} \lambda \zeta^{\delta_f} \mathbf{E}[\Psi_i^{\delta_f}] P_f^{\delta_f} y^{-\delta_f} \right\} \end{cases} \quad (5.2)$$

with $\delta_f = \frac{2}{\alpha_f}$. $I_0^{(a)}$, $I_0^{(s)}$ are independent, yielding to

$$\mathcal{L}_{I_0^{(c)}}(\lambda, y) = \mathcal{L}_{I_0^{(a)} + I_0^{(s)}}(\lambda, y) = \mathcal{L}_{I_0^{(a)}}(\lambda, y) \cdot \mathcal{L}_{I_0^{(s)}}(\lambda, y) \quad (5.3)$$

then,

$$\mathcal{L}_{I_0^{(c)}}(\lambda, y) = \exp \left\{ -\pi \left(\frac{m + n\zeta^{\delta_f}}{M} \right) \lambda \mathbf{E}[\Psi_i^{\delta_f}] P_f^{\delta_f} y^{-\delta_f} \right\} \quad (5.4)$$

Therefore, the original combined interference case is **equivalent** to a modified mainlobe-only homogeneous PPP $\Omega = \Omega_m \cup \Omega_n$ over \mathbb{R}^2 , with intensity:

$$\rho = \frac{m + \boxed{n\zeta^{\delta_f}}}{M} \lambda. \quad (5.5)$$

Is this perturbation trivial to system performance? We will look into the system performance metric of transmission capacity (TC) and area spectral efficiency (ASE) to answer this question.

5.3.3 Performance of Transmission Capacity

Theorem 5.1 *The loss of Transmission Capacity due to existence of OFDM sidelobe interference (σ_{TC}), is a function of parameters m , n , ζ , and δ_f , i.e.*

$$\sigma_{TC} = 1 - \frac{m}{m + n\zeta^{\delta_f}}$$

Proof For the reference victim link on subband l_0 (either first or second tier), denote by P_0 , Ψ_0 , and K_0 the transmit power, channel fading, and penetration loss, respectively. Let γ_0 be the Signal to Interference Ratio (SIR) seen by the reference receiver. The conditional c.d.f. of γ_0 in the combined interference case, if victim link transceivers are in X_0 distance away, is given by:

$$\begin{aligned} F_{\gamma_0|\Psi_0, X_0}(z) &= \Pr\left(\frac{P_0\Psi_0K_0X_0^{-\alpha}}{I_0^c} \leq z|\Psi_0, X_0\right) \\ &= 1 - F_{I_0^c}\left(\lambda_c, \frac{P_0\Psi_0K_0X_0^{-\alpha}}{z}\right) \end{aligned} \quad (5.6)$$

so the unconditioned distribution of γ_0 can be derived as:

$$F_{\gamma_0}(z) = 1 - \mathbf{E}_{\Psi_0, X_0}\left[F_{I_0^c}\left(\lambda_c, \frac{P_0\Psi_0K_0X_0^{-\alpha}}{z}\right)\right] \quad (5.7)$$

For a given SIR threshold Γ_{th} , the link outage probability ϵ is thus derived by:

$$\begin{aligned} \epsilon &= \Pr(\gamma_0 < \Gamma_{\text{th}}) = F_{\gamma_0}(\Gamma_{\text{th}}) \\ &= 1 - \mathbf{E}_{\Psi_0, X_0}\left[F_{I_0^c}\left(\lambda_c, \frac{P_0\Psi_0K_0X_0^{-\alpha}}{\Gamma_{\text{th}}}\right)\right] \\ &= H_c(\lambda_c) \end{aligned} \quad (5.8)$$

where we name $H_c(\cdot)$ as the *outage probability function* which is a monotonically-increasing injective function between combined interferer intensity λ_c and outage probability ϵ .

The transmission capacity TC in the combined interference case (denote as Λ_c) is defined as the maximal allowed Femtocell intensity, so that the **first-tier** outage probability ϵ^m is no greater than a given outage probability target ϵ_{max} , i.e.:

$$\Lambda_c = H_{c,m}^{-1}(\epsilon_{\text{max}}) \quad (5.9)$$

with $H_{c,m}(\cdot)$ as the first-tier version of $H_c(\cdot)$ (with P_0 , Ψ_0 , and K_0 being replaced by the macrocell transmit power P_m , fading gain Ψ_m , and penetration loss K_m) and $H_{c,m}^{-1}(\cdot)$ is the inverse function of $H_{c,m}(\cdot)$.

Therefore, the loss ratio of TC due to the introduction of sidelobe interference gives,

$$\sigma_{\text{TC}} = \frac{\Lambda_a - \Lambda_c}{\Lambda_a} = 1 - \frac{m}{m + n\zeta^{\delta_i}} \quad (5.10)$$

where Λ_a is the corresponding TC in mainlobe-only case. ■

Remark 5.1 Note that the parameters n and ζ are constant, depending only on which transmission scheme (Scheme I, II, III) to adopt. Hence the TC loss σ_{TC} :

1. monotonically decreases with the Femtocell subband allocation m ;

2. monotonically increases with the channel pathloss exponent α_f

Remark 5.2 Specifically, in the case that the channel fading Ψ_m and Ψ_i are all Rayleigh distributed, the TC considering sidelobe interference $\Lambda_c^{\text{Rayleigh}}$ can be given in closed form as:

$$\Lambda_c^{\text{Rayleigh}} = \frac{M}{m + n\zeta^{\delta_f}} \frac{-\ln(1 - \epsilon_{\max})}{\delta_f \Gamma(\delta_f) \Gamma(1 + \delta_f)} \left(\frac{K_m P_m}{K_f P_f \Gamma_{\text{th}}} \right)^{\delta_f} \left(\frac{R_f}{X_0} \right)^2 \quad (5.11)$$

5.3.4 Performance of Area Spectral Efficiency

We denote $D_0^{(2)}$ and $D_0^{(1)}$ as the average data rate on subband l_0 for Femtocell and Macrocell, respectively. We further assume that both link SIRs are in a low or mid region ($> \Gamma_{\text{th}}$), so that for each transmission scheme, the link spectral efficiency can be approximated by a linear function $G(\gamma_0)$ in (bps/Hz), i.e.

$$G(\gamma_0) \approx \begin{cases} 0, & \gamma_0 < \Gamma_{\text{th}} \\ g\gamma_0, & \gamma_0 \geq \Gamma_{\text{th}} \end{cases} \quad (5.12)$$

If both the first and second tiers are adopting channel-blind Round Robin scheduling and all the allocated subbands are fully utilized, then the long term ASE for the first-tier and second-tier in region \mathcal{C} , denoted as $T^{(1)}$ and $T^{(2)}$, respectively, is given by:

$$\begin{aligned} T^{(1)} &= \frac{\sum_i \bar{D}_i^{(1)}}{|\mathcal{C}|} \approx \frac{MD_0^{(1)}}{|\mathcal{C}|} \\ T^{(2)} &= \frac{\lambda |\mathcal{C}| \sum_i \bar{D}_i^{(2)}}{|\mathcal{C}|} \approx \lambda m D_0^{(2)} \end{aligned} \quad (5.13)$$

where $D_i^{(1)}$ / $D_i^{(2)}$ are the average 1st/2nd-tier data rate on l_i .

5.3.4.1 First Tier ASE

In the domain of λ , we have

$$\begin{aligned} T^{(1)} &= \frac{M}{|\mathcal{C}|} \mathbf{E}[G(\gamma_0^{(1)}) | \gamma_0^{(1)} \geq \Gamma_{\text{th}}] \Pr(\gamma_0^{(1)} \geq \Gamma_{\text{th}}) \\ &\approx \frac{M}{|\mathcal{C}|} g \mathbf{E}[\gamma_0^{(1)}] (1 - P(\gamma_0^{(1)} < \Gamma_{\text{th}})) \\ &= \frac{M}{|\mathcal{C}|} g \left[1 - H_{c,m} \left(\frac{M}{m + n\zeta^{\delta_f}} \lambda \right) \right] \int z dF_{\gamma_0^{(1)}}(z) \end{aligned} \quad (5.14)$$

since the both multiplying components of $1 - H_{c,m}(\cdot)$ and $\int z dF_{\gamma_0^{(1)}}(z)$ are monotonically decreasing with λ , thereby,

$$\frac{\partial T^{(1)}}{\partial \lambda} < 0, \quad (5.15)$$

meaning that the first-tier ASE decreases with the increase of Femto users or the Femto subband access rate.

In most of the system designs, as the primary user of the spectrum, the Macrocells occupy higher priority to the Femto ones. We hence define the system constant parameter q , so that

$$\frac{T^{(1)}\big|_{\lambda=0} - T^{(1)}}{T^{(1)}\big|_{\lambda=0}} \leq q, \quad (5.16)$$

meaning that the Macrocell is only willing to sacrifice at most q of its ASE to accommodate the presence of Femtocells in its vicinity. Assume $q = 20\%$, we see from simulation results in Fig. 35 that, for the case of FBC intensity of 1000, in LA Rayleigh+Lognormal fading channel condition (see Section IV for the simulation setups), the subband access rate can be no more than $\frac{1}{M}$. For HA Rayleigh+Lognormal fading channel, the maximal allowed subband access rate is $\frac{3}{M}$. Therefore, when the Femto intensity is high, the system has to decrease the Femto subband access rate to a very low level to prevent a huge loss in the first-tier performance. However, due to the fact that resources are slotted, such adjustment can also lead to a remarkable performance loss.

5.3.4.2 Second Tier ASE

Theorem 5.2 *The loss of 2nd-tier Area Spectral Efficiency due to existence of OFDM sidelobe interference ($\sigma_{ASE}^{(2)}$), is approximately a function of parameters m , n , ζ , and δ_f , i.e.*

$$\sigma_{ASE}^{(2)} \approx 1 - \left(\frac{m}{m + n\zeta^{\delta_f}} \right)^{\delta_f}$$

Proof

To simplify the analysis, we assume that Femtocells are densely deployed and make an approximation to Eq. (5.7) for the combined interference case. The approximation is according to the analysis in [69, Appendix], where $F_{\gamma_0}(z)$ is asymptotically upper bound by

$$\begin{aligned} F_{\gamma_0}(z) &\leq 1 - \exp\{-\lambda \hat{d} \mathbf{E}[\Psi_i^{\delta_f}] \mathbf{E}[\Psi_0^{-\delta_f}] \mathbf{E}[X_0^{\delta_f \alpha_m}] z^{\delta_f}\} \\ &= 1 - \exp\{-\lambda d z^{\delta_f}\} \\ \hat{d} &= \pi P_f^{\delta_f} P_0^{-\delta_f} \\ d &= \hat{d} \mathbf{E}[\Psi_i^{\delta_f}] \mathbf{E}[\Psi_0^{-\delta_f}] \mathbf{E}[X_0^{\delta_f \alpha_m}]. \end{aligned} \quad (5.17)$$

The average data rate for Femtocell $D_0^{(2)}$ in the combined interference case can be derived by:

$$\begin{aligned} D_0^{(2)} &\approx g \left[1 - H_{c,f} \left(\frac{M}{m + n\zeta^{\delta_f}} \lambda \right) \right] \int_{\Gamma_{th}}^{\infty} z dF_{\gamma_0^f}(z) \\ &= g \cdot \exp(-\lambda d \Gamma_{th}^{\delta_f}) (\lambda)^{-\delta_f} J \end{aligned} \quad (5.18)$$

and,

$$J = d^{-\delta_f} \Gamma\left(1 + \frac{1}{\delta_f}, \lambda d \Gamma_{\text{th}}^{\delta_f}\right) \quad (5.19)$$

where $\Gamma(a, \cdot)$ is the upper incomplete gamma function.

Therefore, the second-tier ASE considering sidelobe interference can be written as:

$$T^{(2)} = \lambda J M g(\lambda)^{-\delta_f} \exp(-\lambda d \Gamma_{\text{th}}^{\delta_f}) \quad (5.20)$$

The loss by sidelobe interference $\sigma_{\text{ASE}}^{(2)}$ can thus be interpreted as:

$$\begin{aligned} \sigma_{\text{ASE}}^{(2)} &= \frac{T^{(2)} \Big|_{n=0} - T^{(2)}}{T^{(2)} \Big|_{n=0}} \\ &\approx 1 - \left(\frac{m + n \zeta^{\delta_f}}{m} \right)^{\delta_f} \end{aligned} \quad (5.21)$$

■

Remark 5.3 Specifically in the case when Ψ_0 and Ψ_i are Rayleigh, d in Eq. (20) is given by:

$$d^{\text{Rayleigh}} = \pi \Gamma(1 + \delta_f) \Gamma(\delta_f) \quad (5.22)$$

Therefore, the second tier ASE in Rayleigh channel fading case is:

$$T_{\text{Rayleigh}}^{(2)} = \lambda J M g \lambda^{-\delta_f} \exp(-\lambda d^{\text{Rayleigh}} \Gamma_{\text{th}}^{\delta_f}) \quad (5.23)$$

Corollary 5.1 (Optimal Femto Density) Given a fixed spectrum access rate of $\frac{m}{M}$, the optimal Femto intensity λ that maximizes the 2-tier ASE is:

$$\frac{\partial T^{(2)}}{\partial \lambda} = \frac{\partial J m g(\lambda)^{1-\delta_f} \exp(-\lambda d \Gamma_{\text{th}}^{\delta_f})}{\partial \lambda} = 0 \quad (5.24)$$

approximately, we get

$$\begin{aligned} \lambda^{(a)*} &= \frac{M}{m} (1 - \delta_f) d^{-1} \Gamma_{\text{th}}^{-\delta_f} \\ \lambda^{(c)*} &= \frac{M}{m + n \zeta^{\delta_f}} (1 - \delta_f) d^{-1} \Gamma_{\text{th}}^{-\delta_f} \end{aligned} \quad (5.25)$$

Conclusively, optimal density reduced by $\frac{m}{m+n\zeta^{\delta_f}}$, i.e. σ_{TC}

Corollary 5.2 (Optimal Access Rate) Given a fixed Femto deployment intensity of λ_c , the optimal spectrum access rate of $\frac{m}{M}$ is given by:

$$\frac{\partial T^{(2)}}{\partial m} = 0$$

i.e.

$$\frac{(1 - \delta_f) m + n \zeta^{\delta_f}}{m + n \zeta^{\delta_f}} = \frac{m}{M} \lambda d \Gamma_{\text{th}}^{\delta_f} \quad (5.26)$$

Specifically, in the mainlobe-only case, we have the optimal spectrum access rate as

$$m^{(a)} = \min \left(\lfloor (1 - \delta_f) \lambda^{-1} d^{-1} \Gamma_{\text{th}}^{-\delta_f} M \rfloor, M \right) \quad (5.27)$$

and in the combined interference case

$$m^{(c)} = \min \left(\lfloor (1 - \delta_f) \lambda^{-1} d^{-1} \Gamma_{\text{th}}^{-\delta_f} M - n \zeta^{\delta_f} \rfloor, M \right) \quad (5.28)$$

In a general case, assume that sidelobe interference is small, we have

$$m^{(a)} - m^{(c)} \approx -n \zeta^{\delta_f} \quad (5.29)$$

meaning that the sidelobe interference decreases the optimal subband access rate by $n \zeta^{\delta_f}$.

5.3.5 Short Summary

In summary, by the above analysis, we prove that due to the OFDM sidelobe leakage,

1. the loss of sidelobe on TC is σ_{TC} , which is non-negligible when m is small
2. the loss of sidelobe of ASE is σ_{ASE} ,
 - a) which is generally minor, but can cause
 - b) Access Rate Jump due to the 1st-tier constraint q
3. on the 2nd-tier ASE only
 - a) reduce the Optimal Femto Density, same as σ_{TC}
 - b) may cause reduction of optimal Access Rate, but not always

5.4 NUMERICAL RESULTS

In the simulation, we assume a whole spectrum band of 180 subcarriers. Each subband unit is comprised of 6 consecutive subcarriers (so $M = 30$). We define a channel condition of High Attenuation (HA) as $\alpha_f = 4$ and Low Attenuation (LA) as $\alpha_f = 3$. We generate a number of 3×10^4 Monte-Carlo realizations for each test and the default values of main simulation parameters are listed in Table 6, unless explicitly specified otherwise.

- From all the simulation results in Fig. 5.3-6, we find out that the both performance metrics of TC and ASE are very sensitive to the channel condition. More channel fading randomness (Rayleigh+ Log-normal, composite fading of both distributions) and low attenuation can greatly deteriorate the performance. The reason is that, channel randomness is harmful to low-outage system criteria (as also discussed in Subsection 3.6.2) and low attenuation means a better propagation of interference. Therefore, we name the channel conditions of Rayleigh+ Lognormal and Low Attenuation as the *worstcase*.

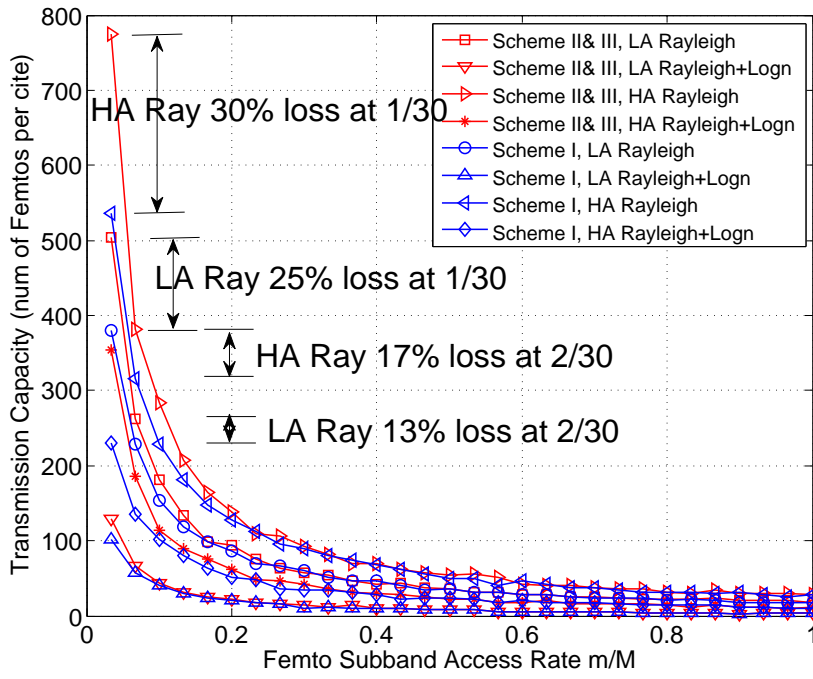


Figure 34: System TC for Accommodating Femtos

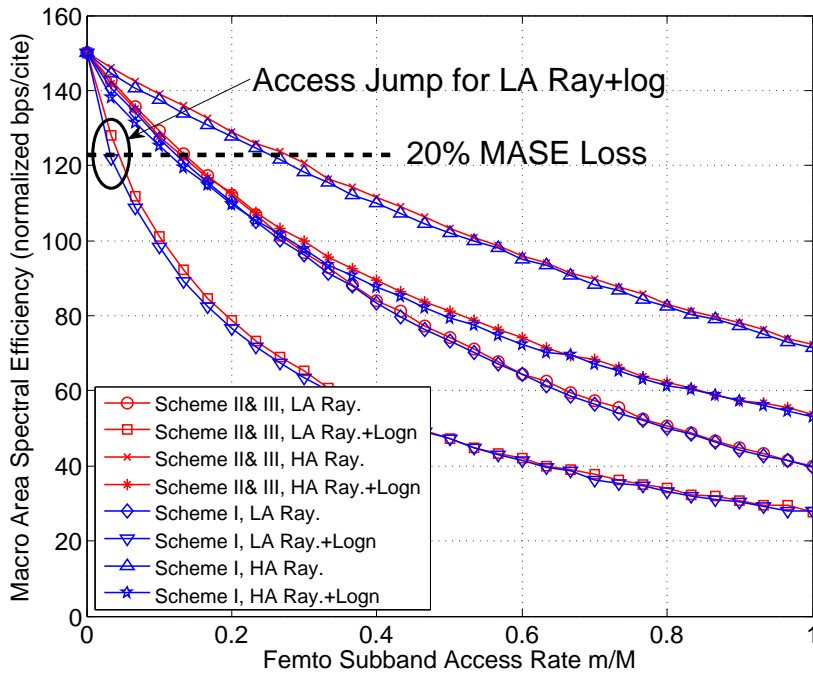


Figure 35: Macrocell ASE vs. Subband Access

Table 6: Default Simulation Parameters for 5.4

Parameter	Description	Value
R_c	Map Size	1000m
P_f	Transmit Power for FBS	15dBm
P_m	Transmit Power for MBS	35dBm
K_0	Victim Link Penetration Loss	-35dB
K_f	Interfering Link Penetration Loss	-55dB
Γ_{th}	Link SIR Target	10 dB
Γ_{max}	Link SIR Cap	20 dB
ϵ_{max}	Outage Probability Target	1%
σ_{LN}	Log-normal Fading Deviation	8 dB
g	Normalized Trans. Efficiency	0.3

- Additionally, in Fig. 34, the presence of sidelobe interference mainly decreases the system transmission capacity in low subband access region. Observe that in HA Rayleigh condition, the loss in capacity can be as high as 40% at $m = 1$, and in LA Rayleigh condition, the loss in capacity is around 24% at $m = 1$.
- Fig. 35 shows that the deployment of either transmission scheme in Femtocell can only slightly affect the Macrocell ASE. However, in some channel conditions such as LA Rayleigh +Lognormal, we notice a very sharp decline of ASE in the low subband access region, meaning that if the system can only accept 20% decline of Macrocell ASE to serve the Femtocell, which is from 150 bps/cite to 120 bps/cite in the Figure, the Femtocells can only take a subband access rate lower than 10%, which turns out to be a very large loss of capacity (shown in Fig. 34), and very large loss of second-tier ASE as well (shown in Fig. 36 and 37).
- In Fig. 36, we observe the optimal Femto spectrum access rate for LA Rayleigh at the region around $[0.8, 0.9]$, but ASE does not decline evidently after the peak value. For other cases in Fig. 36 and 37, the optimal access rate is not present probably because it is not within $[0, 1]$. In addition, we see that Scheme III performs always best in all the channel conditions. Surprisingly, scheme II performs even worse than Scheme I due to its substantial loss in the link spectral efficiency because of the windowing.

If we take the UHF TV band (510-700 MHz) for example, the pathloss exponent in this frequency range is ≈ 3.47 according to the HATA's model in [27].

- In such a case, the FCC's rule on OOB can be translated as $\approx 20 - 25\%$ of more TC at 200 KHz bandwidth than un-regulated system, namely

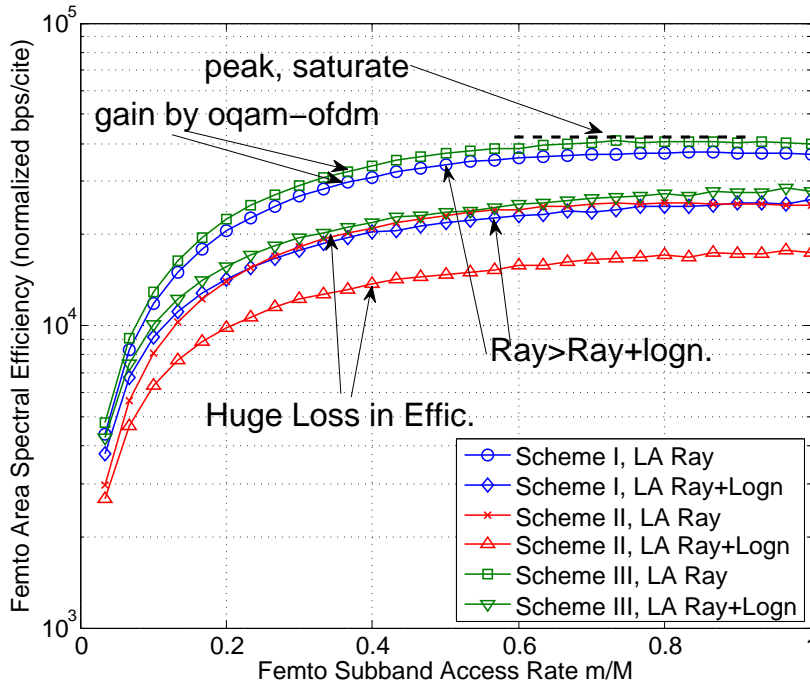


Figure 36: Femto ASE in LA channel vs. Subband Access

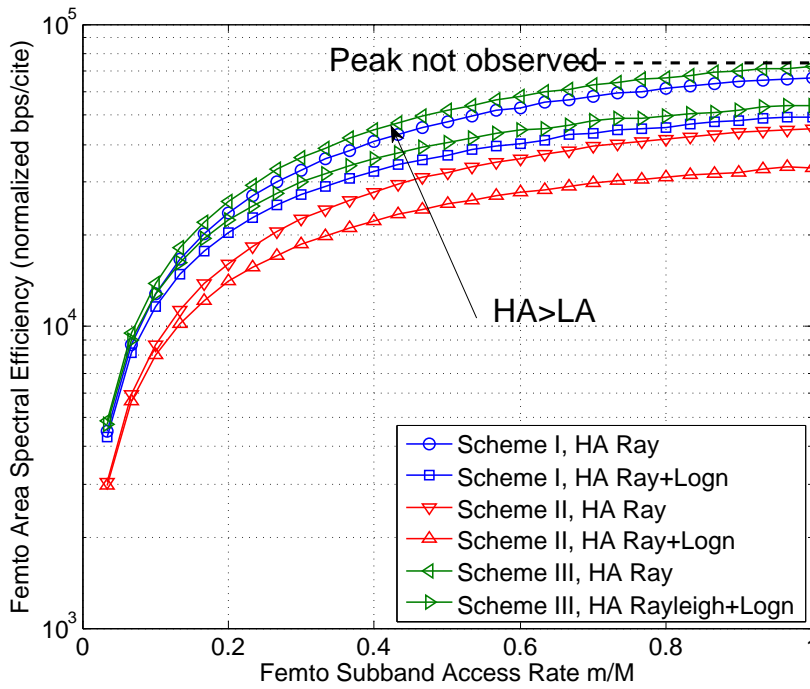


Figure 37: Femto ASE in HA channel vs. Subband Access

it can accommodate around 300 TVWS devices in an area of km^2 . However, this gain diminishes rapidly as the bandwidth increases.

Through all the simulation results, we finally can summarize the comparisons of the three concerned PHY interfaces in Tab. 7. We see a clear trade-off

Table 7: Comparison of the three Schemes

	Loss of TC		Loss of ASE			Complexity
	worstcase	other cases	1st-tier	2nd-tier worstcase	2nd-tier other cases	
Scheme I	high	medium	low	medium	low	$\times 1$
Scheme II	low	low	low	high	high	$\approx \times 1$
Scheme III	low	low	low	low	low	$\approx \times 8$

between complexity and performance. Although Scheme III OQAM-OFDM performs best in many of the cases, it also requires a much higher implementation cost in terms of a fold of 8 for the modulation and demodulation process, according to the results in paper [31].

5.5 CHAPTER SUMMARY

In this chapter, by proper modeling, we successfully abstract the OFDM sidelobe leakage in F-ALOHA Femtocell to an equivalent problem of modified interference intensity in PPP distributed aggressors. From the above theoretic analysis and supporting numerical results, we see that the modified intensity in many cases only leads to minor system performance loss but, in some rare cases, does indeed cause a significant loss, especially when the number of Femtos is high and channel condition is poor.

In such cases, Scheme II is only an intermediate solution because it sacrifices too much in link spectral efficiency. In the mean time, OQAM-OFDM can not only mitigate the adverse sidelobe effect but also maintain a very high system efficiency. Although OQAM-OFDM by state of art is not widely adopted, it is reasonable to consider it as a promising candidate for the future Femtocell application.

FEMTO DEPLOYMENT ISSUE II: ANTENNA SWITCHING

It is a conventional concept that cellular outdoor channel possesses good property in directionality, meaning that directional antenna pattern is effective in improving coverage and providing better QoS to cell edge users. See sector and beam-forming efforts in LTE[1].

However, the two-tier cellular network changes the *design paradigm* of Femtocell. Despite of its own coverage issue, it is also critical for the Femtos to consider the co-existence with the local outdoor Macrocells. As mentioned in Chapter 1, the design goal of Femto is that, it is strictly inferior to the Macro users in the context of causing interference and resource sharing. Therefore, in this chapter, we try to utilize the antenna directionality in Femtocell deployment and investigate those antenna-switching and beam-forming schemes in terms of the co-existence performances with local primary users.

6.1 MOTIVATIONS AND RELATED WORKS

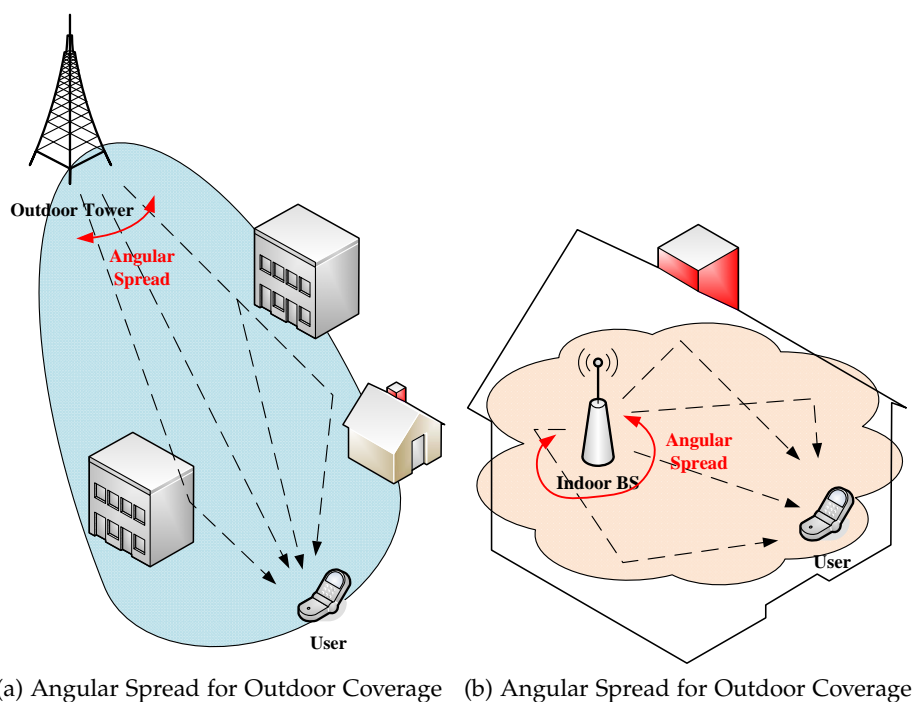


Figure 38: An Example of Outdoor and Indoor Directional Antenna

6.1.1 *Directional Antenna for Indoor Coverage*

Directional antenna is a topic of long history, beginning ever since the era of radio transmission. It is well understood that if the electro-magnetic wave emitted from the transmitting antenna has a strong gain in certain direction, the receiver along this direction will achieve an improved signal strength compared to the isotropic case. It is thus a common technique for the outdoor Macrocell (see in Subfig. 38a) to improve the coverage and cell-edge performance exploiting the antenna directionality, such as cell sectorizing, antenna array, antenna tiltness, and also the recently adaptive beam-forming techniques [57] [56].

On the other hand, directional antenna is generally not a good option for indoor wireless channel because of the following three reasons:

- firstly, indoor wireless channel is usually rich-scattering that channel angular spread (in departure) is relative flat compared to outdoor cases;
- secondly, indoor scenario is rich in coverage deadzones due to the complexity in structure, thick-concrete, furnitures, and obstacles, thereby, directional antenna is doing no better in improving the indoor coverage compared to other antenna techniques like DAS;
- thirdly, for the case that spectrum usage are Equivalent Isotropically Radiated Power (EIRP) regulated instead of transmitting power limited, the directional antenna can have further loss in coverage because of the relatively lower emission power [45].

The indoor wireless channel is relatively flat in angular spread [59] so that directional gain is rather marginal (see in Subfig. 38b). Although adaptive weight-based indoor beam-forming can still perform well because the successful exploit of spatial diversity at transmitter, it has difficulty in implementation in terms of dynamic channel fluctuation and oscillator drift between transceiver pairs, until recently achievement such as [46] but however, the gain presented is achieved when transmitter is equipped with eight antenna elements, which is rather difficult for our FBS to implement for the stakes of size and cost limit.

Additionally, as aforementioned in previous chapter, Femtocell is also one of the promising technologies to dynamically access the spectrum in the future, such as TVWS. These devices are more likely regulated by limiting the EIRP instead of the transmitting power, see FCC's ruling decision on TVWS and ISM [25]. It is obvious that the EIRP cap is a more stringent rule and not beneficial to the directional antenna. [45] gives a detail investigation and proposes a compensation method for the loss of coverage.

6.1.2 *Femto Out-of-Building Emission Leakage*

For the case of Femtocell, the design criteria is not only about the quality of its own transmission link but how to avoid causing huge interference

to the local primary users as well. As some pioneering works like [20][41] revealed, adopting a simple antenna switching scheme can effectively shrink the coverage of Femto pilot signal inside the building, minimize the leakage to the outside of building so that decreasing the number of un-necessary hand-overs and avoid strong Femto-Macro interference case.

Similar to this idea but referring to the outdoor leakage power profile as our main performance criteria, we investigate the possible deployment of two basic smart antenna techniques, namely antenna adaptive pattern-switching and eigen-based beam-forming (or beam-steering) in this chapter.

For these two techniques, we consider a rather more practical configuration at FBS transmitter in DL, i.e. four antenna elements at the transmitter. We argue that for the Femto application, the performance is rather scenario dependent. To overcome this challenge, we use an innovative evaluation method, that using Ray-tracing software to capture the channel propagation and impulse response in time and spatial domain. Then we determine the indoor coverage of certain data rate criteria by means of Effective Exponential SINR Mapping (EESM), which is acknowledged as a precise link-to-system mapping methodology for OFDM systems such as LTE, WIFI, and WIMAX. As for the same level of coverage, we make fair comparisons between conventional omni-directional antenna, antenna switching, and antenna beam-steering.

6.2 CONTRIBUTIONS

The contributions ¹ of this chapter's work can be summarized as follows:

1. we devise an innovative evaluation methodology that can apply various PHY algorithm to predict the Femto-Macro coexisting **system performance**, see also Chapter 7;
2. we investigate the different practical antenna schemes for FBS and find out that they are extremely efficient in decreasing the Femto-to-Macro interference;
3. we find out the best effort performance of antenna switching is very close to beam-steering and totally implementable with no extra modifications on the current LTE standards.

6.3 OUTDOOR LEAKAGE AND ANTENNA SWITCHING

6.3.1 Frequency Selection and TVWS Femto

As the leakage performance is highly dependent on the frequency of the system. We define the following reference frequencies for investigation in this chapter:

- **Freq A:** 580MHz,

¹ A part of this chapter's work is published in [78] and some are included in industrial reports of [67]

- **Freq B:** 760MHz, and
- **Freq C:** 2100MHz,

where Freq A and B are within the TV bands possible for cognitive access in Europe, approximately in the range of 550MHz-780MHz [22], Freq C is the one of the major European LTE bands that we define for the benchmark purposes.

We take the above TVWS Femtos into consideration because it is currently also under considerations by the EU regulators to allow cognitive TVWS devices. Due to the digital switch-over, many reports have revealed that TVWSs are pervasively existent across America and Europe, especially in the rural areas [22]. In the US, the regulation body FCC has given the permissions to the TVWS devices for accessing the UHF TV channels 21-36 (512-680 MHz) and channels 38-51 (614-698 MHz) in year 2008[24] and amended upon the rules in year 2010 [25]. In UK, similar rules were made in year 2009 by the regulation body Ofcom [53].

However, the final decisions in Europe have not been made and we can only assume that some low power short range systems, such as WiFi, Femtocell, Wimax, might possibly be allowed to opportunistically utilize the spectral holes with the sharing modes of "private commons" or "light licensing" in Europe in the future [22].

For this reason, we borrow the US final decisions for reference [25]. In short, the cognitive LTE-Femto concerned in this chapter can be categorized as "Mode II personal/portable devices" by FCC's definition, whose main technical requirements are summarized as the following:

1. *protected contour is 41 dBu with 6.0 km additional separation²;*
2. *power spectral density lower than -1.8 dBm in any 100 KHz band;*
3. *maximal EIRP of 16 dBm per 6 MHz band³;*
4. *maximal -72.8 dB adjacent band emission leakage⁴.*

See Fig.39 as an example, a certain number of cognitive LTE-Femtos that are at a distance of more than 46 km (kilometer) away from the primary DVB-T towers are granted access to the same TV channel. Here we denote FBS as the femto base stations and FUE as the femto user equipments.

6.3.2 Typical Scenarios

Considering the performance of Femtocell is highly relevant to its residential and SOHO applications, we select the two following typical buildings, as:

- **Building A:** a rectangular complex building of size 20m×17m, jointly work from [15]. Its structure is rather irregular and contains three

² can be interpreted as 40 km contour if DVB-T tower is 100m high (HAAT)

³ for those cannot meet adjacent channel separation

⁴ see detail definition in [25]

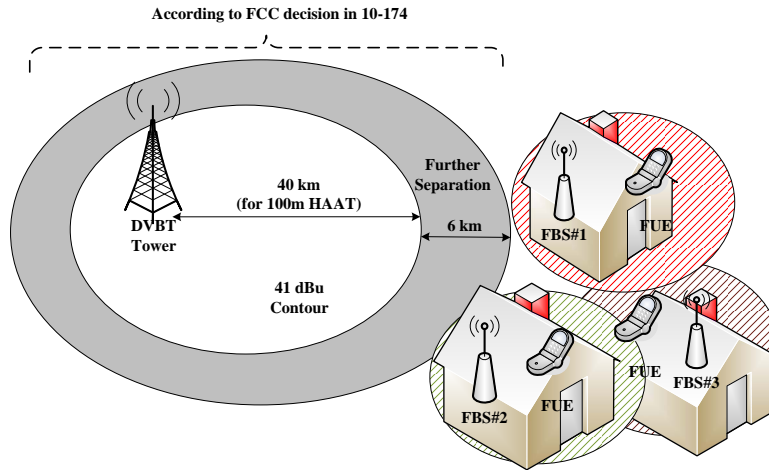


Figure 39: Primary DVB-T and cognitive LTE-Femtos

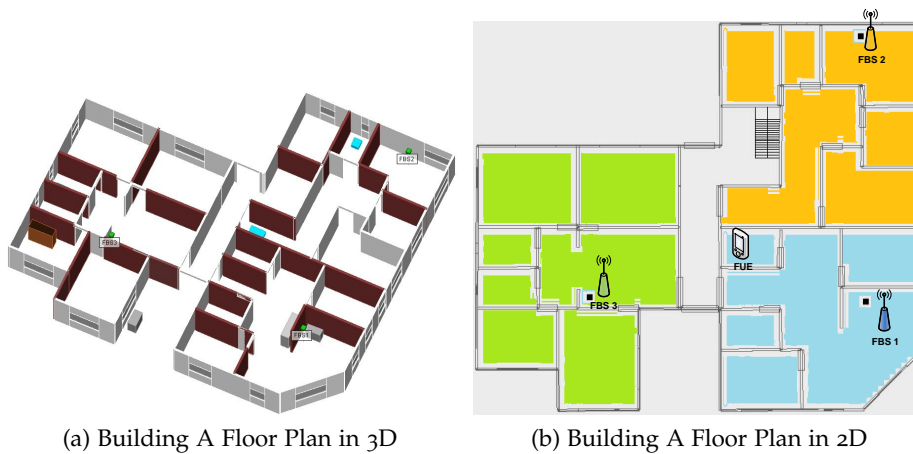


Figure 40: Model of Building A

apartments per floor and equipped with stairs, ceilings, and many furniture setups.

- **Building B:** a quasi-square brick building of size $21\text{m} \times 21\text{m}$, as part of the joint work from [67]. Its structure is rather symmetric and contains four identical apartments per floor and equipped with many brick small compartments and the materials are close to European standards (see Fig. 41a).

We assume that the FBS is randomly located at some specific positions of the both buildings. In Building A, the FBS has three typical positions, i.e. in bedroom, living-room, and corridor of the three apartment (the green, blue, and orange FBSs in Fig.40b). In Building B, the FBS can be positioned either close to window or deep in the building in one of the four apartments, respectively, see in Fig.41b.

It is well known that due to the rich scattering of radio propagation, the wireless channel between any transmitter-receiver pairs inside this building model is corrupted with multi-path fading effect [40]. We thus calculate and

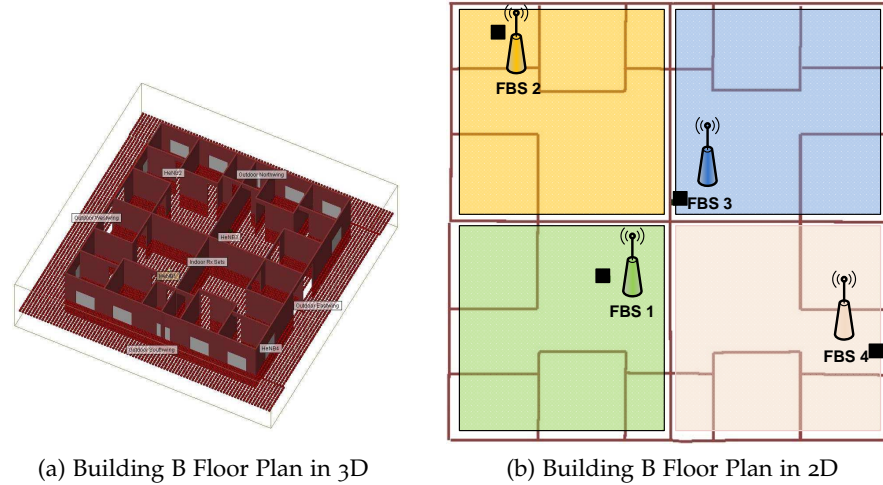


Figure 41: Model of Building B

obtain the channel impulse responses (CIR) by the method of Ray Tracing computer simulation.

The accuracy of Ray Tracing method is proved by [32], where the channel angular property captured by Ray-tracer is well agreed with the real measurement, thereby confirm the validity of the later study which is highly dependent on the computed channel.

6.3.3 Performance Evaluation

The detail simulation methodology will be introduced in Chapter 7. We assume that a referred LTE-Femto system with 5 MHz (FFT size 512) bandwidth (see spec. [2] for detail) is inserted into one frequency hole of the TV channel (6 MHz) and fulfill the FCC requirement which we listed in subsection II-A. We are able to evaluate the coverage performances of such system under different FBS configurations and frequency assumptions. The evaluation method used in this chapter can be described as follows.

- Firstly, the multi-path channel is obtained from Ray-tracer so that we can derive the Signal to Interference and Noise Ratio (SINR) on each of the OFDM subcarrier k , denoted as γ_k .
- Secondly, by using the Effective Exponential SIR Metric (EESM) method [55], the effective SINR for each resource block (RB) γ_{ef} is calculated by

$$\gamma_{ef} = -\beta \ln \left(\frac{1}{N} \sum_k e^{-\frac{\gamma_k}{\beta}} \right) \quad (6.1)$$

where β is a parameter dependent on different modulation and coding schemes (MCS) and N is the number of OFDM subcarriers for one resource block. The detail methodology of this step is given in Chapter 7.

- Afterwards, we map the maximal supportable MCS on each resource block to derive the long term data rate (i.e. throughput) for the reference LTE downlink with adaptive modulation and coding (AMC) transmission schemes. In the next step, we consider the leakage power from the typical Femto-equipped building, denote as P_{leak} . By conducting the computer simulation described above, we are able to obtain the statistics of such leakage power.
- We further assume that this leakage is the major source of co-channel interference that limits the capacity of all the TVWS devices in the area sharing the same white-space channel. We are keen to learn that how many LTE-Femtos this area can accommodate with a pre-defined outage criteria, e.g. Interference over Thermal (IOT) less than 20 dB in the simulation.

To capture the *ad-hoc* nature [69] of user-deployed Femtocell application [17], we assume that the buildings installed with the cognitive LTE-Femtos are obeying the Point Poisson Process (PPP) distributed across the whole reference area [34], which is the Femto model we use throughout the thesis.

- In the next step, we assemble all the interference emitted from the Femto-equipped buildings as the *shot-noise process*. The strength of received interference on reference map point 0, denoted as I_0 , is given by

$$I_0 = \sum_{i \in \Omega} P_{\text{leak}} \Psi_i K \|X_i\|^{-\alpha} \quad (6.2)$$

where Ω is the random set of the Femto equipped buildings, X_i is one of the random locations in the map for each Ω realization, $\|\cdot\|$ denotes the Euclidean distance, K is the constant radio propagation loss, α is the empirical pathloss exponent which is dependent on which frequency band A, B, or C to select, and Ψ_i is the channel fading.

- As the detail methodology is given in Chapter 7, the system statistics of IOT can be derived for different deployment densities of Femtos, allowing for the determination of the maximal Femto density meeting specified IOT criteria and the corresponding system performances such as throughput and ASE are due.

6.3.4 Proposed Antenna Schemes

After setting up the system model and introducing the methodology, we investigate three different antenna schemes that the cognitive LTE-Femtos are possibly deployed with, i.e.

- **Omni-antenna:** baseline for comparison,
- **Scheme I:** Adaptive Pattern Switching,

- **Scheme II: Adaptive Beamforming.**

The latter two directional antenna schemes are conventionally not well recognized for indoor short-range applications due to the fact that indoor wireless channel is of rich-scattering that the angular spread is relatively wide. Thus the antenna gain is restricted by *gain reduction factor* [52] and the improvement of coverage brought by antenna directivity can be rather diminishing.

However, the above discussion only holds for the link improvement of a single Femto case, in the context of its coverage (or throughput). Some recent literatures such as [20] has shown that indoor directional antenna can substantially refrain the FBS from causing harmful interference out of the building.

6.3.4.1 Scheme I: Adaptive Pattern Switching

Similar to what is proposed in [20], in this paper we design a patch antenna for LTE-Femto transmitter with an approximate beamwidth of 80° and 6 dBi gain, see the middle figure in Fig.42 for the azimuth pattern of the designed patch antenna.

We further assume that there are four such patch antenna elements equipped at the FBS, with each element is facing to the direction of $\theta = 0^\circ, 90^\circ, 180^\circ,$ and $270^\circ,$ respectively. By switching only one of these four elements on, the antenna pattern can be facing one of the four θ angles. In addition, by switching two neighboring elements on simultaneously, the synthesized antenna pattern can be also approximately facing the direction of $\theta' = 45^\circ, 135^\circ, 225^\circ,$ and $315^\circ,$ see Fig.43

It is noted that the training process to adapt to the best pattern is enabled by the existing LTE standards. According to Fig. 44, the LTE systems need only a request of regular uplink sounding reference signal (SRS [2]) and measured the corresponding uplink RSSI at the FBS side. The FBS can thus learn which pattern is of maximal gain and switch to the designated pattern. The whole training process only takes one LTE radio frame (20 ms) to complete, which is basically fast enough to capture the indoor user mobility and channel fluctuation.

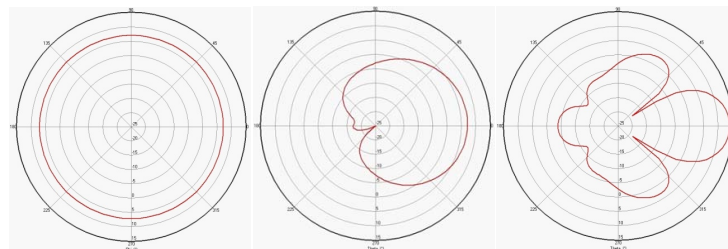


Figure 42: Azimuth Pattern of Designed Antenna, Omni(left), Patch(mid), and Array(right)

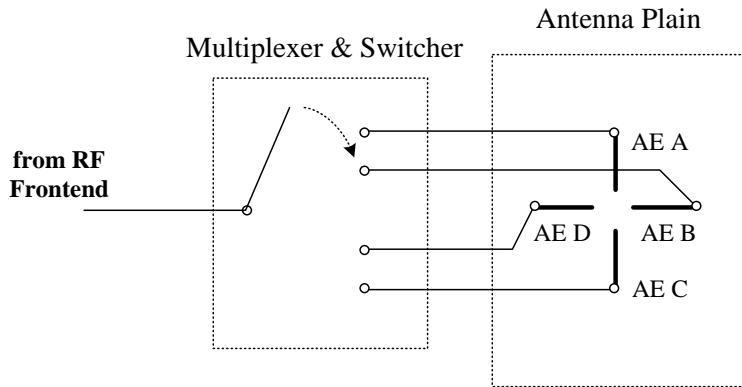


Figure 43: Adaptive switching of 1 or 2 patch antenna elements

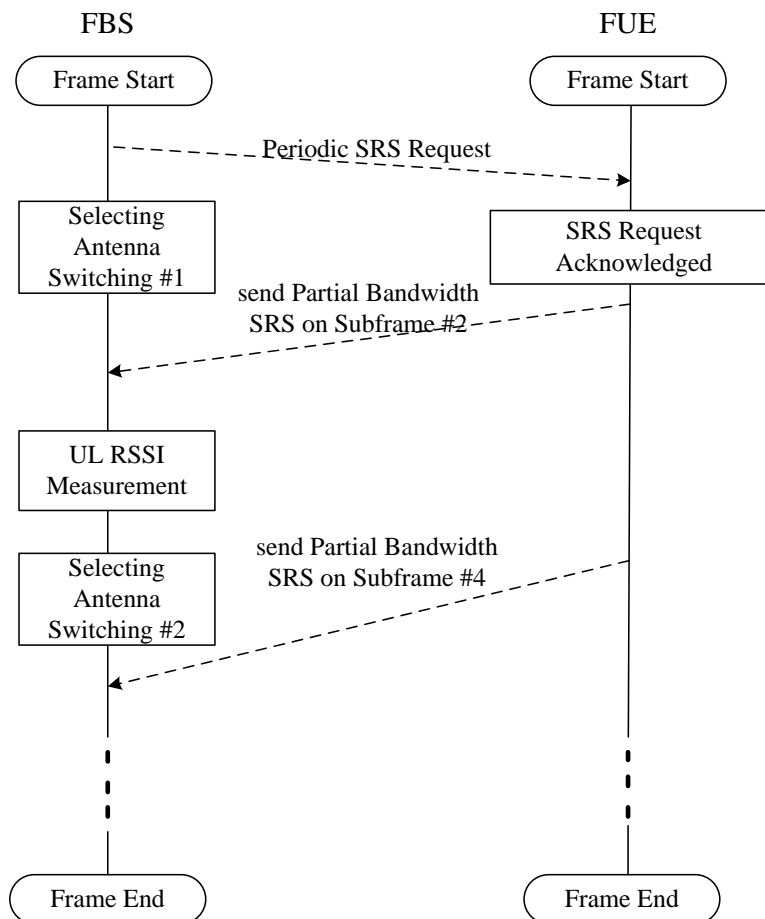


Figure 44: The Training Process of Antenna Switching

6.3.4.2 Scheme II: Adaptive Beamforming

In the second scheme, we assume that the FBS is equipped with a four-element linear uniform antenna array and is capable of performing eigen-based beamforming [4]. We admit that this assumption may be of implementation problems for the TV bands due to the fact that Freq A and B has a rather long wavelength $\approx 50\text{cm}$, so that the aperture of array will be too big for practical indoor applications. Henceforth, it is noted that the beamforming performance here is only for reference purposes.

As seen from the right pattern in Fig. 42, the synthesized array beam pattern is much narrower ($\approx 35^\circ$) compared to the pattern switching case and the gain can be as high as 11 dBi. By a training process similar to that introduced for Scheme I, upon the different user position, the FBS is able to steer its beam to the direction which leads into the maximal antenna gain.

6.4 NUMERICAL RESULTS

The methodology of deriving the simulation performance will be explained in Chapter 8 for detail. Due to a large amount of simulations we have done, here we only present some selected pictures and the numerical results.

In the simulation, we assume that the EIRP for each FBS with all the antenna schemes in Freq A and B is fixed at 16 dBm and the EIRP for Freq C is 23 dBm(20 mW) ⁵. We further assume that the LTE system is FDD (Frame-type I) and we only concern on the downlink performances.

We assume that the training process of adaptive antenna schemes I and II are perfect, i.e. the FBS transmitter can always switch or steer to the best directional pattern. It is noted that this is rather an ideal assumptions and only predict the most optimistic performance. In practice, due to the imperfectness of antenna training, the performance of Scheme I and II have be substantially poorer.

We first conduct the comparisons of the indoor coverage for these FBSs when they are accessing the different frequency channels while adopting different types of antenna schemes. We then obtain the resulting outdoor leakage for these different settings and illustrate their ability to co-exist with many other similar buildings in the area.

6.4.1 Indoor coverage performances

In Fig.45, Fig.46 and Fig.47, for one specified position of FBS 1, we can see that the lower frequency results in less radio attenuation and can indeed improve the indoor coverage substantially. Even though both are in the UHF TV band, Freq A has a slightly higher coverage probability and considerably higher mean data rate than Freq B.

In Fig.47, Fig.48 and Fig.49, we can find that the proposed schemes have a slightly loss of performance in terms of coverage probability and mean

⁵ this band is not subject to the FCC limits and we increase it to compensate for the higher pathloss

throughput. This result matches to other previous studies such like [45] that EIRP constrained systems are not efficient in deploying directional antenna. However, this observed loss from our simulation is not very significant.

If we summon all the results from both Building A and Building B and all the possible FBS positions therein (i.e. FBS 1, 2, 3, ...), we get an overall average view of the coverage performance, see from Tab. 8. From the table, we can draw the following conclusions:

- The current regulated FCC rules are enough to support the Femtocell applications within the whole TV bands, providing a satisfactory coverage for a normal residential or SOHO building.
- The antenna gain is not present in EIRP constrained schemes and instead, antenna schemes I and II have a slightly lower coverage compared to the omni-directional cases. Nevertheless, the loss is only marginal.
- Compare between the two proposed schemes, Scheme II outperforms Scheme I due to fact that directivity brought by pattern-switching antenna is much coarser than the beamforming case. However, the difference is not huge and considering the much higher implementation complexity of beamforming, Scheme I is actually an economically efficient solution for indoor Femto coverage.

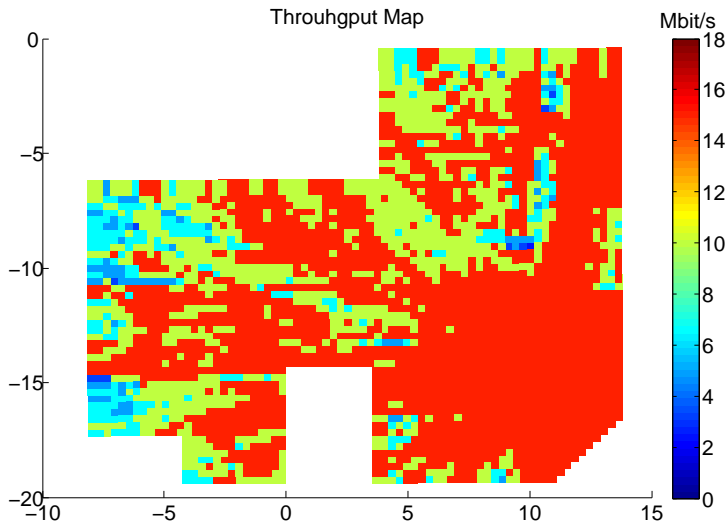


Figure 45: Throughput of Building A with Omni-Antenna when FBS₁ is switched on at Freq A, mean data rate is 12.7 Mbit/s, indoor coverage probability is 100%

6.4.2 Outdoor leakage and co-existence

As mentioned before, after running the indoor coverage simulations, we are able to also acquire the statistics of average outdoor emission leakage for different frequency and antenna settings. From Fig.53, we find out that:

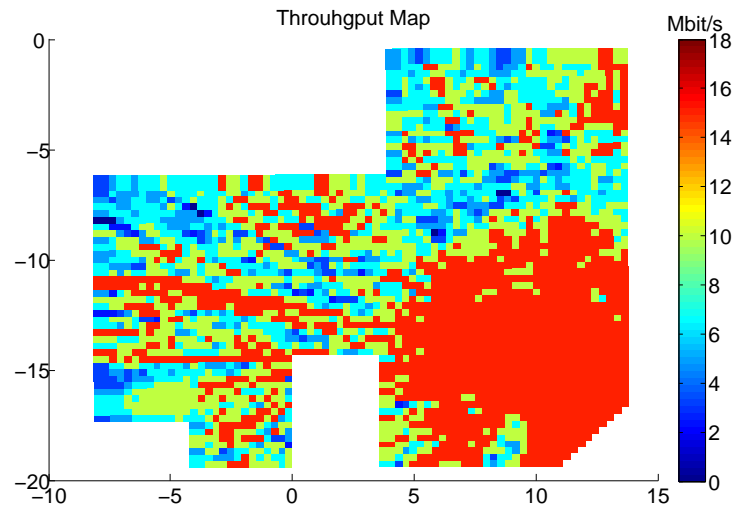


Figure 46: Throughput of Building A with Omni-Antenna when FBS₁ is switched on at Freq B, mean data rate is 10.7 Mbit/s, indoor coverage probability is 98.9%

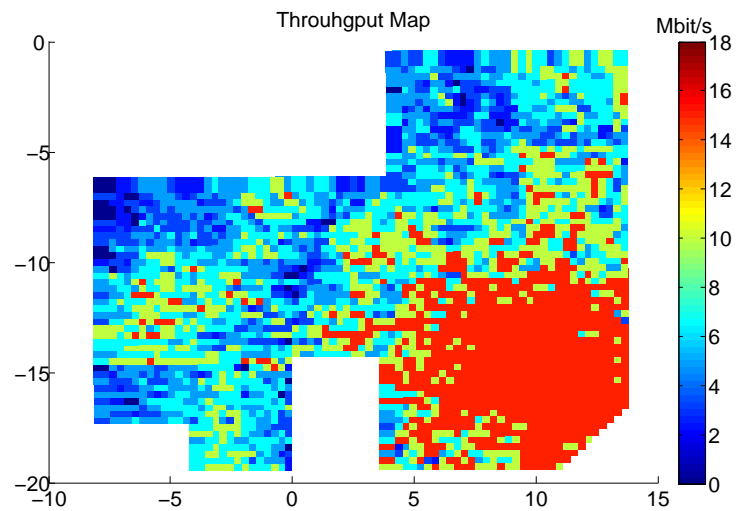


Figure 47: Throughput of Building A with Omni-Antenna when FBS₁ is switched on at Freq C, mean data rate is 8.6 Mbit/s, indoor coverage probability is 95.4%

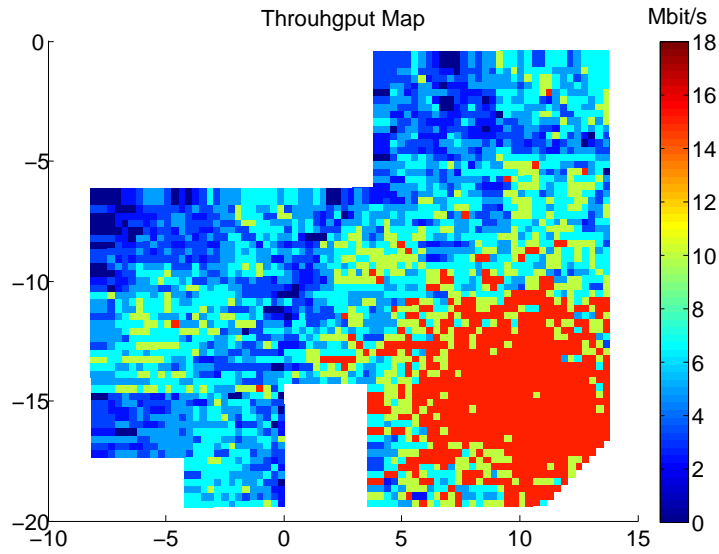


Figure 48: Throughput of Building A with Antenna Scheme II when FBS₁ is switched on at Freq C, mean data rate is 8.1 Mbit/s, indoor coverage probability is 92.2%

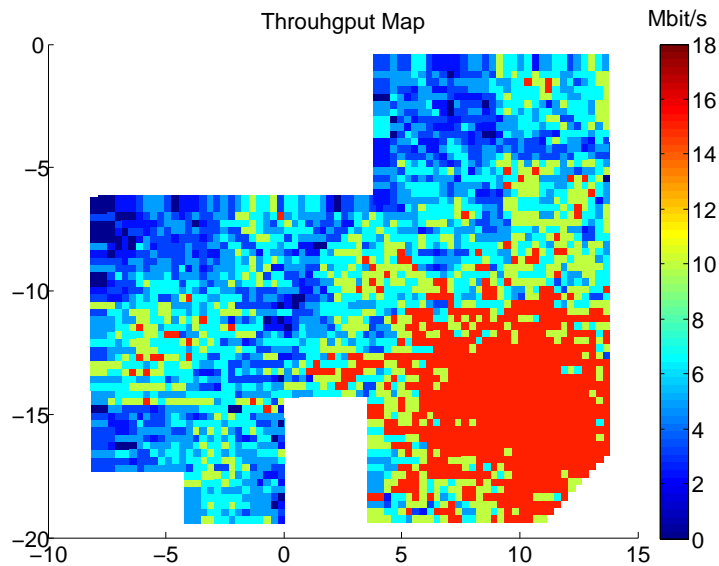


Figure 49: Throughput of Building A with Antenna Scheme III when FBS₁ is switched on at Freq C, mean data rate is 8.4 Mbit/s, indoor coverage probability is 93.3%

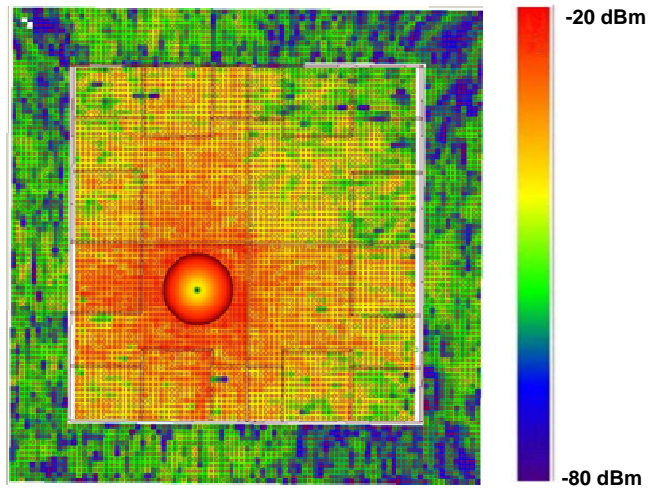


Figure 50: Peripheral emission leakage from Building B when equipped with Omni Antenna

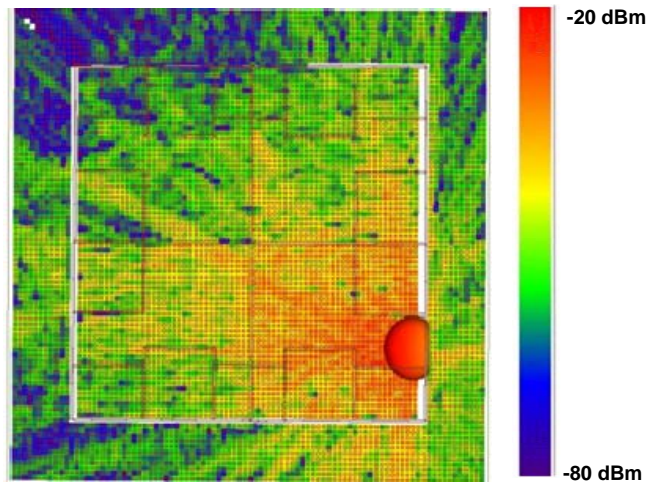


Figure 51: Peripheral emission leakage from Building B when equipped with Antenna Scheme I

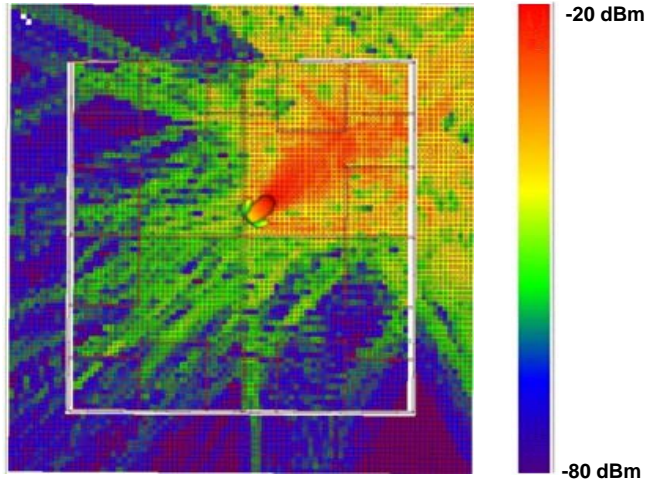


Figure 52: Peripheral emission leakage from Building B when equipped with Antenna Scheme II

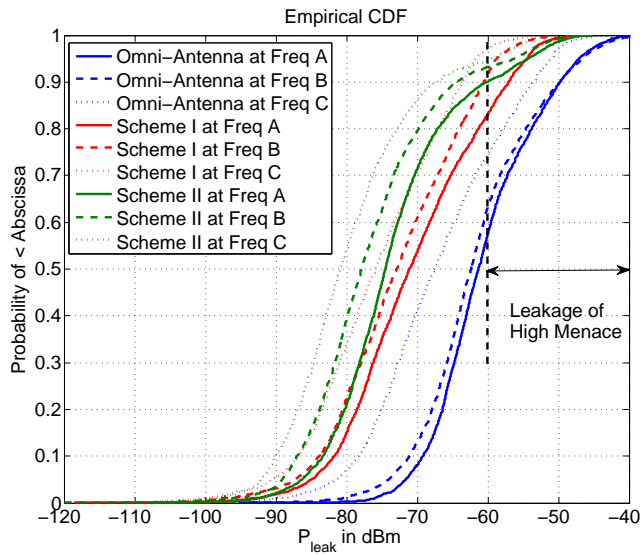


Figure 53: CDF of leakage power

Table 8: Indoor Coverage Probability vs. Antenna Schemes

		Omni-Antenna	Scheme I	Scheme II
Freq A	Building A	99.2%	99.0%	98.4%
	Building B	98.0%	95.8%	96.8%
	Average	98.6%	97.4%	97.6%
Freq B	Building A	97.4%	95.2%	96.7%
	Building B	95.6%	92.8%	94.7%
	Average	96.5%	94.0%	95.7%
Freq C	Building A	90.6%	87.4%	88.3%
	Building B	88.2%	84.6%	86.5%
	Average	88.9%	86.0%	87.4%

- lower frequency leads to a higher leakage for the same limits of EIRP. This is of natural sense because lower frequency also means a better propagation,
- in addition, antenna scheme I and II are found to be extremely efficient in the sense of reducing the leakage power, observing that the median leakage power (of cdf = 50%) is decreased by nearly 10 dB.
- we also note that in the high leakage power range, which is of more menace to the system performance, both the two directional antenna schemes can substantially reduce the probability.

We further define the parameter λ as the average number of deployed cognitive LTE-Femtos per km^2 , i.e. the intensity of PPP distributed Femto-equipped buildings. The thermal noise power in 6 MHz band is assumed to be -106 dBm. Therefore, the co-channel IOT seen by a radio receiver of random position in this area is a ratio between interference power derived by Eq. (6.2) and the noise power. If we further assume that the maximal tolerable IOT for one receiver is 20 dB, we acquire the curves between the interference outage rate and the cognitive LTE-Femto deployment λ in Fig. 54.

- From Fig. 54, we see that the reduced leakage power by antenna Scheme I and II has resulted in a better co-existence for the cognitive LTE-Femtos, reducing the outage rate by almost 50%.
- For a fixed outage rate of 5%, nearly 2 folds of gain in terms of Femto capacity are observed for the proposed schemes.

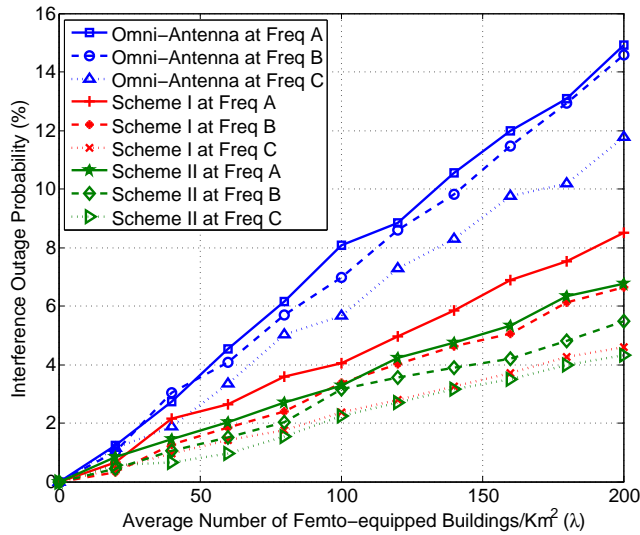


Figure 54: Outage rate vs. LTE-Femto density

6.5 CHAPTER SUMMARY

Combining the overall performance of indoor coverage and outdoor co-existence in the discussion and presented numerical results, we can conclude that for the indoor Femto scenarios, adaptive directional antenna is indeed an satisfactory method of providing the required QoS and remarkably alleviating the interference emitted to the outdoor, as this part of leakage contribute as the major part of Femto-to-Macro cross-tier interference.

Meanwhile, we find out that antenna switching, although very low in complexity and easy to implement with low cost, has a considerable gain in performance, decreasing the average IOT by over 30% and tremendously increase the Femto system capacity by 50%. This performance is even comparable to the beam-forming case. This means that there exists a trade-off for the indoor coverage solutions between coverage, coexistence, and cost. Considering the much lower complexity, antenna switching is indeed a promising candidate for Femto application that can well balance the performance-cost trade-off.

As the simulation results are spread into each of the chapters, this chapter is dedicated to introduce the methodology that we use for evaluating Femtocell in two-tier networks. As mentioned throughout the thesis, the most important performance metrics for Femtocell, i.e. transmission capacity etc., shall not be constrained by the 2nd-tier alone, but the co-existing 1st-tier as well.

However, the transmission capacity of Femtocell is not easy to derive. Only by the framework of stochastic geometry, that performance of ALOHA-based Femtos is possible to be given in tractable approaches, sometimes even in a closed form. However, it is extremely difficult if we consider the overall system and henceforth, we will have to resort to computer-aided simulations to simulate each scheme and evaluate the performance. In this chapter, we introduce how we do for the simulation and how can we capture the precise performance predictions why maintaining a relative low load of computation.

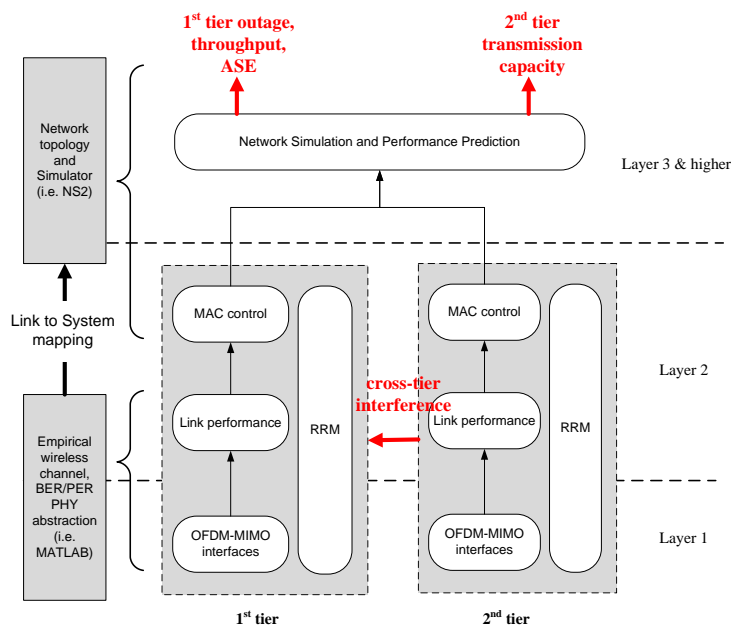


Figure 55: General Simulation Process

7.1 GENERAL DESCRIPTION

To deliver the system performance, the main process of simulation can be depicted in Fig. 55. The whole simulation preserve the OSI layered structure for the modern cellular simulation and contains the decision entity of radio resource management, which coordinates the PHY and MAC layers.

As a layered structure, the simulation tasks of different layers can be assigned to different simulation tools provided the interfaces are well defined. To simulate the 2-tier coexisting behavior, both tiers shall be simulated simultaneously and therein the cross-tier interference are the main connections between the tiers.

The key components of the system simulation are consisting of channel models, link-to-system mapping, and the network simulator that we will describe in the following sections.

7.2 CHANNEL MODEL

The channel models we use in the thesis are *empirical-based models* and *scenario-based models*, which are usually deterministic. In our simulation, we differentiate between indoor and outdoor wireless channels.

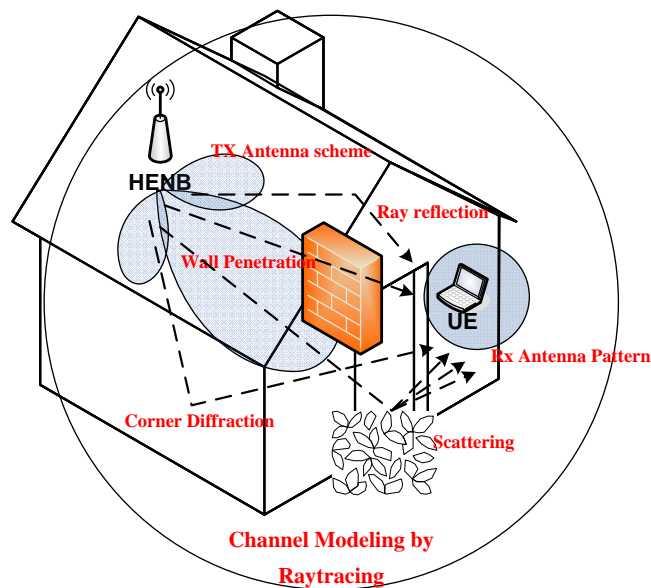


Figure 56: Indoor Channel and Raytracing Method

1. For the indoor case, we use the ray-tracing software to emulate and obtain the scenario-based channel. The reason is that, indoor wireless channels are rich of scatters that they are often corrupted with multipath fading. Therefore, building complex and setup can greatly affect the Femto indoor coverage.

It is critical for us to consider a typical "residential" and "small office" building that matches to the Femtocell application, instead of using the empirical channels which are generally obtained from measurements in general types of buildings.

The accuracy of indoor ray-tracing channel emulation is proven by many literature efforts such as [32][8]. In addition, we also conduct ray-tracing experiments on our own at the institute's office buildings in University of Hannover and compare it with later measurements. Both

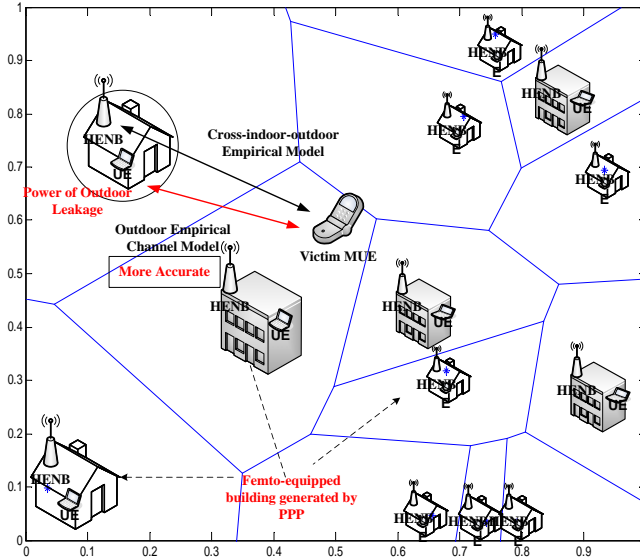


Figure 57: Outdoor Leakage and Empirical Channel

two different studies done in year 2007 with old building structures in [76] and in year 2011 with reconstructions in [16] have shown that ray-tracing is indeed precise and reliable for indoor coverage predictions in UHF bands.

- For the outdoor case, we mainly rely on the empirical channel models that are consented by project partners of Femto Forum [26]. As the MUEs are assumed to be located outdoors, we estimate the 2nd-tier interference seen by the MUE as the source of the emission leakage from Femto-equipped building and propagate through the outdoor-to-outdoor channel, where we use the COST-HATA model for sub-/urban scenarios, i.e.:

$$\begin{aligned}
 L &= 46.3 + 33.9 \log f - 13.82 \log h_B - a(h_R) \\
 &\quad + [44.9 - 6.55 \log h_B] \log d + C + \sigma \\
 a(h_R) &= (1.1 \log f - 0.7)h_R - (1.56 \log f - 0.8) \\
 C &= \begin{cases} 0dB & \text{for medium cities or suburban areas} \\ 3dB & \text{for metropolitan areas} \end{cases}
 \end{aligned} \tag{7.1}$$

where

- f is the frequency
- h_B is the height of MBS tower
- h_R is the height of FBS leakage buildings
- σ is the r.v. of shadowing effect

Compared with the 2nd-tier interference that are assumed to originate from an indoor FBS and propagate through the empirical indoor-to-outdoor channel, our proposed method is of higher accuracy because

Table 9: AMC and Data Rate

MCS Index	Modulation	Code Rate	Spectral Efficiency	Peak Data Rate	EESM β
#1	QPSK	1/3	0.45 bps/Hz	9.19 Mbps	1.79
#2	QPSK	1/2	0.67 bps/Hz	13.78 Mbps	1.78
#3	QPSK	3/4	1 bps/Hz	20.67 Mbps	1.46
#4	16QAM	1/2	1.33 bps/Hz	27.56 Mbps	5.26
#5	16QAM	3/4	2 bps/Hz	41.34 Mbps	4.58
#6	64QAM	3/4	3 bps/Hz	62.01 Mbps	8.41

the outdoor empirical channel is more precise and consented by many in research.

7.3 LINK-TO-SYSTEM MAPPING

Link-to-System Mapping is for mapping the contemporary channel/interference condition to the corresponding link performance. Since the main scope of this thesis is to study the OFDMA Femtocells, we explicitly assume that both the 1st-tier and 2nd-tier are LTE-like systems.

Hereby we shortly introduce the LTE system physical layer which is generally based on OFDM-MIMO physical interfaces with extra features of AMC, turbo/convolution channel coding, scrambling and interleaving, and Hybrid-ARQ mechanism. In the study, we assume that there are six different Modulation and Coding Schemes (MCSs) and the LTE link can adaptively transmit with highest possible MCS to maximize the spectral efficiency. The six defined MCSs are given by Tab. 9

We also use two methods for the LTE link-to-system mapping. They are:

1. **bit-based simulation** is a matlab based signal-level simulation, see Fig. 58. The main process is to simulate for each source bit 0 or 1 from being randomly generated, coded, then modulated into baseband signal and transmitted from RF front-end (by transmitter simulation), then on-the-fly propagated through the wire channel with Channel Impulse Response (CIR) obtained by ray-tracing (by on-the-fly simulation), to finally received and detected by the LTE receiver (by receiver simulation).
2. **EESM-based simulation** is an empirical method that maps effective SINR on each OFDM subcarriers directly to the link packet error rate. Even though it is much easier than faster than the bit-based simulation, the accuracy is also good because the parameter β of it is acquired based on numerous experiments.

For the EESM simulation conducted in Chapter 6, the effective SINR γ_{ef} is given by:

$$\gamma_{\text{ef}} = -\beta \ln \left(\frac{1}{N} \sum_k^N e^{-\frac{\gamma_k}{\beta}} \right) \quad (7.2)$$

where γ_k is the SINR experienced by each OFDM subcarrier and β is referenced to the work from [55].

7.4 NETWORK SIMULATION

In this thesis, we assume that each Femtocell is using ALOHA-based scheduler so that the network simulation is relatively easy. It is worthy to mention that we assume the FBSs and the FBS-equipped buildings are distributed in the law of homogeneous PPP.

To generate a homogeneous PPP process by computer simulation, we need to exploit the property of homogeneous PPP that the number of points appeared in each closed map is a random variable with Poisson distribution and conditioned on the numbers, each point is uniformly distributed. Therefore, the simulation PPP random process can be generated as in Fig. 59.

7.5 SIMULATION SUMMARY

To summarize, the system simulation conducted in this thesis can be depicted in the flowchart of Fig. 60.

The simulation tasks are evenly assigned to two PCs (each with due core) in the laboratory. It is necessary to point out that, since the whole simulation are Monte-Carlo based and the considered map is pretty large in size, it normally takes a huge number of loops to see the convergence of simulation results. As also mentioned when introducing the simulation results in Chapter 3, the number of loops can be at the scale of 10^4 to 10^5 that took these two PCs over 40 hours to finish simulating for one scenario.

Nevertheless, the obtained simulation results are quite well agreed with what has been predicted by the theoretic analysis, proving that stochastic geometry and PPP framework are indeed very useful tools to deliberate the performances of ad-hoc deployment networks.

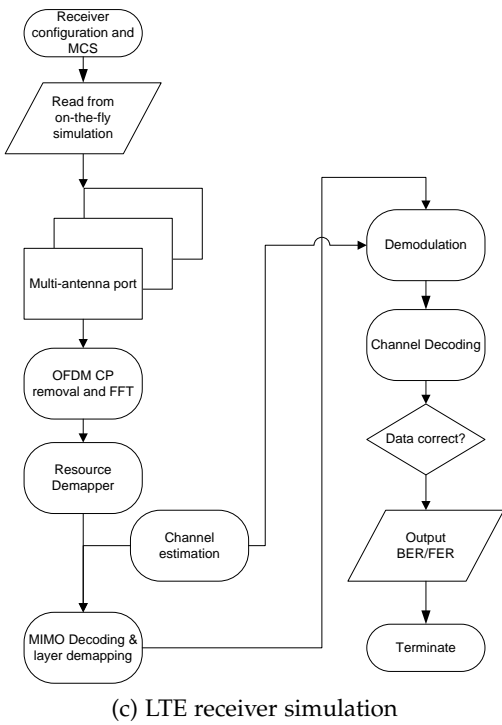
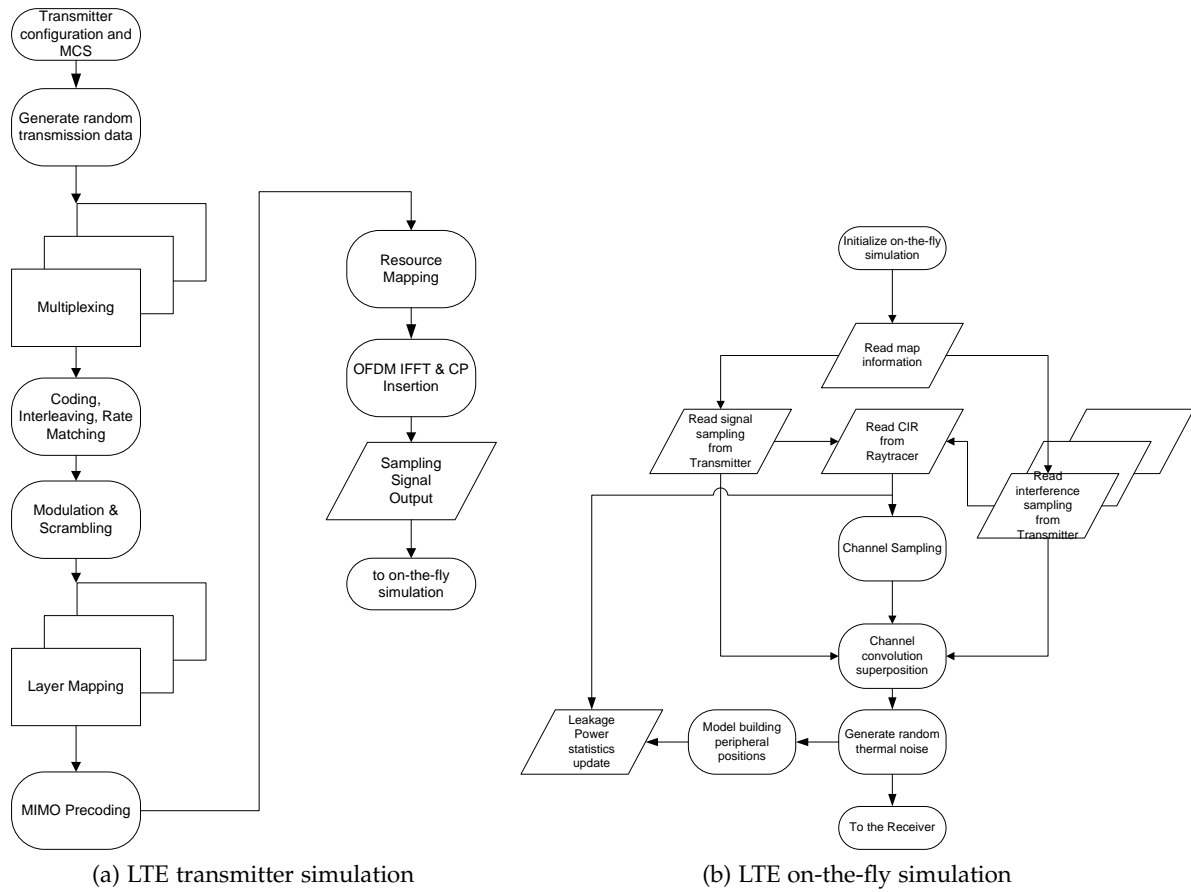


Figure 58: The Process of Bit-Based LTE Simulation

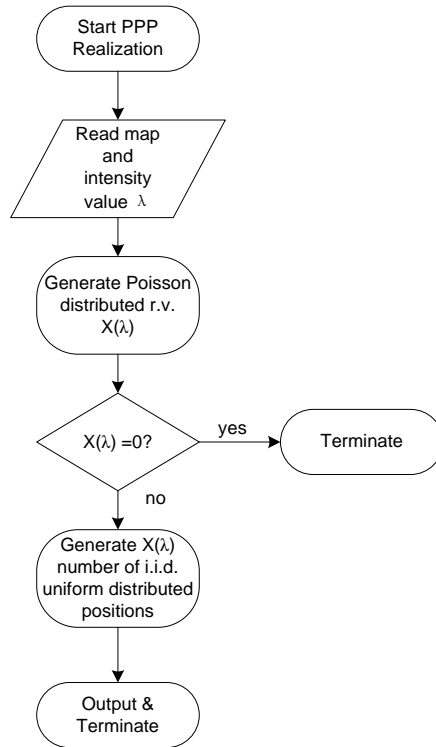


Figure 59: Generate PPP Positions

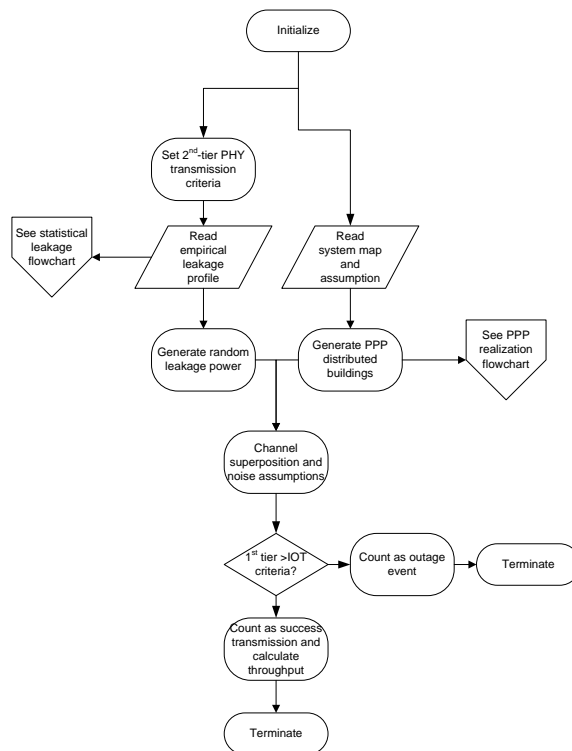


Figure 60: The Overall Simulation Process

CONCLUSIONS AND FUTURE WORKS

In this chapter, we will summarize the conclusions that we have achieved from the thesis work, discuss and explain the yet open problems and extend to the plans of the future.

8.1 CONCLUDING REMARKS

In this thesis, we study the interference management issue for the two-tier Macro-Femto coexisting cellular systems. This issue has become a topic of great importance to decide the successful deployment of LTE indoor (esp. residential and SOHO) deployment. It is also technically challenging because of the strict limits in aspects of practice, cost, implementation, and regulation.

Our thesis work focuses on the F-ALOHA access schemes for Femtocells to reuse a portion of the primary spectrum. Previous theoretic work has shown that F-ALOHA is a rather simple but efficient scheme to maximize the transmission capacity.

- **In Chapter 3 and Chapter 4**, our work is focused to answer the extended spectrum access question: what if the 2-tier overlay infrastructure has a clear preference of which subband to access for the underlying Femtos? Can we have a simple mechanics to notify the Femtos about this terrestrial preference and can the Femtos thereupon behave in a manner to cooperate for the best coexistence?

Our work has revealed that the answer to the above questions is *yes*.

In the FFR uplink, it is only necessary to broadcast the basic 1st-tier FFR config information to the co-located Femtocells, so that the Femtocells can respond adaptively with the proposed algorithms to partially-biased access the subbands and always achieve the maximal transmission capacity for the system.

In the FFR downlink, our study reveals that totally-biased access is optimal for the Femtos as long as its transmitting power is kept low and the system is very sensitive to the outage. Therefore, the heuristic algorithms estimating which subband the local region is least possible to access to, is a very critical to the Femtocell performances.

After devising some simple and useful estimation methods, we successfully propose a unified uplink-downlink framework, so that the Femtocells can exchange the Macro FFR information and utilizes the measurables by its attached FUEs. This framework has been proved by both analysis and simulation that it performs well under many circumstances, being robust to noise, general fadings, and other cell

layouts. It also keeps an excellent track of the current Femto design, so that the framework itself is easily realizable in the sense of low cost, low message burden, and completely standardization compatible.

- In Chapter 5 and Chapter 6, we consider some practical deployment issues of Femtocell. Due to the special ad-hoc deployment of Femtocell, we revisit the old questions about the sidelobe leakage and indoor-to-outdoor building emission leakage and deliver the results in new perspectives.

For the sidelobe leakage, we find out that although often neglected in research, the bad channel condition and high Femto density may lead to a substantial loss of coexistence performance. Although the regulators have a grip on the leakage control, e.g. the FCC's decision on the TVWS devices, it is reasonable for the developers to consider some air-interface alternatives to lower the leakage and better accommodate to the network heterogeneity.

Similar results are also found in the building emission leakage study. Although the regulators have carefully defined an EIRP limit for many secondary spectrum users, it may discourage the Femtos from using directional antennas because of the coverage loss compared to transmit power limited case. However, our study based on LTE system level simulation reveals that the coverage loss in the application of residential and small office building cases are not very evident, and if we consider the coexistence performance, the directional antenna is clearly a favor due to its excellent ability of lowering the emission out of the buildings.

- In Chapter 7, we briefly introduce the methodologies that are used in facilitating the simulations and we also explain how to evaluate the LTE systems for indoor coverage and throughput performances.

Summing up from all the works that have been done in this thesis, we conclude that to improve the coexistence of two-tier cellular systems, a well designed framework that can combine the theory and practice and evolves with different level of radio resource management optimization upon different level of radio cognition is extremely important. Although the current stage of Femto development may be restricted by many implementation and regulation limits, it is reasonable to believe that the Femtocells can tackle with the interference issues and become one of the most promising enablers for the future wireless communication.

8.2 FUTURE OUTLOOK

Most of the study in this thesis is based on F-ALOHA and Poisson Point Process assumptions. Often these assumptions lead to pessimistic performance predictions. Therefore in the future work, we need to consider the cases more close to reality, including:

- the real-case deployment for Femtocell, which shall be in the midst of PPP and regular patterns, so that in the process of evaluation, it might be necessary to consider the complex building structures, position-clustering, user behaviors, and so on.
- the real-case channel access for Femtocell, which shall be in between the F-ALOHA assumptions and CSMA, meaning that the Femtocell may possess some basic radio sensing and monitoring abilities to opportunistically avoid the potential interference.

Moreover, it should not be overlooked that, by the advances in the communication and signal processing, the transmitter and receiver design [10][72] nowadays have a strong feature of pre-avoiding, mitigating or fully canceling the interference. Such advances may challenge the conventional view of interference and cell layout, such as the higher SINR interference is, the easier it can be successfully decoded at the receiver, even totally annihilated from the receiving signal.

Despite the above mentioned theoretical limitations of this thesis that our future work is planning to solve, we realized through the study that, the cognitive sensing abilities and the multi-FBS coordination features can indeed provide much greater performance gain than the current quasi-blind and stand-alone Femtocell designs.

These abilities and features are currently in the early stage of development because of the low cost requirement. However, it is reasonable to believe that, as the Femtocell penetrates further into the market and the ascending computer power in Moore's law, the sensing and coordination will be eventually implemented at the Femtocell.

By that moment, the house-hold Femto Base Station will grow as a powerful and intelligent access point, responsible of providing high speed wireless coverage, provisioning the seamless hand-over between the outdoor networks, and organizing the entire network inside the building. This is indeed the *great convergence* of mobile, nomadic, and fixed wireless communication technologies and the scope of Femtocells is thereupon shifting from what this thesis currently stands to the paradigm of playing an important role in the future wireless networks.

This appendix is to provide the mathematical background of Poisson Point Process for supporting Chapter 3, 4, 5, and 6. The following contents are mainly cited from [43] [66], [12], and IEEE tutorial of [34].

A.1 DEFINITIONS

A point process Ω is defined as a measurable mapping from some probability space \mathcal{P} to the space of point measures \mathcal{E} . A point process Ω is called Poisson Point Process on \mathcal{E} , if it is simple and

1. for all disjoint subsets $\mathcal{A}_1, \mathcal{A}_2, \dots, \mathcal{A}_n$ on \mathcal{E} , the random variables $\Omega(\mathcal{A}_i)$ are independent;
2. for all sets \mathcal{A} on \mathcal{E} , the random variables $\Omega(\mathcal{A}_i)$ are Poisson distributed, i.e.

$$\mathbf{P}(\Omega(\mathcal{A}) = k) = \frac{\Lambda(\mathcal{A})^k e^{-\Lambda(\mathcal{A})}}{k!} \quad (\text{A.1})$$

with parameter $\Lambda(\mathcal{A}) \triangleq \mathbf{E}[\Omega(\mathcal{A})]$ called as intensity measure.

Intuitively, for any disjoint subsets $\mathcal{A}_1, \mathcal{A}_2, \dots, \mathcal{A}_k$, the joint distribution can be given as:

$$\mathbf{P}(\Omega(\mathcal{A}_1) = n_1, \dots, \Omega(\mathcal{A}_k) = n_k) = \prod_{i=1}^k \left(e^{-\Lambda(\mathcal{A}_i)} \frac{\Lambda(\mathcal{A}_i)^{n_i}}{n_i!} \right) \quad (\text{A.2})$$

If the case that for any sets \mathcal{A} on \mathbb{R}^d , we have

$$\Lambda(\mathcal{A}) = \lambda |\mathcal{A}|,$$

we call the process Ω (with intensity measure Λ) as the *homogeneous Poisson Point Process* (hPPP), and name constant λ as the intensity of this hPPP.

A.2 OPERATIONS PRESERVING PPP

There are some operations that can preserve the Poisson PP law, they are:

- **Superposition**

The superposition of independent Poisson PP with intensities Ω_k is a Poisson PP with intensity measure $\sum_k \Omega_k$ if and only if the latter is a locally finite measure.

- **Thinning**

The thinning of Ω with retention function p is a PP given by

$$\Omega^p = \sum_k \delta_k \epsilon_{x_k}$$

where the random variables δ_k are independent given Ω . The thinning of the Poisson PP of intensity measure Λ with retention probability p yields a Poisson PP of intensity measure $p\Lambda$ with $(p\Lambda)(A) = \int_A p(x)\Lambda(dx)$

- **Transformation**

When the point transformation is independent given Ω , with probability $\mathbf{P}(y_k \in B|\Omega) = p(x_k, B)$, the transformation of the PPP *Omega* of intensity measure Λ by a probability kernel p is the PPP with intensity measure $\Lambda'(A) = \int_{\mathbb{R}^d} p(x, A)\Lambda(dx)$, with $A \subset \mathbb{R}^d$

A.3 PALM THEORY

We will skip the introduction of the Palm Measure but give the two most important theorems regarding the property of PPP.

Theorem A.1 (Slivnyak-Mecke or Slivnyak's Theorem) *Let Ω be a PPP with intensity measure Λ , For all most all $x \in \mathbb{R}^d$,*

$$\mathbf{Pr}_x^!(\cdot) = \mathbf{Pr}\{\Omega \in \cdot\}$$

that is, the reduced palm distribution $\mathbf{Pr}_x^!(\cdot)$ of the PPP is equal to its original distribution.

The Slivnyak's theorem guarantees that we can select a *typical* PPP distributed BS or receiver, assuming at the origin o of the coordinates, the conditional PPP seen from it is equivalent to the original PPP assumptions.

Henceforth, throughout the thesis, we use the technique of selecting the typical reference point and omit the denotation of reduced palm measure.

Theorem A.2 (Mecke's Theorem) *Let Λ be a point process with a σ -finite mean measure Λ (i.e. there exists a countable partition of \mathbb{R}^d such that Λ is finite on each element of this partition). Then Λ is the PPP with intensity measure Λ if and only if*

$$\mathbf{Pr}_x^!(\cdot) = \mathbf{Pr}\{\Omega \in \cdot\}.$$

Provided by Mecke's Theorem, we learn that PPP is indeed a very special type of point process that it is uniquely tractable.

A.4 SUM OF POISSON POINT PROCESS

Theorem A.3 (Campbell's Theorem) *Let Ω be a PPP on \mathbb{R}^d with intensity measure Λ , and let $f : \mathbb{R}^d \rightarrow \mathbb{R}$ be any function. Then the sum*

$$\Sigma = \sum_{X \in \Omega} f(X)$$

is absolutely convergent with probability if and only if

$$\int_{\mathbb{R}^d} \min(|f(x)|, 1) \Lambda(dx) < \infty. \quad (\text{A.3})$$

If this condition holds, then

$$\mathbf{E}(e^{\theta\Sigma}) = \exp \left\{ \int_{\mathbb{R}^d} (e^{\theta f(x)} - 1) \Lambda(dx) \right\}$$

for any complex θ for which the integral on the right converges.

The Campbell's theorem is the direct enabler for the analysis of the **shot-noise** interference process in the thesis.

A.5 SHOT-NOISE INTERFERENCE

Assuming the interference nodes are in a law of PPP Ω distributed with intensity measure of Λ , and the radio propagation is following the power decaying in loss, i.e. the pathloss model of

$$KW\|X\|^{-\alpha},$$

where K is penetration constant, W is independent fading, $\|X\|$ is the euclidean distance and α is the pathloss exponent, we are then able to obtain the interference seen from the origin, which is the sum of all the signals from the interference nodes as:

$$I = \sum_{X \in \Omega} KW\|X\|^{-\alpha}.$$

The Laplacian transform of the r.v. I is thus derived as:

$$\begin{aligned} \mathcal{L}_I(s) &\triangleq \mathbf{E}[e^{-sI}] \\ &= \exp \left\{ - \int_{\mathbb{R}^d} \mathbf{E}_W \left[1 - e^{-sKW\|X\|^{-\alpha}} \right] \Lambda(dX) \right\} \end{aligned} \quad (\text{A.4})$$

For $\alpha \leq d$, we have $I = \infty$ as the consequence of the cumulated interference from the many far transmitters whose signal powers do not decay fast enough to keep the interference power finite.

Therefore, throughout the thesis, we assume the exponent $\alpha > 2$ in 2-D cases, which also matches with the radio propagation property in practice.

BIBLIOGRAPHY

- [1] 3GPP 36.104. Base Station (BS) Radio Transmission and Reception, 2011. URL www.3gpp.org.
- [2] 3GPP 36.211 Rel. 8. Evolved Universal Terrestrial Radio Access (E-UTRA) Physical Channels and Modulation, December 2008. URL www.3gpp.org.
- [3] 3GPP 36.921. Home eNodeB (HeNB) Radio Frequency (RF) requirements analysis, January 2010. URL www.3gpp.org.
- [4] 3GPP RAN1. RAN1-090133 Huawei Beamforming enhancement in LTE-Advanced, January 2009. URL www.3gpp.org.
- [5] G. Alfano, M. Garetto, and E. Leonardi. Capacity scaling of wireless networks with inhomogeneous node density: upper bounds. *IEEE J. Select. Areas Commun.*, 27(7):1147–1157, September 2009. ISSN 0733-8716. doi: 10.1109/JSAC.2009.090911.
- [6] G. Alfano, M. Garetto, E. Leonardi, and V. Martina. Capacity Scaling of Wireless Networks With Inhomogeneous Node Density: Lower Bounds. *IEEE/ACM Trans. Networking*, 18(5):1624–1636, October 2010. ISSN 1063-6692. doi: 10.1109/TNET.2010.2048719.
- [7] M.-S. Alouini and A.J. Goldsmith. Area Spectral Efficiency of Cellular Mobile Radio Systems. *IEEE Trans. Veh. Technol.*, 48(4):1047–1066, jul 1999. ISSN 0018-9545. doi: 10.1109/25.775355.
- [8] H.R. Anderson. Site-specific BER analysis in frequency-selective channels using a ray-tracing propagation model. In *Global Telecommunications Conference, 1994. GLOBECOM '94. Communications: The Global Bridge.*, IEEE, volume 3, pages 1441–1445 vol.3, November 1994. doi: 10.1109/GLOCOM.1994.513015.
- [9] Jeffrey G. Andrews, François Baccelli, and Radha Krishna Ganti. A Tractable Approach to Coverage and Rate in Cellular Networks. *CoRR*, abs/1009.0516, 2010.
- [10] J.G. Andrews. Interference cancellation for cellular systems: a contemporary overview. *IEEE Wireless Commun. Mag.*, 12(2):19–29, April 2005. ISSN 1536-1284. doi: 10.1109/MWC.2005.1421925.
- [11] J.G. Andrews, S. Weber, and M. Haenggi. Ad hoc networks: To spread or not to spread? [ad hoc and sensor networks]. *IEEE Commun. Mag.*, 45(12):84–91, december 2007. ISSN 0163-6804. doi: 10.1109/MCOM.2007.4395371.

- [12] F. Baccelli and B. Blaszczyszyn. *Stochastic Geometry and Wireless Networks Volume I Theory*. Now Publisher, 1st edition, 2009.
- [13] H. Bolcskei, P. Duhamel, and R. Hleiss. Design of pulse shaping OFDM/OQAM systems for high data-rate transmission over wireless channels. In *IEEE International Conference on Communications, ICC '99*, volume 1, pages 559–564, 1999. doi: 10.1109/ICC.1999.768001.
- [14] G. Boudreau, J. Panicker, Ning Guo, Rui Chang, Neng Wang, and S. Vrzic. Interference coordination and cancellation for 4G networks. *IEEE Commun. Mag.*, 47(4):74–81, April 2009. ISSN 0163-6804. doi: 10.1109/MCOM.2009.4907410.
- [15] H. Boulaaba. Advanced antenna selection for the interference management of femtocell systems (supervised by z. zhao). Master's thesis, Leibniz University of Hannover, 2011.
- [16] H. Cao, M. El-Hadidy, Z. Zhao, W. Niy, and T. Kaiser. Measurement and Ray-tracing of Wideband Indoor Channel in UHF TV White Space. In *Proc. of 4th International Conference on Cognitive Radio and Advanced Spectrum Management (submitted to)*, 2011.
- [17] V. Chandrasekhar and J. Andrews. Spectrum Allocation in Tiered Cellular Networks. *IEEE Trans. Commun.*, 57(10):3059–3068, Oct. 2009. ISSN 0090-6778. doi: 10.1109/TCOMM.2009.10.080529.
- [18] V. Chandrasekhar, J. Andrews, and A. Gatherer. Femtocell Networks: a Survey. *IEEE Commun. Mag.*, 46(9):59–67, Sep. 2008. ISSN 0163-6804. doi: 10.1109/MCOM.2008.4623708.
- [19] V. Chandrasekhar, M. Kountouris, and J.G. Andrews. Coverage in Tiered Cellular Networks with Spatial Diversity. In *Global Telecommunications Conference, 2009. GLOBECOM 2009. IEEE*, pages 1–6, 30 2009-dec. 4 2009. doi: 10.1109/GLOCOM.2009.5425918.
- [20] H. Claussen and F. Pivit. Femtocell Coverage Optimization Using Switched Multi-Element Antennas. In *Communications, 2009. ICC '09. IEEE International Conference on*, pages 1–6, Jun. 2009. doi: 10.1109/ICC.2009.5199033.
- [21] H. Claussen, L.T.W. Ho, and L.G. Samuel. Financial Analysis of a Pico-Cellular Home Network Deployment. In *Communications, 2007. ICC '07. IEEE International Conference on*, pages 5604–5609, June 2007. doi: 10.1109/ICC.2007.929.
- [22] COGEU Project. European TV White Spaces Analysis and COGEU use-cases, January 2009. URL www.ict-cogeu.org.
- [23] Harpreet S. Dhillon, Radha Krishna Ganti, François Baccelli, and Jeffrey G. Andrews. Modeling and Analysis of K-Tier Downlink Heterogeneous Cellular Networks. *CoRR*, abs/1103.2177, 2011.

- [24] Federal Communications Commission. Second Report and Order and Memorandum Opinion and Order. 23 FCC Rcd 16807, 2008. URL www.fcc.gov.
- [25] Federal Communications Commission. FCC SECOND MEMORANDUM OPINION AND ORDER on Unlicensed Operation in the TV Broadcast Bands. FCC 10-174, 2010. URL www.fcc.gov.
- [26] Femto Forum. OFDMA Interference: Proposed System Simulation Methodology, Nov. 2008. URL www.femtoforum.org.
- [27] Femto Forum. Interference Management in UMTS Femtocells, Aug. 2009. URL www.femtoforum.org.
- [28] Femto Forum. Femtocell Business Case Whitepaper, Jun. 2009. URL www.femtoforum.org.
- [29] Femto Forum. Interference Management in OFDMA Femtocells, Mar. 2010. URL www.femtoforum.org.
- [30] Femto Forum. Femtocell Synchronization and Location Whitepaper, Mar. 2011. URL www.femtoforum.org.
- [31] Martin Fuhrwerk, Christoph Thein, and Lars Häring. Performance comparison of cp-ofdm and oqam-ofdm based wifi systems. In *Proceedings of the 16th International OFDM-Workshop (submitted to)*, 2011.
- [32] G. German, Q. Spencer, L. Swindlehurst, and R. Valenzuela. Wireless indoor channel modeling: statistical agreement of ray tracing simulations and channel sounding measurements. In *Acoustics, Speech, and Signal Processing, 2001. Proceedings. (ICASSP '01). 2001 IEEE International Conference on*, volume 4, pages 2501–2504 vol.4, 2001. doi: 10.1109/ICASSP.2001.940509.
- [33] D. Gonzalez, S. Ruiz, M. Garcia-Lozano, J. Olmos, and A. Serra. System level evaluation of lte networks with semidistributed intercell interference coordination. In *Personal, Indoor and Mobile Radio Communications, 2009 IEEE 20th International Symposium on*, pages 1497–1501, sept. 2009. doi: 10.1109/PIMRC.2009.5449773.
- [34] M. Haenggi, J.G. Andrews, F. Baccelli, O. Dousse, and M. Franceschetti. Stochastic Geometry and Random Graphs for the Analysis and Design of Wireless Networks. *IEEE J. Select. Areas Commun.*, 27(7):1029–1046, Sep. 2009. ISSN 0733-8716. doi: 10.1109/JSAC.2009.090902.
- [35] Kaibin Huang, V.K.N. Lau, and Yan Chen. Spectrum Sharing between Cellular and Mobile Ad Hoc Networks: Transmission-Capacity Trade-off. *IEEE J. Select. Areas Commun.*, 27(7):1256–1267, Sep. 2009. ISSN 0733-8716. doi: 10.1109/JSAC.2009.090921.
- [36] A.M. Hunter, J. Andrews, and S. Weber. Transmission capacity of ad hoc networks with spatial diversity. *IEEE Trans. Wireless Commun.*, 7(12): 5058–5071, Dec. 2008. ISSN 1536-1276. doi: 10.1109/T-WC.2008.071047.

- [37] J. Ilow and D. Hatzinakos. Analytic alpha-stable noise modeling in a Poisson field of interferers or scatterers. *IEEE Trans. Signal Processing*, 46(6):1601–1611, June 1998. ISSN 1053-587X. doi: 10.1109/78.678475.
- [38] Infonetics Research Inc. Mobile Market Research Report, Mar. 2007. URL www.infonetics.com.
- [39] Infonetics Research Inc. 2G/3G/4G Femtocell Equipment Quarterly Markets, Shares, and Forecasts, Jun. 2011. URL www.infonetics.com.
- [40] W.C. Jakes. *Microwave Mobile Communications*. New York: Wiley, 1974.
- [41] Yi Jiang, Yan Zhou, Mohit Anand, Farhad Meshkati, Norman Ko, and Mehmet Yavuz. Benefits of Transmit and Receive Diversity in Enterprise Femtocell Deployments. In *Proceedings of IEEE WiOpt'11 Workshop on Indoor/Outdoor Femtocell*, 2011.
- [42] N. Jindal, J. Andrews, and S. Weber. Bandwidth Partitioning in Decentralized Wireless Networks. *IEEE Commun. Mag.*, 7(12):5408–5419, Dec. 2008. ISSN 1536-1276. doi: 10.1109/T-WC.2008.071220.
- [43] J.F. C. Kingman. *Poisson Processes*. Oxford University Press, 1993.
- [44] Parag Kulkarni, Woon Hau Chin, and Tim Farnham. Radio resource management considerations for LTE Femto cells. *Computer Communication Review*, 40(1):26–30, 2010.
- [45] Alexandr M. Kuzminskiy. Downlink beamforming subject to the equivalent isotropic radiated power constraint in WLAN OFDM systems. *Signal Processing*, 87(5):991–1002, 2007. ISSN 0165-1684. doi: DOI:10.1016/j.sigpro.2006.09.009. URL <http://www.sciencedirect.com/science/article/pii/S0165168406003148>.
- [46] S. Lakshmanan, K. Sundaresan, R. Kokku, A. Khojastepour, and S. Rangarajan. Towards adaptive beamforming in indoor wireless networks: An experimental approach. In *INFOCOM 2009, IEEE*, pages 2621–2625, april 2009. doi: 10.1109/INFCOM.2009.5062199.
- [47] Jin-Woo Lee, June Moon, and Yong-Hwan Lee. Other-Cell Interference Reducing Resource Allocation in OFDM-Based Asynchronous Cellular Systems. *EURASIP Journal on Wireless Communications and Networking*, 2008:doi:10.1155/2008/378097, 2008.
- [48] D. Lopez-Perez, A. Valcarce, G. de la Roche, and Jie Zhang. OFDMA Femtocells: A Roadmap on Interference Avoidance. *IEEE Commun. Mag.*, 47(9):41–48, September 2009. ISSN 0163-6804. doi: 10.1109/MCOM.2009.5277454.
- [49] S.B. Lowen and M.C. Teich. Power-law shot noise. *IEEE Trans. Inform. Theory*, 36(6):1302–1318, November 1990. ISSN 0018-9448. doi: 10.1109/18.59930.

- [50] Y. Medjahdi, M. Terre, D. Le Ruyet, D. Roviras, J.A. Nossek, and L. Baltar. Inter-cell interference analysis for ofdm/fbmc systems. In *Signal Processing Advances in Wireless Communications, 2009. SPAWC '09. IEEE 10th Workshop on*, pages 598–602, june 2009. doi: 10.1109/SPAWC.2009.5161855.
- [51] P. Mogensen, Wei Na, I.Z. Kovacs, F. Frederiksen, A. Pokhariyal, K.I. Pedersen, T. Kolding, K. Hugl, and M. Kuusela. Lte capacity compared to the shannon bound. In *Vehicular Technology Conference, 2007. VTC2007-Spring. IEEE 65th*, pages 1234–1238, april 2007. doi: 10.1109/VETECS.2007.260.
- [52] A.F. Molisch, L.J. Greenstein, and M. Shafi. Propagation issues for cognitive radio. *Proceedings of the IEEE*, 97(5):787–804, May 2009. ISSN 0018-9219. doi: 10.1109/JPROC.2009.2015704.
- [53] Office of Communications. Digital dividend: cognitive access Statement on licence-exempting cognitive devices using interleaved spectrum, July 2009. URL <http://www.ofcom.org.uk/>.
- [54] Chang-Yeong Oh, Min Young Chung, Hyunseung Choo, and Tae-Jin Lee. A Novel Frequency Planning for Femtocells in OFDMA-Based Cellular Networks Using Fractional Frequency Reuse. In *ICCSA (3)*, pages 96–106, 2010.
- [55] J. Olmos, A. Serra, S. Ruiz, M. Garcia-Lozano, and D. Gonzalez. Exponential Effective SIR metric for LTE downlink. In *Personal, Indoor and Mobile Radio Communications, 2009 IEEE 20th International Symposium on*, pages 900–904, September 2009. doi: 10.1109/PIMRC.2009.5449772.
- [56] A. Paulraj, D. Gore, and R.t Nabar. *Introduction to Space-Time Wireless Communications*. Cambridge University Press, 2008.
- [57] J. Proakis. *Digital Communications*. McGraw Hill, 4 edition, 2000.
- [58] S. Rangan. Femto-macro cellular interference control with subband scheduling and interference cancelation. In *GLOBECOM Workshops (GC Wkshps), 2010 IEEE*, pages 695–700, December 2010. doi: 10.1109/GLOCOMW.2010.5700410.
- [59] T. Rappaport. *Wireless Communications-Principles and Practice*. Prentice Hall, January 1996.
- [60] S. Shamai and A.D. Wyner. Information-theoretic considerations for symmetric, cellular, multiple-access fading channels. i. *IEEE Trans. Inform. Theory*, 43(6):1877–1894, November 1997. ISSN 0018-9448. doi: 10.1109/18.641553.
- [61] S. Shamai and A.D. Wyner. Information-theoretic considerations for symmetric, cellular, multiple-access fading channels. ii. *IEEE Trans. Inform. Theory*, 43(6):1895–1911, November 1997. ISSN 0018-9448. doi: 10.1109/18.641554.

- [62] P. Siohan, C. Siclet, and N. Lacaille. Analysis and design of OFDM/O-QAM systems based on filterbank theory. *IEEE Trans. Signal Processing*, 50(5):1170–1183, May 2002. ISSN 1053-587X. doi: 10.1109/78.995073.
- [63] O. Somekh and S. Shamai. Shannon-theoretic approach to a Gaussian cellular multiple-access channel with fading. *IEEE Trans. Inform. Theory*, 46(4):1401–1425, July 2000. ISSN 0018-9448. doi: 10.1109/18.850679.
- [64] T. Stitz, T. Ihalainen, A. Viholainen, and M. Renfors. Pilot-Based Synchronization and Equalization in Filter Bank Multicarrier Communications. *EURASIP Journal on Advances in Signal Processing*, 2010:1–18, 2010. doi: 10.1155/2010/741429.
- [65] D. Stoyan, W. S. Kendall, and J. Mecke. *Stochastic Geometry and Its Applications*. John Wiley & Sons, Chichester, 1987.
- [66] D. Stoyan, W. S. Kendall, and J. Mecke. *Stochastic Geometry and Its Applications*. John Wiley & Sons, 2nd edition, 1996.
- [67] C. Thein, M. Fuhrwerk, and Z. Zhao. 1st Milestone Deliverables of CogFemto Project. Technical report, Huawei, 2011.
- [68] David Tse and Pramod Viswanath. *Fundamentals of Wireless Communication*. Cambridge University Press, 2005.
- [69] S. Weber, J.G. Andrews, and N. Jindal. The Effect of Fading, Channel Inversion, and Threshold Scheduling on Ad Hoc Networks. *IEEE Trans. Inform. Theory*, 53(11):4127–4149, November 2007. ISSN 0018-9448. doi: 10.1109/TIT.2007.907482.
- [70] S. Weber, J.G. Andrews, and N. Jindal. An overview of the transmission capacity of wireless networks. *IEEE Trans. Commun.*, 58(12):3593–3604, December 2010. ISSN 0090-6778. doi: 10.1109/TCOMM.2010.093010.090478.
- [71] S.P. Weber, X. Yang, J.G. Andrews, and G. de Veciana. Transmission capacity of wireless ad hoc networks with outage constraints. *IEEE Trans. Inform. Theory*, 51(12):4091–4102, December 2005. ISSN 0018-9448. doi: 10.1109/TIT.2005.858939.
- [72] S.P. Weber, J.G. Andrews, Xiangying Yang, and G. de Veciana. Transmission capacity of wireless ad hoc networks with successive interference cancellation. *IEEE Trans. Inform. Theory*, 53(8):2799–2814, aug. 2007. ISSN 0018-9448. doi: 10.1109/TIT.2007.901153.
- [73] T. Weiss, J. Hillenbrand, A. Krohn, and F.K. Jondral. Mutual interference in OFDM-based spectrum pooling systems. In *Vehicular Technology Conference. VTC 2004-Spring. IEEE 59th*, volume 4, pages 1873–1877, May 2004. doi: 10.1109/VETECS.2004.1390598.
- [74] J.-S. Wu, J.-K. Chung, and M.-T. Sze. Analysis of uplink and downlink capacities for two-tier cellular system. *IEE Proceedings- Communications*,

- 144(6):405–411, December 1997. ISSN 1350-2425. doi: 10.1049/ip-com:19971648.
- [75] A. D. Wyner. Shannon-Theoretic Approach to a Gaussian Cellular Multiple-Access Channel. *IEEE Trans. Inform. Theory*, 40(4):1713–1727, November 1994.
- [76] Z. Zhao, Q. Cai, and S. Sczyslo. Final Report of MOLDAS Project. Technical report, ADC Wireless, 2008.
- [77] Z. Zhao, A. Wilzeck, and T. Kaiser. Downlink Frequency Reuse and Hopping for OFDMA Femtocells. *Frequenz Journal of RF-Engineering and Telecommunications*, 64:185–190, October 2010.
- [78] Z. Zhao, M. Schellmann, H. Boulaaba, and E. Schulz. Interference Study for Cognitive LTE-Femtocell in TV White Spaces. In *Technical Symposium at ITU Telecom World 2011 ITU WT11'*, Geneva, Switzerland, July 2011.
- [79] Z. Zhao, C. Thein, F. Zheng, and T. Kaiser. Analysis of the Influence of OFDM Sidelobe Interference on Femto Rich Systems. In *Proceedings of IEEE WiOpt'11 Workshop on Indoor/Outdoor Femtocell*, May 2011.
- [80] Z. Zhao, F. Zheng, A. Wilzeck, and T. Kaiser. Femtocell Spectrum Access Underlaid in Fractional Frequency Reused Macrocell. In *Proceedings of IEEE ICC'11 Workshop on Heterogeneous Networks*, June 2011.

WISSENSCHAFTLICHER WERDERGANG

Zhao Zhao

männlich, geboren am 19.08.1982 in Shanghai in China

wohnhaft in der Dorotheenstr. 5B in 30419 Hannover, Deutschland

1997-2000	Studium an der Jinshan Senior High School in Shanghai in China
2000-2004	Studium der Elektrotechnik an der Shanghai Jiaotong University in Shanghai in China
07.2004	Verleihung des akademischen Grades Bachelor of Science (B. Sc.) durch die Shanghai Jiaotong University in Shanghai in China
2004-2007	Studium der Elektrotechnik an der Shanghai Jiaotong University in Shanghai in China
03.2007	Verleihung des akademischen Grades Master of Science (M. Sc.) durch die Shanghai Jiaotong University in Shanghai in China
2007-heute	Wissenschaftlicher Mitarbeiter am Institut für Kommunikationstechnik an der Gottfried-Wilhelm-Leibniz-Universität Hannover

